Łukasz Komorowski, MSc

Lymphoid-specific role of the thioredoxin system in survival and drug sensitivity of leukemia with BCR-ABL1 translocation

Dissertation for a doctorate degree in Medical and Health Sciences

in the discipline of Medical Sciences

Supervisor: Małgorzata Firczuk, PhD

Department of Immunology

PhD thesis defense before the Medical Sciences Discipline Council

Medical University of Warsaw

Warsaw, 2022

Keywords: Leukemia, B cell acute lymphoblastic leukemia, chronic myeloid leukemia, Philadelphia chromosome, BCR-ABL1, peroxiredoxin 1, thioredoxin system, DNA damage repair

Słowa kluczowe: Białaczka, wywodząca się z prekursorów limfocytów B ostra białaczka limfoblastyczna, przewlekła białaczka szpikowa, chromosom Filadelfia, BCR-ABL1, peroksyredoksyna 1, system tioredoksyny, naprawa uszkodzeń DNA

Funding of the project

SONATA BIS 2015/18/E/NZ5/00723 grant funded by the National Science Centre, entitled „Novel pro-oxidative strategies in the treatment of B cell acute lymphoblastic leukemia". Principal investigator: dr Małgorzata Firczuk.

Grant financed by the Ministry of Science and Higher Education within the call "Regionalna Inicjatywa Doskonałości" (RID), 013/RID/2018/19, entitled „Strategies for the research development in the field of immune-oncology" (iONKO)". Principal investigator: prof. Jakub Gołąb.

I wish to sincerely thank my supervisor dr Małgorzata Firczuk, for her time, support, and effort to help me discover and use my potential.

I'd also like to thank all collaborators involved in the project, especially:

dr Agata Pastorczak and dr Joanna Madzio for numerous scientific discussions and their invaluable help with the project;

dr Max Bielecki for guiding me through newly discovered grounds of R programming and helping with clarification of statistical intricacies, always with a smile;

dr Klaudyna Fidyt, for introducing me to the team's methods and procedures, patience and understanding of the beginner's mistakes, and support throughout the whole project's duration;

Prof. Tomasz Stokłosa for sharing his knowledge, know-how, and materials, without which this project would be lacking.

Dr Martyna Poprzeczko for continuous help throughout the project without complaints, even when they were justified;

Kacper Szczygieł for starting the project and laying the foundation for my work;

Jaromir Hunia for relieving me of part of my duties, helping with the timely realization of the project;

Many thanks to my family and friends for their support. Special thanks to my wife Ada for her indulgence and bravely taking care of our daughter, allowing me to finish this PhD thesis in time, and to Julia for not giving her mother too hard time during the writing of this dissertation.

Last, but not least, I'd like to thank prof. Jakub Gołąb, for creating a professional environment in the Department of Immunology MUW, allowing me to conduct research with access to state-of-the-art equipment, and all my colleagues from the Department for always being there with great advice and a good word.

Table of contents

List of figures

List of tables

Abbreviations

ABL1	V-abl Abelson murine leukemia viral oncogene homolog 1
ADE	adenanthin
AKT	protein kinase B
ALL	acute lymphoblastic leukemia
allo-HSCT	allogeneic hematopoietic stem cell transplantation
altNHEJ	alternative non-homologous end joining
AML	acute myeloid leukemia
ANXA5	annexin A5
AP	accelerated phase
AP1	activator protein 1
APOC2	apolipoprotein C-II
APOC4	apolipoprotein C-IV
ASCI	asciminib
ASXL1	additional sex combs like 1
ATF4	activating transcription factor 4
ATM	ataxia telangiectasia mutated
ATR	ataxia telangiectasia and Rad3-related protein
AUR	auranofin
B-ALL	B cell acute lymphoblastic leukemia
B-CLL	B cell chronic lymphocytic leukemia
BCR	breakpoint cluster region
BCRec	B cell receptor
BMPR1A	bone morphogenetic protein receptor type 1A
BOSU	bosutinib
BP	blast phase
BRCA1/2	breast cancer type 1/2 susceptibility proteins
BTG1	B cell translocation gene 1
CASD1	CRISPR-associated protein 1 domain containing 1
CAT	catalase
CBL	casitas B-lineage lymphoma
CDKN2A/B	cyclin dependent kinase inhibitor 2A/B
CFU	colony forming unit
CHEK1	checkpoint kinase 1
CHOP	C/EBP homologous protein
CIITA	class II major histocompatibility complex transactivator
CML	chronic myeloid leukemia
cNHEJ	classical non-homologous end joining
CP	chronic phase
CtIP	C-terminal binding protein 1 interacting protein
CUZD1	CUB and zona pellucida like domains 1

CYBB	cytochrome B-245 beta chain
Cys	cysteine
DAB2	disabled homolog 2
DASA	dasatinib
DDR	DNA damage response
DNA-PKcs	DNA-dependent protein kinase catalytic subunit
DNMT3A	DNA methyltransferase 3A
DSB	double strand break
EBF1	early B cell factor 1
ER	endoplasmic reticulum
ETV6	ETS translocation variant 6
FABD	F-actin binding domain
FES	tyrosine kinase feline sarcoma/Fujinami avian sarcoma oncogene homolog
FYN	FYN proto-oncogene
GEMA	gene expression and mutation analysis
GPx	glutathione peroxidase
GSEA	Gene Set Enrichment Analysis
GSH	glutathione
HIF-1α	hypoxia inducible transcription factor 1α
HLA	human leukocyte antigen
HR	homologous recombination
IKZF1	IKAROS family zinc finger 1
IL	interleukin
IMAT	imatinib
IRF8	interferon regulatory factor 8
ITGB2	integrin subunit beta 2
JAK	Janus kinase
JNK	c-Jun N-terminal kinase
KDM1A	(K)-specific demethylase 1A
KHDRBS3	KH RNA Binding Domain Containing, Signal Transduction Associated 3
LBP	lymphoid blast phase
LCK	lymphocyte cell-specific protein-tyrosine kinase
LIG3	DNA ligase III
LIG4	DNA ligase IV
LIX1	limb and CNS expressed 1
LRRC26	leucine rich repeat containing 26
LYN	V-Yes-1 Yamaguchi Sarcoma Viral Related Oncogene Homolog
MAPK	mitogen-activated protein kinases
MBP	myeloid blast phase
MLF1	myeloid leukemia factor 1
MLL	myeloid/lymphoid or mixed-lineage leukemia 1

MPAL	mixed phenotype acute leukemia
MRE11	meiotic recombination 11 homolog
MSH6	mutS homolog 6
mTOR	mammalian target of rapamycin
NADPH	reduced nicotinamide adenine dinucleotide phosphate
NBS1	nibrin
NFKB1	nuclear factor kappa B subunit 1
NF-κB	nuclear factor kappa-light-chain-enhancer of activated B cells
NGS	next generation sequencing
NHEJ	non-homologous end joining
NHEJi	non-homologous end joining inhibitor
NILO	nilotinib
NIRA	niraparib
NOX	NADPH oxidase
NRF2	nuclear factor erythroid 2-related factor 2
OLAP	olaparib
OxS	oxidative stress
p53	tumor protein 53
PARP1	poly(ADP-ribose) polymerase 1
PARPi	poly(ADP-ribose) polymerase inhibitor
PBS	phosphate buffered saline
PCA	principal component analysis
PCDHGC3	protocadherin gamma subfamily C, 3
Ph	Philadelphia chromosome
Ph+ B-ALL	Philadelphia chromosome positive B cell acute lymphoblastic leukemia
PI	propidium iodide
PI(4,5)P2	phosphatidylinositol 4,5-bisphosphate
PI3K	phosphoinositide 3-kinases
PKC	protein kinase C
PLCB1	phospholipase C beta 1
PLEK	pleckstrin
PONA	ponatinib
PP2A	serine/threonine-protein phosphatase 2A
PRAME	preferentially expressed antigen of melanoma
PRDX1	peroxiredoxin 1
PRKAR2B	protein kinase CAMP-dependent type II regulatory subunit beta
PTEN	phosphatase and tensin homolog
PURO	puromycin
RAD50	DNA repair protein RAD50
RAD51	DNA repair protein RAD51 homolog 1
RAG	recombinase activating gene
RAS	rat sarcoma virus GTPase

RB1	retinoblastoma 1
ROS	reactive oxygen species
RPL29	ribosomal protein L29
RUCA	rucaparib
RUNX	runt-related transcription factor 1
SAMHD1	SAM and HD domain containing deoxynucleoside triphosphate
SH3/2	Src-homology2/3
SHC	SH2 domain protein C
SHIP1	SRC homology 2 domain containing inositol polyphosphate 5-phosphatase 1
SOD	superoxide dismutase
SPARC	secreted protein acidic and cysteine rich
SRC	V-Src Avian Sarcoma (Schmidt-Ruppin A-2) Viral Oncogene Homolog
SRCIN1	SRC kinase signaling inhibitor 1
SSB	single strand break
ssDNA	single strand DNA
STAT	signal transducer and activator of transcription protein
TALA	talazoparib
TCF3	transcription factor 3
TET2/3	Tet methylcytosine dioxygenase 2/3
TKI	tyrosine kinase inhibitor
TKIres	resistant to tyrosine kinase inhibitors
TKIsen	sensitive to tyrosine kinase inhibitors
TPRG1	tumor protein p63 regulated 1
TXN	thioredoxin
TXNi	thioredoxin system inhibitors
TXN-R	thioredoxin reductase
UPR	unfolded protein response
XLF	X-ray repair cross-complementing protein 4-like factor
XRCC4	X-ray repair cross-complementing protein 4

Abstract in English

A fusion of the *breakpoint cluster region* (*BCR*) and *V-abl Abelson murine leukemia viral oncogene homolog 1* (*ABL1*) genes (*BCR-ABL1*) is a result of translocation between chromosomes 9 and 22. It causes formation of the aberrant Philadelphia chromosome (Ph), encoding BCR-ABL1, a constitutively active tyrosine kinase. BCR-ABL1 is the hallmark and main oncodriver of chronic myeloid leukemia (CML). Even though CML historically had a poor outcome, the introduction of tyrosine kinase inhibitors (TKIs) made it a maintainable and mostly treatable disease. Apart from CML, Ph is also found in a subset of another leukemia type, B cell acute lymphoblastic leukemia (B-ALL). This leukemia is a common pediatric malignancy, characterized by the accumulation of immature lymphocytes, but it also occurs in adults. It is mainly treated with chemotherapy, but in a substantial fraction of patients, it returns as a difficult to cure, chemotherapy-resistant disease, therefore novel therapeutic approaches are urgently needed. Philadelphia chromosome-positive B-ALL (Ph^+ B-ALL) is one of the high-risk subtypes of B-ALL. Even though CML responds very well to treatment with TKIs, Ph^+ B-ALL has a relatively poor survival prognosis, with approximately 50% of cases relapsing post initial treatment. For this reason, the search for novel Ph^+ B-ALL targets is of utmost importance.

One of the hallmarks of cancer is the dysregulation of redox homeostasis caused by elevated levels of reactive oxygen species (ROS). To counteract the effects of ROS accumulation and prevent cell death, malignant cells upregulate elements of antioxidant machinery. Recent studies have shown increased levels of ROS and increased expression of the thioredoxin (TXN) family antioxidant enzymes in B-ALL cell lines and primary cells. Particular dysregulation of redox homeostasis was observed in Ph^+ B-ALL.

The main aim of the presented thesis was to assess the TXN system as a therapeutic target in Ph-positive (Ph^+) leukemias. Another objective was to propose potential drug combination and to test it in *in vitro* cell models of Ph^+ leukemias.

Initial experiments showed that the inhibition of the TXN system with either auranofin (AUR) or adenanthin (ADE) caused increased cell death in lymphoid Ph^+ cell lines and sensitized them to TKIs. Moreover, increased expression of peroxiredoxin 1 (PRDX1), one of

the TXN system elements, was found in lymphoid Ph^+ cell lines and primary cells in comparison to myeloid CML cells. CRISPR-Cas9 mediated knockout of PRDX1 significantly reduced lymphoid, but not myeloid, Ph^+ cells' proliferation and sensitized them to TKIs. These results strongly indicated that PRDX1 plays a lineage-specific role in Ph^+ leukemias. RNAseq analysis of genome-wide changes in imatinib -induced gene expression patterns in lymphoid Ph^+ cell line upon PRDX1 knockout revealed dysregulation of some genes and pathways crucial to cell maintenance and survival, further verifying PRDX1 key role in lymphoid Ph^+ cells. Moreover, no significant changes in ROS levels and endoplasmic reticulum stress upon PRDX1 knockout were identified. Further investigations of the mechanism of cell death triggered by imatinib in PRDX1-deficient cells led to the recognition of increased DNA damage and non-homologous end joining (NHEJ) as a vulnerability of lymphoid Ph^+ cells. A triple combination of TKIs, NHEJ, and TXN system inhibitors showed promising responses in both lymphoid Ph^+ cell lines and patient-derived Ph^+ B-ALL primary cells.

In summary, the role of PRDX1 in Ph^+ cells was shown to be associated with cell survival, resistance to therapy, and maintenance of genomic integrity in a lymphoid-specific manner. Moreover, the TXN system was identified as a new therapeutic target in Ph^+ B-ALL, the inhibition of which enhanced the effectiveness of standard therapy. NHEJ was also discovered as a previously unknown vulnerability in Ph^+ B-ALL and should be further investigated. Overall, these studies uncover novel potential targets that can contribute to the improvement of the effectiveness of Ph^+ B-ALL therapy in the future.

Abstract in Polish

Specyficzna dla komórek limfoidalnych rola systemu tioredoksyny w przeżywalności oraz wrażliwości na leki białaczek z translokacją BCR-ABL1

Fuzja genów *BCR* oraz *ABL1* jest rezultatem translokacji pomiędzy chromosomami 9 i 22. Powoduje ona powstanie nieprawidłowego chromosomu Filadelfia (Ph), kodującego BCR-ABL1, konstytutywnie aktywną kinazę tyrozynową. BCR-ABL1 jest charakterystyczną cechą i głównym onkogenem przewlekłej białaczki szpikowej (CML). Pomimo, iż CML jest chorobą o historycznie złych rokowaniach, wprowadzenie do użytku klinicznego inhibitorów kinazy tyrozynowej (TKIs) w znakomitej większości przypadków znacznie poprawiło skuteczność leczenia. Poza CML, chromosom Ph występuje również u części chorych na ostrą białaczkę limfoblastyczną z prekursorów limfocytów B (B-ALL). B-ALL jest częstym nowotworem pediatrycznym, charakteryzującym się akumulacją niedojrzałych limfocytów, występuje jednak również u dorosłych. W leczeniu B-ALL stosowana jest głównie chemioterapia, jednak w wielu przypadkach choroba nawraca w trudnej do leczenia, lekoopornej postaci. Z tego powodu, nowe strategie leczenia są pilnie potrzebne. Podtyp B-ALL z chromosomem Ph (Ph^+ B-ALL) związany jest z wysokim, około 50% ryzykiem nawtoru choroby i niekorzystnym rokowaniem. Z tego względu, poszukiwanie nowych celów w terapii Ph^+ B-ALL jest bardzo ważne.

Jedną z typowych cech wielu nowotworów jest zaburzenie homeostazy redoks, spowodowane nadmierną produkcją reaktywnych form tlenu (ROS). Aby przeciwdziałać szkodliwym efektom akumulacji ROS, komórki nowotworowe muszą zwiększać aktywność mechanizmów odpowiedzi antyoksydacyjnej. Badania wykazały wzmożoną produkcję ROS oraz podwyższoną ekspresję antyoksydacyjnych enzymów z rodziny tioredoksyn (TXN) w liniach komórkowych oraz materiale pierwotnym pochodzącym od chorych na B-ALL. Ponadto, wzmożone zaburzenie homeostazy redoks zostało zaobserwowane w podtypie Ph^+ B-ALL.

Głównym celem poniższej pracy była ocena układu TXN jako potencjalnego celu terapeutycznego w Ph-pozytywnych (Ph^+) białaczkach. Kolejnym celem było zaproponowanie nowej kombinacji leków i przetestowanie jej aktywności cytotoksycznej w badaniach *in vitro* w modelach komórkowych białaczek Ph-pozytywnych.

Pierwsze eksperymenty wykazały, że zahamowanie aktywności układu TXN za pomocą auranofiny (AUR) lub adenantyny (ADE) spowodowało wzmożoną śmierć limfoidalnych komórek Ph^+ oraz uwrażliwiło je na TKIs. Ponadto, w porównaniu do mieloidalnych komórek CML, zaobserowano podwyższoną ekspresję proksyredoksyny 1 (PRDX1), elementu układu TXN, zarówno w liniach komórkowych jak i materiale pierwotnym. Wyciszenie ekspresji PRDX1 za pomocą techniki CRISPR-Cas9 obniżyło żywotność, proliferację oraz zwiększyło wrażliwość na TKIs w limfoidalnych komórkach Ph^+, natomiast w komórkach mieloidalnych nie zaobserwowano podobnych efektów. Wyniki te sugerują specyficzną dla komórek limfoidalnych rolę PRDX1 w białaczakch Ph^+. Ponadto analiza RNAseq wykazała, że wyciszenie PRDX1 w limfoidalnych komórkach Ph^+ spowodowało zaburzenia ekspresji wielu genów i szlaków niezbędnych dla podtrzymywania oraz przeżycia komórek, potwierdzając rolę PRDX1 w limfoidalnych komórkach Ph^+. Co ciekawe, nie wykazano istotnych różnic w poziomach ROS oraz stresu siateczki śródplazmatycznej pomiędzy komórkami kontrolnymi i komórkami z wyciszeniem PRDX1. Zaobserwowano natomiast podwyższony poziom uszkodzeń DNA oraz zwiększenie ekspresji genów związanych z naprawą DNA poprzez scalanie niehomologicznych końców (NHEJ). Dalsze badania wykazały, że komórki Ph^+ B-ALL są szczególnie wrażliwe na zahamowanie NHEJ, szczególnie przy jednoczesnym zahamowaniu układu TXN. Potrójna kombinacja TKIs, układu TXN oraz inhibitorów NHEJ dała obiecujące rezultaty, zarówno na liniach komórkowych jak i komórkach pierwotnych pochodzących od chorych na Ph^+ B-ALL.

Podsumowując, w pracy wykazano specyficzną dla Ph^+ komórek limfoidalnych rolę PRDX1 w żywotności, wrażliwości na terapię oraz utrzymaniu integralności DNA. Ponadto, układ TXN został wytypowany jako nowy cel terapeutyczny w Ph^+ B-ALL, którego zahamowanie potęguje efekty standardowej terapii. Mechanizm NHEJ został również rozpoznany jako dotychczas nieznany słaby punkt Ph^+ B-ALL, warty dodatkowych badań. Podsumowując, przedstawione w poniższej pracy wyniki ukazują nowe potencjalne cele terapeutyczne, które w przyszłości mogą przyczynić się do poprawienia skuteczności terapii Ph^+ B-ALL.

1. Introduction

1.1. BCR-ABL1 rearrangement

Philadelphia chromosome (Ph) is a short aberrant chromosome formed by a reciprocal t(9;22)(q34;q11) translocation between the chromosomes 9 and 22. It contains a fusion gene consisting of the breakpoint cluster region (*BCR*) and the V-abl Abelson murine leukemia viral oncogene homolog 1 (*ABL1*), encoding constitutively active tyrosine kinase BCR-ABL1, first found in chronic myeloid leukemia (CML)[1]. BCR-ABL1's distinctive characteristic is the ability to trigger malignant transformation in hematopoietic precursors without any accompanying genetic events[2]. It comes in several different isoforms[3] and is found in distinct diseases[4–6]. Apart from BCR-ABL1 presence in up to 95% of CML cases[7], its expression is also observed in up to 2-4% of pediatric and 50% adult B-cell acute lymphoblastic leukemia (B-ALL) patients [8,9]. Although, BCR-ABL1 is the main oncogenic driver in these diseases, their diverse genetic background and lineage commitment make up their characteristic profiles, which is reflected in their different sensitivity to pharmaceutical inhibition of BCR-ABL1[7]. This shows that BCR-ABL1 impact on transformed cells goes beyond its tyrosine kinase activity, with a complex role in the cells.

1.1.1. BCR-ABL1 isoforms and their occurrence in hematological malignancies

The site of a breakpoint during Ph formation determines the BCR-ABL1 isoform. The typical and most common BCR-ABL1 transcripts are: 1) e1a2, encoding 185-190kDa variant (also known as p190), 2) e13a2 and e14a2, both coding 210kDa variant (p210) and 3) e19a2, which encodes 230kDa form (p230)[3]. p210 isoform is mostly associated with CML, as it is present in approximately 95% of cases, and p190 is identified in 70% of Ph-positive B-ALL (Ph^+ B-ALL)[7,10]. p230 is present only in rare cases of acute myeloid leukemia (AML) or specific subtypes of CML[10], and is not further discussed in this study. The precise mechanism of Ph formation and the breakpoint site determination has not been fully elucidated yet, although non-homologous end joining (NHEJ) and single-strand annealing are proposed to play a role in those processess[11]. Moreover, an analysis of p190 and p210 genomic breakpoints provided

some evidence for differential mechanisms underlying both isoforms formation, although the precise events promoting any of them are still unclear[12].

Both p190 and p210 contain the same truncated ABL1 fragment (aa 46-1149), containing a well-characterized Src-homology2/3 (SH3/2)-kinase unit, necessary for the ABL1 activity and F-actin binding domain (FABD), allowing for BCR-ABL1 association with the cytoskeleton. The main difference between those variants lies in the BCR fragment, as only p210 contains Dbl-homology and Pleckstrin-homology domains[4], indicating their importance in distinct disease phenotypes caused by both variants.

1.1.2. BCR-ABL1 signaling

BCR-ABL1 aberrant signaling is caused by a constitutive activation of the ABL1 kinase domain in the fusion protein. ABL1 is a member of the ABL non-receptor tyrosine kinases family with a diverse role in the cell, including regulation of cell growth and proliferation. It was also shown to be required for mice neonatal development, as its knockout caused lethality in approximately 50% of animals. Regulation of the ABL1 activity is related to its structural changes, with an “open” active and “closed” inactive states[13]. Effects of ABL1 are dependent on its subcellular localization – in the cytoplasm, it promotes cell proliferation and survival, while in the nucleus it inhibits the cell cycle and activates cell death. In cells expressing BCR-ABL1, normal ABL1 is also present, acting as a tumor suppressor[14]. In this context, FABD at the C-terminus of BCR-ABL1 is crucial for its effects, as it allows it to remain in the cytoplasm, despite the nuclear localization signal’s presence[15].

The BCR-ABL1 is responsible for triggering of several pathways, including the rat sarcoma virus GTPase (RAS)/mitogen-activated protein kinases (MAPK) and the nuclear factor kappa-light-chain-enhancer of activated B cells (NF-κB), which together contribute to increased cell growth, cell cycle progression, and survival. Also, the Janus kinase (JAK)/signal transducer and activator of transcription protein (STAT) pathway is upregulated, improving cell survival and causing cytokine independence. Moreover, BCR-ABL1 activates the mammalian target of rapamycin (mTOR) and phosphoinositide 3-kinases (PI3K)/protein kinase B (AKT), preventing apoptosis and ameliorating cells viability[16].

Despite having the same kinase domains, p190 and p210 are preferentially found in very distinct diseases, which indicates major differences in both isoforms' signaling. Moreover, in an *in vivo* study, mice injected with bone marrow cells transduced with p190 developed aggressive B-cell leukemia and recipient animals of p210-expressing cells showed milder signs of CML-like disease[17]. Despite that knowledge, no in-depth research comparing BCR-ABL1 isoforms signaling wasn't conducted until 2017, when a proteomic studies of p190 and p210 interactomes was published[18]. BCR-ABL1 interactomes and phosphoproteomes were investigated *in vitro* utilizing IL-3 dependent murine hematopoietic Ba/F3 cell line, transduced with either p190 or p210. Results of those studies revealed the differential BCR-ABL1 binding partners, probably linked to differential structure of both isoforms. Even though both are localized in the cytoplasm, p190 was shown to preferentially bind to cytoskeleton remodeling proteins, while p210 to proteins in the cell membrane proximity[18]. Interestingly, the Pleckstrin-homology domain, present only in p210, was also shown to strongly interact with phosphatidylinositol 4,5-bisphosphate ($PI(4,5)P_2$), which is a component of cell membranes. Interestingly, mutants of p210 unable to bind $PI(4,5)P_2$ displayed a very similar localization pattern to p190, while binding strength of p210-specific partners by p210 was decreased to almost identical levels as their unspecific binding with p190[4]. Those observations indicate that the Pleckstrin-homology domain, present in p210 and absent in p190, may be a key element of differential signaling of those two BCR-ABL1 isoforms.

1.2. Philadelphia-positive leukemias

Among leukemias most commonly associated with BCR-ABL1 expression are CML and Ph^+ B-ALL. Despite the shared main oncodriver, CML and Ph^+ B-ALL are very distinct diseases. Their main characteristics and features are discussed in the next paragraphs.

1.2.1. CML

CML is a myeloproliferative disease and its development can be triggered by BCR-ABL1 expression alone[17], without any accompanying mutations in approximately 90% of cases[19]. One per 100,000 people are diagnosed with it annually in Europe, usually at a mild and manageable chronic phase (CP)[20].

CML in CP is almost asymptomatic and leukemic cells undergo similar to normal maturation and regulation[21]. More recently, single cell analysis of newly diagnosed CML samples allowed for identification of fairly frequent additional mutations (25-30% of tested cases) of genes related to methylation control, such as *Tet methylcytosine dioxygenase 2/3* (*TET2/3*), DNA methyltransferase 3A (*DNMT3A*), a*dditional sex combs like 1* (*ASXL1*), (K)-specific demethylase 1A (*KDM1A*), and mutS homolog 6 (*MSH6*)[22,23]. Unfortunately, there was no further investigation of this observations' significance up to date.

Although CML is now a highly treatable disease with cure rate reaching 90-95%, in some cases it progresses to a more aggressive accelerated phase (AP) and subsequently to a mostly fatal blast phase (BP). CML progresses to a myeloid BP (MBP) in 70% of cases, while the remaining 30% undergo a lineage shift to lymphoid-like phenotype, entering lymphoid BP (LBP)[24]. Cells in BP exhibit accumulation of additional genetic mutations, and cannot longer differentiate, resulting in clonal expansion and accumulation of immature progenitors[25]. Even though exact mechanism and timeline of CML progression to BP are still not fully understood, it is certainly linked to the increase of BCR-ABL1 expression, resulting in genomic instability and accumulation of additional mutations[26]. Genetic aberrations other than BCR-ABL1 translocation are present in 70-80% of all CML BP cases, while only 10-30% patients in CP exhibit additional mutations[19,22,23]. MBP and LBP mutational landscapes are very diverse. In MBP, the most frequently mutated gene is epigenetic regulator *ASXL1*, mutated in 40% of MBP cases. Other frequent mutations include tumor suppressor genes, such as *runt-related transcription factor 1* (*RUNX1*, 40% of cases) and *tumor protein 53* (p53, 20% of cases). In LBP on the other hand, the most common mutations occur in *IKAROS family zinc finger 1* (*IKZF1*) and *cyclin dependent kinase inhibitor 2A/B* (*CDKN2A/B*), present in 55% and 50% of LBP cases, respectively, which are also the most frequently mutated genes in Ph^+ B-ALL[26–28]. Moreover, characteristics of CML in LBP, including response to treatment, phenotype and disease's clinical picture is more similar to Ph^+ B-ALL than to CML in CP , and is often misdiagnosed as Ph+ B-ALL[29].

Currently, the first line treatment of CML consists of tyrosine kinase inhibitors (TKIs), a group of potent BCR-ABL1 inhibitors. TKIs are small, orally available compounds, that inhibit

kinase activity of BCR-ABL1, downregulating its oncogenic signaling[30]. TKIs approved for CML monotherapy by both the U.S. Food and Drug Administration (FDA) and the European Medicines Agency (EMA), can be divided into two subgroups: competitive (imatinib [IMAT], nilotinib [NILO], dasatinib [DASA], and bosutinib [BOSU], ponatinib [PONA])[7] and allosteric (asciminib [ASCI])[31,32] BCR-ABL1 inhibitors. In case of poor or no response to monotherapy treatment, often meaning progression to AP and BC, intensive chemotherapy (including use of anthracycline, cytosine arabinoside, etoposide, carboplatin, fludarabine, 5-azacitidine, decitabine, or HCVAD) is added to TKIs[7]. Unfortunately, the results of TKIs and chemotherapy combinations are still usually poor, with 10% response rate in MBP and up to 50% in LBP, although the median survival still not exceeds 10 months[7].

1.2.2. B-ALL

Every year, approximately 1 in 78,000 of adults and 1 in 24,000 of children are diagnosed with acute lymphoblastic leukemia (ALL)[33,34], and 75% of all ALL cases are of B cell origin – B-ALL[35], characterized by the accumulation of abnormally proliferating immature B cell progenitors in the bone marrow. In most cases, the disease develops *de novo* in healthy individuals, although some factors predisposing to ALL development have been previously proposed (including Down syndrome, Ataxia-Telangiectasia, and Nijmegen breakage syndrome)[36]. More recently, genome-wide association studies identified a set of genes linked to susceptibility of ALL development, encoding tumor suppressors and transcription factors regulating hematopoietic and lymphoid development. Among those genes, some crucial for B cell maturation were recognized, including *IKZF1* and *Paired box 5* (*PAX5)*[37].

B-ALL is a very genetically heterogenous disease. Currently, there are more than 30 identified subtypes[38,39]. Most of B-ALL cases are diagnosed in children with achievement of complete remission in up to 90% pediatric patients. Even though, some risk-associated genetic factors, including rearrangements of *transcription factor 3* (*TCF3), myeloid/lymphoid or mixed-lineage leukemia 1 (MLL), BCR/ABL1* translocation, or *IKZF1* status[39], cause development of therapy-resistant aggressive disease, and approximately 20% of pediatric and 40% adult patients experience relapse, significantly lowering their survival chances[39–41]. Among the most prevalent high-risk subtypes is Ph^+ B-ALL, characterized by *BCR/ABL1*

translocation. Its incidence increases with patients age, with approximately 2-4% in pediatric and up to 50% in adult cases of B-ALL[8,9]. Unlike in CML, BCR-ABL1 expression alone is insufficient for malignant transformation in B cells and additional mutations are required for the development of this leukemia subtype, indicating more complex genetic landscape of Ph^+ B-ALL[42].

1.2.3. Molecular profile of Ph+ B-ALL

Ph^+ B-ALL is a genetically complex disease, with diverse mutations accompanying BCR-ABL1 expression. Even though many alterations are unique to specific cases, several recurrent mutations were discovered. Interestingly, two most frequently mutated genes in Ph^+ B-ALL, *IKZF1* and *CDKN2A/B,* are also common in CML LBP.

Loss-of-function mutations in *IKZF1* are observed in over 70% of Ph^+ B-ALL cases[43,44]. They are the result of either mono-allelic (in rare cases also bi-allelic) or partial *IKZF1* deletion, resulting in a dominant-negative IK6 isoform expression[43,44]. Elevated recombinase activating gene (RAG) activity in Ph^+ B-ALL is attributed to deletions resulting in the generation of this isoform[44,45]. In a cohort of one hundred *de novo* Ph^+ B-ALL patients, elevated IK6 expression correlated with BCR-ABL1 levels, additional mutations occurrence, increased risk of relapse, decreased relapse-free and overall survival (OS)[46]. Normal IKZF1 is required for lymphopoiesis, and its reconstitution in *IKZF1*-deleted B-ALL cells was shown to induce energy deficit through downregulation of several proteins involved in glucose transport and metabolism, indicating its role as a gatekeeper preventing malignant transformation[47].

PAX5 is another gene frequently deleted in Ph^+ B-ALL, as its mutations are identified in up to 40-45% of Ph^+ B-ALL cases[48]. PAX5 is a transcription factor involved in the regulation of B cells' maturation and similarly to IKZF1 acts as a tumor suppressor by downregulating glucose metabolism in Ph^+ B-ALL cells[47]. Monoallelic PAX5 deletion has been also shown to be a sufficient additional event to p190 expression for the development of B-ALL in approximately 90% of tested mice[49].

CDKN2A/B gene is mutated in 45% of Ph^+ B-ALL cases[48]. Its product acts as a tumor suppressor, able to cause cell cycle arrest and activate p53[48]. *CDKN2A/B* mutations are a

prognostic factor for poor Ph+ B-ALL outcomes in patients and its higher frequencies were observed after relapse, regardless of age[50,51]. Interestingly, alterations in *CDKN2A/B* were identified in all B-ALL patients harboring *PAX5* mutations, independently of disease subtype, indicating a strong link between those two proteins and their significance in normal and malignant B cells[52].

Among less frequently identified alterations, mutations of *B cell translocation gene 1 (BTG1)* and *retinoblastoma 1 (RB1),* in 18% and 14% of Ph+ B-ALL cases respectively, were observed[48]. Both genes are involved in the negative regulation of cell cycle progression, thus acting as tumor suppressors[48]. Moreover, mutations in *early B cell factor 1* (*EBF1*; 13% of cases) and *ETS translocation variant 6* (ETV6; 5%) were discovered in Ph+ B-ALL patients. Although the occurrence of those aberrations is relatively low, EBF1 and ETV6 are transcription factors engaged in the regulation of B-cells maturation[48]. This could indicate that dysregulation of transcription factors specific to B cells is a genetic event needed for Ph+ B-ALL development in addition to BCR-ABL1 expression.

Apart from genetic alterations, the Ph+ B-ALL phenotype is also heavily shaped by its B cell origin. During normal B cell maturation, cells undergo two selection stages: positive, in which cells with too low pre-B cell receptor (BCRec) signaling activation undergo apoptosis, and negative, removing cells that exhibit overactivation of downstream pre-BCRec signaling caused by auto-antigens[53]. Even though Ph+ B-ALL cells lack pre-BCRec subunits required for positive selection, BCR-ABL1 activates pre-BCR downstream signaling, allowing for cell survival. On the other hand, hyperactive BCR-ABL1 could eliminate cells through negative selection[54]. To prevent cell death, precise regulation of BCR-ABL1 is needed in Ph+ B-ALL cells. One of such mechanisms is the overexpression of phosphatase and tensin homolog (PTEN) in B-ALL cells, which is surprising, as PTEN is considered to be a tumor suppressor in most malignancies. It downregulates PI3K/AKT signaling to a level preventing negative selection of cells, and PTEN silencing causes overactivation of AKT, leading to cell death[55]. Ph+ B-ALL cells can also escape negative selection by expression of surface inhibitory receptors, recruiting inhibitory SRC homology 2 domain containing inositol polyphosphate 5-phosphatase 1

(SHIP1) phosphatase, which diminishes BCR-ABL1 signaling to an appropriate, intermediate level[54].

1.2.4. Ph+ B-ALL treatment and prognosis

Historically, the prognosis for Ph^+ B-ALL patients was very poor with essentially no long-term survivors without allogeneic hematopoietic stem cell transplantation (allo-HSCT). Fortunately, in recent years, great progress in the management of Ph^+ B-ALL has been made due to the introduction of IMAT, the first drug in the class of TKIs. Apart from IMAT, two other TKIs are FDA-approved for Ph^+ B-ALL treatment – a second-generation TKI - DASA and a third-generation PONA. These inhibitors were designed to overcome IMAT resistance developed by some patients, caused mainly by mutations in BCR-ABL1, rendering IMAT ineffective[7,30]. Since the introduction of the TKIs to Ph^+ B-ALL treatment, a significant improvement of OS has been observed. However, in adult Ph+ B-ALL patients the 5-year OS achieved with currently approved therapies is still relatively low not exceeding 50% and in Ph+ B-ALL pediatric patients prognosis is still worse than for other B-ALL subtypes[56,57].

Current frontline Ph^+ B-ALL therapy in Europe consists mostly of TKIs and chemotherapy in several treatment stages. During the induction phase, the usually used drugs include prednisone, cyclophosphamide, vincristine, and anthracycline alone or with L-asparaginase. In the consolidation phase, cytosine arabinoside, L-asparaginase, cyclophosphamide, and methotrexate are used[7]. In case of relapse, if the leukemic cells qualify for immunotherapy, antibodies against CD22 (inotuzumab ozogamicin) and CD19 (blinatumomab) are used[58,59]. Moreover, TKIs usage help to obtain a high complete remission rate in Ph^+ B-ALL patients. This allows for more patients to undergo allo-HSCT, although its legitimacy is debatable, as it is burdened with the high treatment-related mortality (even up to 40%).

Despite the introduction of TKIs significantly improved short-term OS in Ph^+ B-ALL, the overall long-term survival is still relatively low. This is mainly due to the acquisition of TKIs resistance by the leukemic cells in a manner either dependent or independent of BCR-ABL1. BCR-ABL1-dependent resistance is caused by point mutations in the *ABL1*, decreasing the

TKIs' affinity, thus lowering their effectiveness. The most well-described mutation, causing resistance to IMAT and DASA is the T315I mutation[60,61]. Even though PONA is still an effective inhibitor of T315I mutated BCR-ABL1, some parallel mutations, such as F359V or D276G, induce PONA resistance[60,61]. Among BCR-ABL1-independent mechanisms of resistance to therapy, overactivation of BCR-ABL1 downstream signaling pathways was identified. AKT/mTOR and RAS/MAPK pathways were found to play a role in IMAT-induced therapy resistance in Ph^+ B-ALL cell lines and primary cells[62–64]. Moreover, the microenvironment of leukemic cells may also contribute to their resistance. A study investigating the impact of TKIs on mesenchymal stem cells (MSC) present in the bone marrow, revealed that MSCs subjected to IMAT treatment elevated secretion of several molecules, such as interleukin 7, activating pro-survival pathways through overactivation of JAK1 and JAK3 in Ph^+ B-ALL cells[65].

As a significant percentage of Ph^+ B-ALL patients don't respond or relapse post-treatment, new approaches to ameliorate therapy effectiveness are intensively tested in clinical trials. A large portion of those tests focuses on the combination of the first, second, and third-generation TKIs with chemotherapy and immunotherapy. Even though regimens including TKIs with intensive chemotherapy in the clinical tests achieved high rates of 5-year OS (up to 80%), its adverse side effects, preventing its application for the elderly and unfit patients, prompted search for chemotherapy-free approaches[30]. Steroids combination with IMAT and NILO was shown to be safe for older or unfit patients, although OS wasn't significantly improved due to high remission rates, in many cases related to T315I mutation of BCR-ABL1[66,67]. Despite this, preliminary results of another ongoing study investigating efficacy of PONA with prednisone in older or unfit patients population indicate that studies of this approach shouldn't be abandoned yet[68]. Also, combinations of TKIs with blinatumomab, a drug approved for ALL treatment, were studied in several clinical tests. Preliminary results of study investigating combination of DASA with blinatumomab and steroids, showed promising results, with 2-years OS reaching 87%, although some relapses due to T315I were observed[69]. Another phase 2 trial, assessing same combination with modified protocol reported 100% of 1-year OS, with estimated 85% 3-year OS median[70]. Some clinical trials are still ongoing, testing such combinations as DASA and consolidation

therapy with either vincristine and prednisone or high-dose methotrexate and cytarabine (NCT05026229), or PONA with blinatumomab or IMAT and chemotherapy (NCT04722848), although no preliminary data is available. Nevertheless, combination of some TKIs with blinatumomab might not be desirable, as DASA and PONA were shown to abrogate *in vitro* efficacy of blinatumomab towards Ph^+ B-ALL cells[71].

Moreover, ASCI is investigated in the context of Ph^+ B-ALL treatment. A registered, although not yet recruiting, phase 4 study aims to compare ASCI monotherapy and its combination with IMAT effectiveness in Ph^+ B-ALL and CML to other TKIs in monotherapy (NCT04877522). Two other active phase 1 studies are also testing ASCI combinations with either DASA and prednisone (NCT03595917) or with either IMAT, DASA, or nilotinib (NCT02081378).

Even though many clinical trials are ongoing, also other, more selective and potent approaches to Ph^+ B-ALL treatment are seeked in pre-clinical studies, aiming to utilize some of its vulnerabilities to potentially improve clinical outcomes of patients. One of such strategies is targeting altered metabolic and molecular pathways in leukemias. Exploiting specific changes in redox homeostasis or DNA repair have already been studied in some leukemias[47,72–74], although more studies are still needed to assess their relevance to the Ph^+ B-ALL subtype.

1.3. Oxidative stress

The hallmark of multiple cancers is increased oxidative stress (OxS), caused by dysregulation of ROS production and metabolism[75]. Disrupted redox homeostasis might be a target for therapy of cancer, and its potential has been studied in several malignancies, including those of B cell origin, with promising outcomes[73,75–77].

1.3.1. Oxidative stress in B-ALL

The main source of ROS in the cell is oxidative metabolism. Although ROS are present in the cells physiologically, playing a role in redox signaling, their levels must be precisely controlled to prevent their accumulation. Sources of ROS in the cell may be either intra- or extracellular. Among intrinsic producers of ROS are, apart from mitochondrial oxidative

phosphorylation, protein folding in the endoplasmic reticulum (ER), and fatty acid oxidation, with a plethora of ROS-generating enzymes, such as reduced nicotinamide adenine dinucleotide phosphate (NADPH) oxidases (NOXs) or cytochrome P450. Some of the extrinsic ROS sources are microenvironment, pollutants, and various therapies, including radiation[78,79]. OxS occurs when there is an imbalance between ROS production, uptake and removal, and this prolonged state potentially causes disruption of redox homeostasis, cell damage, and eventually cell death.

Elevated ROS level is a characteristic trait of many cancers, including leukemias, and increased OxS was also observed in primary B-ALL samples[74]. A study measuring circulating OxS markers in B-ALL patients discovered their prominent increase, with concomitant downregulation of non-enzymatic and enzymatic antioxidants, such as superoxide dismutase (SOD), catalase (CAT), glutathione (GSH), and glutathione peroxidase (GPx)[80]. In pediatric ALL patients, lowered GPx level was shown with a parallel accumulation of OxS markers, such as 8-hydroxy-2'-deoxyguanosine (8-OHdG; a derivative of DNA oxidation)[81,82]. This observation was confirmed to be lymphoid specific, as such changes weren't detected in CML cells[72].

Increased ROS production in B-ALL cells results from several factors. First, increased proliferation rate and accelerated metabolism elevate ROS levels in malignant cells, induced by oncogenic signaling, which is responsible for ROS overproduction[83–85]. Moreover, ROS accumulation is caused by a leukemia-characteristic overactivation of such pathways as PI3K/PTEN/AKT/mTOR, JAK/STAT, or rapidly accelerated fibrosarcoma (RAF)/MAPK kinase (MEK)/extracellular signal-regulated kinase (ERK)[86,87]. Activation of these pathways is often induced by many oncoproteins, including BCR-ABL1, making them partially responsible for elevated ROS levels in B-ALL cells[88].

1.3.2. BCR-ABL1 impact on redox homeostasis

The direct link between BCR-ABL1 and redox homeostasis was shown in the past. Inducible expression of BCR-ABL1 in several hematopoietic cell lines, including IL-3 dependent pro-B cells, showed an increase in H_2O_2 production and activation of PI3K pathway elements[89,90]. Pi3K/AKT activation subsequently increased mitochondrial and NOXs activity,

further elevating ROS levels[91]. Interestingly, the extrinsic addition of H_2O_2 to cells caused activation of several BCR-ABL1 substrates, such as casitas B-lineage lymphoma (CBL), SH2 domain protein C (SHC), and ABL1 itself[90]. This indicates that BCR-ABL1-dependent ROS accumulation provides a signaling feedback loop, potentiating oncogenic signaling.

Induction of OxS by BRC-ABL1 was also shown to promote genomic instability in CML, resulting in accumulation of mutations that could benefit the cell's survival and accelerate disease progression. OxS-induced mutations can occur in BCR-ABL1, granting cells' resistance to TKIs such as IMAT. In studies utilizing both *in vitro* and *in vivo* models, reduction of ROS levels in IMAT-treated groups revealed significantly lower rate of mutagenesis and acquisition of resistance to treatment[92,93].

1.3.3. Mechanisms of protection of cancer cells from oxidative damage

Prolonged OxS can lead to major consequences in cells, eventually even to their death. That is why leukemic cells must compensate for higher ROS production to avoid apoptosis. To do so, cancer cells induce several transcription factors linked to redox-response, such as NF-κB, hypoxia inducible transcription factor 1α (HIF-1 α), p53, activator protein 1 (AP-1), or nuclear factor erythroid 2-related factor 2 (NRF2)[94–97]. Those transcription factors initiate expression of antioxidant small molecules and enzymes, such as GSH, NADPH, bilirubin, and thioredoxins (TXNs), thioredoxin reductases (TXN-Rs) peroxiredoxins (PRDXs), heme oxygenase or CAT[98,99].

NADPH supply in B-ALL is indispensable for maintenance of redox homeostasis, as NADPH reducing potential is required for renewal of several main antioxidant enzymes. This demand is met by upregulation of PPP by serine/threonine-protein phosphatase 2A (PP2A). PP2A also downregulates AKT, subsequently activating the Forkhead box proteins, inducing antioxidant response[72].

GSH and TXN systems are two main antioxidant pathways in the cell, and some of their elements are frequently upregulated in leukemia. Many studies indicate the TXN system plays a major role in B cell malignancies[77,100].

1.3.4. TXN system

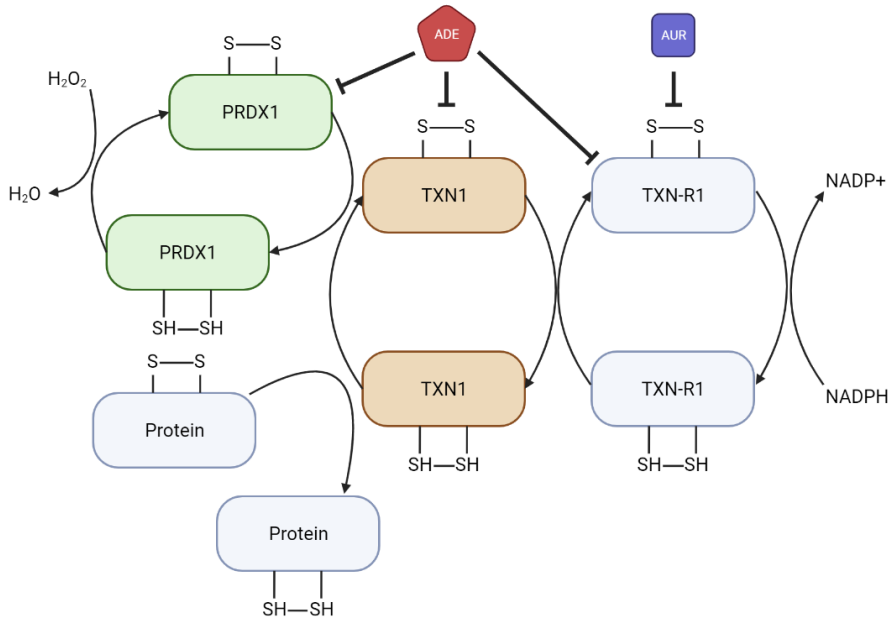

Fig. 1. Simplified illustration of TXN system elements and inhibitors. Briefly, PRDX1 is oxidized while decomposing H_2O_2 to H_2O. Oxidized PRDX1 is in turn reduced by TXN1, which is subsequently reduced by TXN-R1. TXN-R1 restoration requires NADPH reduction potential, generating $NADP^+$. Two TXN system inhibitors ADE and AUR with their targets are also indicated. Based on a publication by Karlenius and Tonissen[101]. ADE – adenanthin, AUR – auranofin, PRDX1 – peroxiredoxin 1, TXN1 – thioredoxin 1, TXN-R1 – thioredoxin reductase 1.

PRDX, TXN, and TXN-R are three groups of enzymes making up the TXN system (Fig. 1). TXN system is involved in the regulation of gene expression, antioxidant response, apoptosis and proliferation[102]. Its antioxidant role is exerted through reduction of disulfide bond in protein substrates. Additionally, PRDX is involved in a reduction of H_2O_2 to water, and is subsequently regenerated by reducing capabilities of TXN and TXN-R with the utilization of NADPH[102]. TXN1 was also shown to stimulate antiapoptotic response through activation of NF-κB[103], blocking apoptosis signal-regulating kinase 1[104] and inhibiting caspase 3's active site[105]. Moreover, TXN1 was shown to activate PI3K/AKT signaling by inhibition of its negative regulator PTEN, stimulating cells proliferation[106].

1.3.5. PRDX1 and its role in cancer

PRDXs are a large family of antioxidant enzymes, categorized by several conserved cysteine (Cys) residues: 2-Cys (PRDX1-4), atypical 2-Cys (PRDX5), and 1-Cys (PRDX6). PRDX1 contains two conserved Cys at positions 53 and 173, which are required for its catalytic

function[107]. PRDX1 is usually present in both cytoplasm and nucleus in catalytically active dimers, which forms decamers under specific conditions, such as high PRDX1 concentration or low pH, reduced state. Upon hyperoxidation, PRDX1 decamers can also form higher form aggregates functioning as chaperones under stress conditions[108–110].

PRDX1, apart from protection from ROS accumulation, may play a significant role in cancer cells, some of which are not dependent on its catalytic function. Interestingly, it was discovered that PRDX1 inhibits wild type ABL1 (also called c-ABL)[111]. Normal ABL1 was later shown to be expressed in CML, acting as a tumor suppresor[14]. PRDX1 can also bind and inhibit c-Jun N-terminal kinase (JNK), preventing overactivation of JNK-induced stress signaling[107]. PRDX1 was also shown to interact with such transcription factors as androgen receptor or NF-κB, suppressing cell death[112]. PRDX1 expression was also linked to cell maintenance and drug resistance in several cancer types, including breast[113–115], lung[116], and follicular lymphomas[117]. Those results indicate that PRDX1 plays a supportive role in some malignancies, providing rationale for its targeting in anticancer approaches.

1.3.6. Inhibition of antioxidant pathways as a potential anticancer therapy

As malignant B cells exert elevated ROS levels and their survival heavily depends on antioxidant systems activity, enhancement of oxidative stress seems a feasible therapeutic approach for B cell leukemias. Indeed, inhibition of GSH or L-cysteine depletion exerts cytotoxic effects in B cell malignancies[118,119]. Interestingly, pharmacological inhibition of the TXN system showed significant cytotoxicity in B cell leukemias, especially in combination with other drugs (i.e. venetoclax)[74,120] or prooxidative compounds, such as L-ascorbate[73].

Auranofin (AUR) and adenanthin (ADE) are two of the existing TXN system inhibitors, often used in the studies of the TXN system. AUR is an FDA approved drug in rheumatoid arthritis, inhibiting TXN-R1/2, causing disruption of the whole TXN system by removing the reducing potential of TXN-R1/2[121]. Apart from the TXN system inhibition, AUR was also shown to regulate PI3K/AKT/mTOR signaling[122], HIF-1α[123], and deubiqitinases[124]. AUR effects were studied in several cancer types, including B cell malignancies, with promising effects[73,74,121]. ADE is the second TXN system inhibitor with an ability to bind to active Cys residues in TXN

system elements (TXN, TXN-R, and PRDX), rendering them inactive [125]. Even though ADE's efficacy in killing cancer cells have been confirmed[74,126,127], it was also shown to be less selective towards cancer cells than AUR, as it more prominently killed normal peripheral blood mononuclear cells[74]. Moreover, ADE disrupted functions of human natural killer cells[128], suggesting its use should be limited to *in vitro* studies of the TXN system.

1.4. DNA damage response

Maintaining DNA integrity is crucial for cells, as the accumulation of DNA damage can lead to apoptosis or malignant transformation. DNA lesions occur in physiological conditions due to external factors, such as ionizing or UV radiation, and internal, like errors in DNA replication or activity of certain enzymes. DNA damage can take the form of single-strand (SSB) or double-strand break (DSB). DSB is the deadliest type DNA damage, as it can lead to permanent mutations, inhibition of DNA replication and ultimately accumulation of DNA lesions induces apoptosis[129]. In response to accumulating DSB, cells initiate various types of DNA damage response (DDR). One of the early events in DDR is the rapid recruitment of ataxia telangiectasia mutated (ATM) serine/threonine kinase to a single strand DNA (ssDNA), created during early steps of DNA repair mechanisms[130,131]. ATM is considered to be one of the most important coordinators of DNA repair mechanisms, orchestrating recruitment and activation of proteins involved in DDR[130]. One of the ATM activation consequences is phosphorylation of histones H2AX on Ser139 in proximity to DNA break site. Phosphorylated H2AX, often called γH2AX, is an early marker of DSB, serving as a signal for other proteins engaged in DDR[132]. ATM was also shown to be involved in regulating the cell cycle checkpoint proteins and mediators of apoptosis[130,131]. If DNA damage persists and ssDNA presence is prolonged, ataxia telangiectasia and Rad3-related protein (ATR) is also recruited to a DNA break site[133]. ATR is another DDR regulator, and its key function is activation of checkpoint kinase 1 (CHEK1), which induces cell cycle arrest. This gives cell more time for DNA repair, preventing premature mitosis or DNA damage-induced apoptosis[133]. ATR also phosphorylates a number of ATM targets, potentiating DDR signaling, and prevents the replication fork collapse[133].

1.4.1. Main DSB repair pathways

The two major types of DSB repair are homologous recombination (HR) and non-homologous end joining (NHEJ)[134]. HR is a more conservative pathway with higher fidelity than NHEJ, but it is dependent on the presence of sister chromatids, limiting its activity to the S and G2 phases of the cell cycle. NHEJ, on the other hand, while more error-prone, can act throughout all cell cycle phases[135–137]. Graphical summary of main DSB repair pathways is presented on Figure 2.

There are three steps of HR: 1) DSB recognition, 2) synthesis-dependent strand annealing and 3) break-induced replication. In short, a ssDNA is cut from the DSB, which forms a D-loop structure with the homologous templates (usually sister chromatids). The resected single strand binds to the DSB site, inserting a homologous DNA sequence, serving as a template for DNA repair[134]. Among the plethora of proteins engaged in HR, DNA repair protein RAD51 homolog 1 (RAD51) is a core protein in this pathway. It catalyzes the ssDNA transfer at the broken DNA site to its undamaged homologue and promotes resynthesis of the broken DNA region[138]. RAD51 present at DSB recruits a complex consisting of meiotic recombination 11 homolog (MRE11), DNA repair protein RAD50 (RAD50) and nibrin (NBS1) (MRN complex). This complex, along with breast cancer type 1/2 susceptibility proteins (BRCA1/2), are crucial for DNA end resection. BRCA1/2 were also shown to be indispensable for HR activity, as it is involved in RAD51 ssDNA loading, HR stages progression and facilitation of RAD51-mediated pairing of homologous sequences[139].

NHEJ is another type of DNA repair and can be divided into two main subtypes – classical (cNHEJ) and alternative (altNHEJ). In the cNHEJ, a Ku70 and Ku80 heterodimer binds to the DSB ends and recruits DNA-dependent protein kinase catalytic subunit (DNA-PKcs), a member of the PI3K family[140]. DNA-PKcs can phosphorylate other NHEJ factors and DNA damage checkpoint proteins[133], although its autophosphorylation is thought to be the only activity crucial for cNHEJ activity, as it's required for forming a synaptic complex that bridges DNA ends in DSB[141]. Activated DNA-PKcs recruits subsequent proteins involved in DSB ends processing, including an endonuclease Artemis, tyrosyl DNA phosphatase 1, polynucleotide kinase/phosphatase, AP endonuclease 1, that in turn bind the X-ray repair cross-

complementing protein 4 (XRCC4)-XRCC4-like factor (XLF)-DNA ligase IV (LIG4) complex, ligating the DNA ends[140].

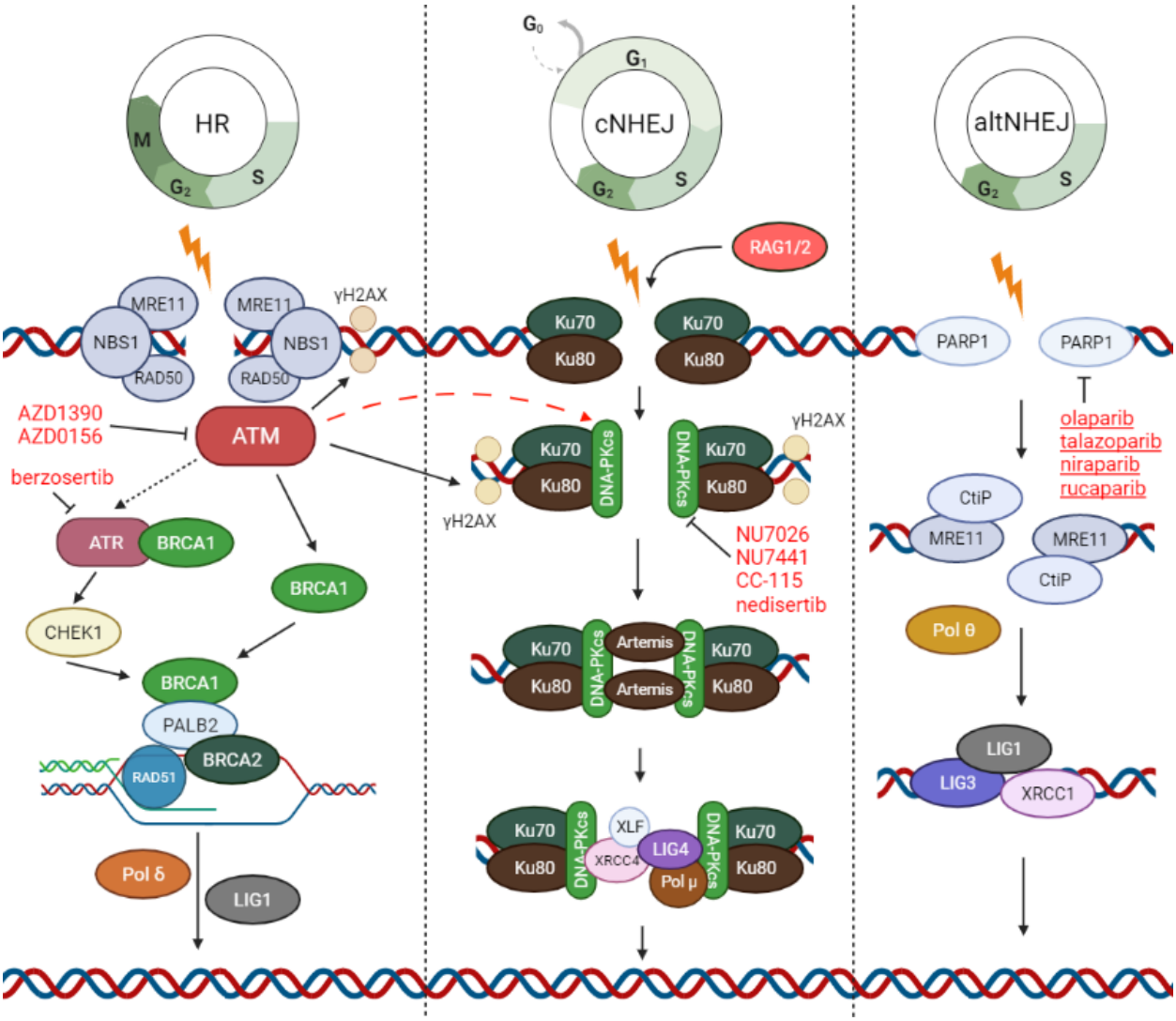

Fig. 2. DDR pathways. Three main mechanisms of DNA DSB repair, their major proteins and selected inhibitors are presented on the ilustation in red font. Underlined are the compounds approved for use in the clinic. Dotted arrow indicates indirect regulation, while red dashed arrow shows non-essential activation. More detailed description of DDR pathways can be found in the text. Based on Perkhofer et al. publication[142]. ATM - ataxia telangiectasia mutated, ATR - ataxia telangiectasia and Rad3-related protein, BRCA1/2 - breast cancer type 1/2 susceptibility proteins, CHEK1 - checkpoint kinase 1, DNA-PKcs - DNA-dependent protein kinase catalytic subunit, LIG1/3/4 – ligase 1/3/4, MRE11 - meiotic recombination 11 homolog, NBS1 – nibrin, PALB2 – partner and localizer of BRCA2, PARP1 - poly(ADP-ribose) polymerase 1, Pol θ/μ/δ – DNA polymerase θ/μ/δ, XLF - XRCC4-like factor, XRCC4 - X-ray repair cross-complementing protein 1/4.

AltNHEJ is a backup DSB repair pathway, acting when HR and cNHEJ are unable to repair damaged DNA[139,143,144]. It is independent of the components of cNHEJ, such as LIG4,

DNA-PKcs, and Ku70, relying on microhomology regions on both sides of DSB[145]. Poly(ADP-ribose) polymerase 1 (PARP1) is the initiator of altNHEJ, binding to DSB ends, which are then resected by the recruited C-terminal binding protein 1 interacting protein (CtIP)/MRN complex, and finally, DSB ends are ligated by polymerase theta and DNA ligase III (LIG3)[134].

PARP1 is one of the 18 proteins making up the PARP family[146]. PARP1 catalyzes a reaction of attaching ADP-ribose chains to proteins in a process called polyADP-ribosylation, which is a highly evolutionary conserved post-translational modification[147]. PARP1 was shown to be involved in relaxation of chromatin, DNA repair[147], DNA expression regulation[147,148], and ribosome biogenesis[148]. Moreover, PARP1's involvement in telomere maintenance is also hypothesized[149].

Apart from PARP1's crucial role in altNHEJ, it also supports cNHEJ and HR activities, although it's not required for those processes[146,150]. PARP1 is involved in cNHEJ through additional stimulation of DNA-PKcs by its PARP-ylation and PARP1's inhibition was shown to synergize with DNA-PKcs inhibition in suppressing cancer cells survival[146,151]. In HR, PARP1 promotes recruitment of the MRN complex and resection of DSB ends, although it was shown to play a rather supporting and non-essential role in initiation of HR[146,150]

1.4.2. DSB repair in cancer and leukemia

Genetic instability is a hallmark of most cancer types, induced by a plethora of factors characteristic for cancer cells, such as elevated OxS, proliferative stress or impaired DDR. Even though disrupted genomic stability can be beneficial in malignant cells to some extent, being source of pro-survival or therapy-resistance related mutations, accumulation of too many unrepaired DNA lesions could lead to apoptosis. Therefore, in cancers at least partial activity of DDR is maintained to protect them from death, often with upregulation of unfaithful DNA repair pathways, maintaining high mutational potential[137,152,153].

HR alterations are frequently present in several malignancies. *BRCA1/2* were the first genes, which mutations have been attributed to severe HR impairment, serving as a therapeutic marker[154,155]. Analysis of 17,152 primary samples from 55 cancer types identified *BRCA1/2* mutations in 4.9% of all analyzed cases, while 53% of them were breast, ovary,

prostate, or pancreatic cancers, which are often associated with *BRCA1/2* loss of function[154]. BRCA1/2 is also frequently downregulated in AML and CML[156,157]. Downregulation and mutations of several other genes, including *RAD51, RAD50, MRE11, NBS1*, were also found to cause HR inactivation[158–160], revealing that *BRCA1/2* mutations may not be the only markers of inactivated HR. Accordingly, a term "BRCAness" was proposed for non-*BRCA1/2* mutated cancers that share molecular features of *BRCA1/2*-deficient malignancies and which could benefit from similar therapeutic approaches[161].

As cNHEJ is the predominant DSB repair mechanism, its preservation is crucial for normal and cancer cells survival. Indeed, no cases of Ku70 or Ku80 mutations, two core cNHEJ proteins, have been reported. The knockout of either of these proteins in human cell lines caused cell death, possibly due to the reduction of telomere length[162]. Mutations in other cNHEJ elements (incl. DNA-PKcs, LIG4, XRCC4) are rare, and lead to severely impaired DSB repair, radiosensitivity and elevated predisposition to malignancies[153]. Even though absolute inactivation of cNHEJ is very rare, downregulation of some of its elements was found in endometrial[163], breast[164], uterine, cervix, and breast[165] cancers, promoting genomic instability. Also, lower cNHEJ activity was observed in most CML, even though cNHEJ-related proteins' expression wasn't consistently downregulated CML cells[166]. It is hypothesized that this effect is due to the BCR-ABL1-induced ROS accumulation, as activity of Ku70 and DNA-PKcs is blocked by OxS[167]. LIG4 is also considered to be downregulated in CML, although the significance of this observation isn't fully elucidated[166]. On the other hand, cNHEJ was discovered to be overactivated in AML patients, leading to unfaithful DSB repair and accumulation of genetic aberrations[168]. In B cell chronic lymphocytic leukemia (B-CLL), high levels of DNA-PKcs are associated with therapy-resistance by allowing cells to escape apoptosis[169]. Moreover, increased altNHEJ activity, caused by overexpression of PARP1 and LIG3, was correlated with therapy-resistant phenotype in CML[167].

1.4.3. DSB repair in ALL

ALL cells, like other malignancies, also exhibit disruptions in DSB repair pathways. Genetic analysis of ALL primary material revealed downregulation of HR and cNHEJ elements expression, with deficiency of DSB repair systems present in up to 25% of Ph^- subtypes and

all tested cases of Ph+ B-ALL[170]. This is most likely due to previously shown downregulation of both BRCA1 and DNA-PKcs by BCR-ABL1 activity[171,172]. Interestingly, even though inhibition of BCR-ABL1 with IMAT partially restored BRCA1 and DNA-PKcs levels, it significantly downregulated other proteins involved in HR (RAD51) and cNHEJ (LIG4)[173,174]. Expression of oncogenic K-RAS protein in ALL was also shown to induce overexpression of LIG3 and PARP1, enhancing altNHEJ[175].

Some disruptions of DNA damage repair pathways in ALL could be linked to their lymphoid origin. Physiologically, to be able to recognize a diverse repertoire of antigens, developing pre-B cells carry out a process called V(D)J recombination, which provides formidable variability of B cell receptors. V(D)J recombination process involves introduction of DBS by RAG1/2, which is then repaired through cNHEJ[176]. As V(D)J recombination is restricted to G0/G1 phase of the cell cycle, HR cannot take part in repair of RAG1/2, as it is active only in S and G2 phases[176]. It is not fully understood how RAG proteins recruit specifically cNHEJ, but not altNHEJ, to the site of the cleavage, although recent results suggest involvement of Ku70 in altNHEJ suppression in progenitor B cells[144].

As B-ALL cells are often stalled at the pre-B stage, they're still maintaining RAGs activity. Two studies investigating pediatric B-ALL primary material showed ongoing V(D)J recombination in the vast majority of tested cases[177,178]. A study in murine pre-B cell model and primary Ph+ B-ALL samples revealed that inhibition of BCR-ABL1 by IMAT causes AKT and NF-kB downregulation, leading to activation of RAGs, even in the S phase[179]. This could have dire consequences, as RAG activity in S phase has been linked to leukemogenesis[180].

As V(D)J recombination and RAGs are only present in T and B cells[181], significance of cNHEJ seems to be more pronounced in the cells of lymphoid lineage. This hypothesis is supported by the finding that mRNA of all core elements of cNHEJ in pediatric ALL is overexpressed[182]. Moreover, inhibition of DNA-PKcs in addition to daunorubicin treatment caused persistent accumulation of the DBS in the SUP-B15 Ph+ B-ALL cell line, while HR inhibition didn't affect DNA repair in those cells[182], indicating that Ph+ B-ALL cells might heavily rely on cNHEJ activity for DSB repair.

1.4.4. DNA repair inhibitors as anticancer drugs

In some cancers, a disruption of one DDR pathway and consequent dependence on the sole remaining DDR pathway is observed. Researchers are trying to take advantage of this fact with specific inhibitors that could induce synthetic lethality in cancer cells (Table 1). A great example of successful utilization of this approach is the development and usage of PARP inhibitors (PARPi) in BRCA1/2-mutated breast and ovarian cancer. *BRCA1/2* mutation in those cells impairs HR, and inhibition of PARP, which is required for backup DDR pathways, causes apoptosis of cancer cells, but not healthy, HR-prominent cells[183,184]. Currently, there are four clinically approved PARPi – olaparib (OLAP), talazoparib (TALA), niraparib (NIRA), and rucaparib (RUCA). In the clinic, they are used alone or in combination with other therapeutics, mainly chemotherapy, with numerous clinical trials testing different combinations of PARPi in leukemia (mainly AML) underway (NCT03953898, NCT03878524). Safety of PARPi was investigated in a meta-analysis of randomized controlled trials and a retrospective study of the WHO pharmacovigilance database, which revealed that PARP inhibition may increase the risk of developing the myelodysplastic syndrome and AML, although its possibility was still low (0.73% in PARP-treated group vs 0.47% in general population)[185], showing that using PARPi is a safe therapeutic approach. Up to date, the exact mechanism of PARPi-exerted cell death isn't fully elucidated. Published results indicate that PARPi may cause apoptosis through either trapping PARP on DNA and stalling the replication fork, cNHEJ overactivation and subsequent catastrophic genomic instability, disruption of Okazaki fragments processing, although no consensus over PARPi mechanism was reached[186].

DSB repair pathway	Name	Target	Stage	Ref.
altNHEJ	Olaparib	PARP1	FDA-approved	[187]
	Talazoparib	PARP1	FDA-approved	[188]
	Niraparib	PARP1	FDA-approved	[189]
	Rucaparib	PARP1	FDA-approved	[190]
cNHEJ	NU7026	DNA-PKcs	pre-clinical	[191]
	NU7441	DNA-PKcs	pre-clinical	[192]
	Nedisertib	DNA-PKcs	I/II	NCT03983824
	CC-115	DNA-PKcs, mTOR	II	NCT02977780
HR and cNHEJ	AZD1390	ATM	I	NCT02588105
	AZD0156	ATM	I	NCT05182905
HR	Berzosertib	ATR	I, I/II, II	NCT04768296, NCT04802174, NCT04052555
	Ceralasertib	ATR	II	NCT05061134, NCT04417062, NCT03328273

Table 1. List of selected DSB repair inhibitors in development and clinical trials. AltNHEJ – alternative NHEJ, ATM - ataxia telangiectasia mutated, ATR - ataxia telangiectasia and Rad3-related protein, cNHEJ – classicall non-homologous end joining, DNA-PKcs - DNA-dependent protein kinase catalytic subunit, HR – homologous recombination, NHEJ – non-homologous end joining, PARP1 - poly(ADP-ribose) polymerase 1.

In a comprehensive study, briefly mentioned earlier, a personalized approach to test patients' susceptibility to PARPi has been proposed[170]. The complex approach called gene expression and mutation analysis (GEMA) assessing mutational and quantitative changes in DDR elements through multiple techniques, such as reverse transcription-quantitative PCR, microarrays, next generation sequencing (NGS), and flow cytometry, allowing for the identification of HR- and cNHEJ-deficient leukemias that could benefit from the use of PARP inhibitors. Indeed, patient-derived cells from several leukemic types selected through GEMA were highly sensitive to PARPi treatment, especially in combination with standard therapeutics specific for each leukemia type (i.e. daunorubicin for AML, IMAT for CML)[170]. Moreover, *in vitro* and *in vivo* models of BRCA- and cNHEJ-deficient leukemias showed the

efficacy of OLAP and TALA in proliferating as well as quiescent leukemic cells, indicating the promising potential of GEMA in the clinic[170].

Even though PARPi are shown to be effective in some cases and safe for clinical use, they have several side effects. Among them, the most frequent for whole class of drugs are nausea, hematological toxicity and fatigue, observed in approximately 75%, 50% and 60% of patients treated with PARPi, respectively[193]. Among less common side effects, also constipation, decreased appetite, diarrhea, dizziness and headaches are also reported[193]. Also, some pre-existing and acquired PARPi resistance is observed in a significant fraction of patients (even up to 40% of *BRCA1/*2 mutated cases of ovarian cancers)[194]. Some proposed mechanisms responsible for that are: reversion mutations in *BRCA1/2* restoring HR activity, protection of replication fork stalling, drug efflux, specific miRNA expression pattern changes, and compensation of PARP function by PARP-independent mechanisms[194–198].

cNHEJ components can also be a promising target for targeted anticancer therapy. Out of cNHEJ inhibitors (cNHEJi), some targeting DNA-PKcs are currently in clinical trials, although no cNHEJi were approved in clinic yet. To identify predictive markers for DNA-PKcs inhibition outcomes, an integrative study of 67 cancer cell lines revealed mutations of *BRCA1, BRCA2, ATM, PAXIP1,* and *RAD50* to correlate with cells dependence on DNA-PKcs activity[199]. DNA-PKcs inhibitors NU7026 and NU7441 were shown to enhance radiosensitivity in neuroblastoma[191] and liver cancer[192]. Another selective DNA-PKcs inhibitor, nedisertib (NEDI; also known as peposertib or M3814), helps to overcome drug resistance in lung cancer cells[200], and several clinical trials, including tests in AML in combination with standard therapy, are ongoing (NCT03983824). A phase I trial, testing NEDI in solid tumors, showed its good overall tolerance, although in monotherapy the best achieved response was a stable disease in 12 patients out of 31 enrolled[201]. Dual inhibition of mTOR and DNA-PKcs by CC-115 was also studied, with promising pre-clinical outcomes in CLL[202]. A completed phase I study of CC-115 showed good tolerance to treatment, with partial response and a stable disease in some tested cancer types (38% and 25% in CLL, respectively)[203].

Other DBS repair elements are also being investigated as a potential anticancer drug targets. Inhibition of ATM was shown to be beneficial in radiosensitization of glioma[204], prostate[205], and brain[206] cancer. Two of the ATM inhibitors, AZD1390 and AZD0156, are currently tested in phase I clinical trials, although no results have been published yet (NCT02588105, NCT05182905). Also, ATR inhibition is intensively tested, including several clinical trials. Berzosertib, highly selective ATR inhibitor[207], is currently a subject of over 15 ongoing or recruiting clinical trials (NCT04768296, NCT04802174, NCT04052555), and some already completed, showing promising effects (i.e. in combination with gemcitabine and cisplatin in advanced solid tumors[208]). Another promising ATR inhibitor, ceralasertib, shown to induce cell death in various tumor models in a monotherapy and in combination with DNA damaging agents, PARPi or radiotherapy[209], is currently studied in clinical trials in mono- (NCT05061134) and combination therapies, including combination with olaparib in osteosarcoma (NCT04417062) or acalabrutinib in CLL (NCT03328273).

Even though intensive pre-clinical and clinical research of DNA repair targeting in cancer, much more studies are needed to harness its potential. This is especially apparent for NHEJi, as they're showing promising outcomes in pre-clinical and preliminary clinical results, and no NHEJi are approved for clinical use are available up to date.

2. Aims of the study

Ph^+ B-ALL is one of the high-risk B-ALL subtypes. Although introduction of TKIs significantly improved treatment outcomes, high rates of relapse in patients require more specific and effective therapies. To achieve this goal, a better understanding of the Ph^+ B-ALL biology is needed, possibly uncovering some specific vulnerabilities serving as potential therapeutic targets. Disrupted redox homeostasis in B-ALL leukemias was exploited through inhibition of TXN system, one of the main antioxidant systems in B-ALL, although TXN system role wasn't investigated in Ph^+ B-ALL subtype and other Ph^+ leukemias. The first goal in this study was to evaluate the TXN system targetability in Ph^+ leukemias and assess role of PRDX1 in those malignancies. Secondly, this project was aimed at developing novel combinations of drugs to ameliorate Ph^+ B-ALL therapies efficacy.

Detailed aims of this study were:

- assessment of TXN system as a potential target in Ph^+ leukemia cell lines;
- assessment of the expression of TXN system elements in primary Ph^+ leukemias;
- evaluation of PRDX1's role of in viability of Ph^+ cells and their sensitivity to TKIs and NHEJi;
- assessment of TKIs and NHEJi combination efficacy in Ph^+ cell lines;
- investigation of the TKIs and NHEJi efficacy in PRDX1-deficient Ph^+ cell lines;
- testing novel triple combinations involving TKIs, AUR and NHEJi in lymphoid Ph^+ cell lines and PDXs.

3. Materials and methods

3.1. Materials

3.1.1. Cell lines

Human Ph^+ cell lines and representing myeloid (K562, KU-812, LAMA-84, MEG-A2) or lymphoid (BV173, SUP-B15, TOM-1) lineages were purchased from DSMZ (Braunschweig, Germany). BV173, SUP-B15, TOM1, K562, KU-812 and LAMA-84 cells were maintained in RPMI 1640 medium (Gibco), supplemented with either 10% (BV173, K562, LAMA-84) or 20% (TOM1, KU-812, SUP-B15) FBS (HyClone) and 1% penicillin/streptomycin solution (BV173, SUP-B15, K562; Sigma-Aldrich). MEG-A2 cells were cultured in IMDM medium (Gibco), supplemented with 20% FBS (HyClone). All cell lines were kept in a humidified atmosphere at 37°C and 5% CO_2 and checked for Mycoplasma contamination routinely.

3.1.2. Mice

Transgenic immunodeficient NSG mice (NOD scid gamma, NOD.Cg-*Prkdc*^{scid} *Il2rg*^{tm1Wjl}/SzJ) were purchased from The Jackson Laboratory. *In vivo* procedures were carried out after permission of the II Local Ethics Committee for animal research based in Warsaw University of Life Sciences (WAW2/095/2019). All mice were kept in specific pathogen free standard animal facility, in individually ventilated cages.

3.1.3. Patient derived material for PDXs generation

For generation of PDXs, primary material isolated form Ph^+ B-ALL patients' bone marrow was used. The blasts were isolated by centrifugation of bone marrow samples in Lymphoprep (STEMCELL Technologies) gradient. Upon isolation, cells were either cryopreserved or injected into 6–12-week-old NSG female or male mice immediately. 1-5mln of cells were injected into recipient animals' tail vein, and leukemia burden was assessed by cytometric assessment of $hCD19^+hCD34^+$ cells percentage in mice peripheral blood weekly. Antibodies used for monitoring of mice are listed in Table 2.

Antibody	Clone	Catalogue no.	Manufacturer
anti-mCD45 APC	30-F11	17-0451-83	eBioscience
anti-hCD45 PE	HI30	12-0459-42	eBioscience
anti-hCD19 FITC	HIB19	11-0199-42	eBioscience

Table 2. List of antibodies used for monitoring of leukemia progression in NSG mice.

Mice were sacrificed when one of the following conditions was met: 1) ratio of human $CD19^+CD34^+$ and mouse $CD34^+$ cells in peripheral blood reached 1:1, 2) severe splenomegaly or 3) rear legs paralysis was observed, or 4) mice overall condition was visibly declining. PDX human cells were isolated from the spleen using centrifugation in Lymphoprep gradient and if less than 80% of isolated cells were $hCD19^+$, additional purification with CD19-specific magnetic beads was performed. PDX cells isolated this way were either taken for experimental procedures immediately or cryopreserved in liquid nitrogen until needed. Patients, whose material was used for generation of PDXs, are characterized in Table 3.

Patient symbol	Type	Cohort	Sex	TKI sensitivity
PDX#1	Ph+ B-ALL	adult	M	resistant
PDX#2	Ph+ B-ALL	pediatric	M	resistant
PDX#3	Ph+ B-ALL	pediatric	M	resistant
PDX#4	CML LBP	adult	M	sensitive
PDX#5	CML LBP	adult	F	sensitive
PDX#6	Ph+ B-ALL	pediatric	F	sensitive

Table 3. Characteristics of patients, whose donated material was used for generation of PDXs. CML LBP – chronic myeloid leukemia in lymphoid blast phase, Ph^+ B-ALL – Philadelphia positive B cell acute lymphoblastic leukemia.

3.1.4. Drugs and chemicals

Compounds used in experimental procedures were: imatinib, dasatinib, nedisertib, olaparib (IMAT, DASA, NEDI, OLAP; Selleckchem), auranofin, puromycin, hydrogen peroxide, catalase (AUR, PURO, H_2O_2, CAT; Sigma-Aldrich), adenanthin (ADE, Faces Biochemical Co.), and sodium pyruvate (Thermo Fisher Scientific). Other reagents were purchased from either

Sigma-Aldrich or Thermo Fisher Scientific. All compounds were dissolved either in water or DMSO and stored in 4°C or -20°C, according to manufacturer's recommendations.

3.2. Methods

3.2.1. PDX Ph^+ lymphoid cell culture

Freshly isolated or thawed PDX cells were immediately taken for experimental procedures. Prior to cytotoxic assays, dead cells were discarded through centrifugation in Lymphoprep gradient. PDX cells were cultured in SFEM II medium (Gibco), supplemented with 20% FBS (Gibco), 20ng/ml recombinant human interleukin 3 and 10ng/ml recombinant human interleukin 7 (R&D Systems), called SFEM-full medium.

3.2.2. CRISPR/Cas9 generation of genomic PRDX1 knockout in BV173 and K562 cell lines

BV173 and K562 cells genomic PRDX1 knockout was obtained using a second-generation CRISPR/Cas9 lentiviral system. HEK293T cells were co-transfected with 4µg lentiCRISPRv.2 (Addgene plasmid #52961) encoding gRNA targeting PRDX1 (sequence: ATCAATGATAAAAAGGCCCCTGG), 4µg packaging psPAX2 and 2µg envelope pMD2.G vectors. LentiCRISPRv.2 encoding non-targeting gRNA sequence (sequence: ACGGAGGCTAAGCGTCGCAA) was used as a control. Cells modified with PRDX1 targeting, or non-targeting gRNA are referred to as sgPRDX1 and sgNTC, respectively. 48h after transfection, virus containing media from HEK293T cells was filtered through 0.45µm filter and target cell lines were infected in the presence of 4µg/ml polybrene. Selection of modified cells was performed by culturing infected cells in the presence of 2µg/ml PURO, 1mM sodium pyruvate and 50µg/ml catalase. For BV173 cells, selection of clones was also performed. In short, cells were seeded onto 96-well plate in density of 1 cell/well in the presence of presence of 2µg/ml PURO, 1mM sodium pyruvate and 50µg/ml catalase. Next, wells with singular cell were marked. After allowing single cells to grow, three selected BV173 sgPRDX1 clones were mixed in 1:1:1 ratio and used throughout the project. PRDX1 knockout was confirmed by immunoblotting. After the selection, sgPRDX1 cells were cultured in the medium supplemented with 1mM sodium pyruvate and 50µg/ml catalase (ROS scavengers).

In experiments not involving ROS scavengers, cells were deprived of ROS scavengers for 2-3 days prior to the experiment.

3.2.4. Reconstitution of PRDX1 in BV173 sgPRDX1 cells

Reconstitution of either WT or mutated PRDX1 in BV173 sgPRDX1 cells was obtained using a second-generation lentiviral expression system. HEK293T cells were co-transfected with 4µg expression plasmid pLV-SFFV-hPRDX1:T2A:EGFP (Vector Builder) encoding either WT or mutated PRDX1, 4µg packaging psPAX2 and 2µg envelope pMD2.G vectors. Mutations in PRDX1-coding sequences are summarized Table 4. 48h after transfection, virus-containing media from HEK293T cells were filtered through 0.45µm filter and the target cell lines were infected in the presence of 4µg/ml polybrene. Modified cells ($EGFP^+$) were sorted using BD FACSAria™ III Cell Sorter (BD Biosciences). After sorting, cells were cultured with the addition of ROS scavengers.

PRDX1 variant	PRDX1 coding sequence
C52A C83A C173A	ATGTCTTCAGGAAATGCTAAAATTGGGCACCCTGCCCCCAACTTCAAAGCCACAGCTGTTATG CCAGATGGTCAGTTTAAAGATATCAGCCTGTCTGACTACAAAGGAAAATATGTTGTGTTCTTC TTTTACCCTCTTGACTTCACCTTTGTGTGCCCCACGGAGATCATTGCTTTCAGTGATAGGGCAG AAGAATTTAAGAAACTCAACTGCCAAGTGATTGGTGCTTCTGTGGATTCTCACTTCTGTCATCT AGCATGGGTCAATACACCTAAGAAACAAGGAGGACTGGGACCCATGAACATTCCTTTGGTAT CAGACCCGAAGCGCACCATTGCTCAGGATTATGGGGTCTTAAAGGCTGATGAAGGCATCTCG TTCAGGGGCCTTTTTATCATTGATGATAAGGGTATTCTTCGGCAGATCACTGTAAATGACCTCC CTGTTGGCCGCTCTGTGGATGAGACTTTGAGACTAGTTCAGGCCTTCCAGTTCACTGACAAAC ATGGGGAAGTGTGCCAGCTGGCTGGAAACCTGGCAGTGATACCATCAAGCCTGATGTCCAA AAGAGCAAAGAATATTTCTCCAAGCAGAAG

Table 4. Coding sequence of PRDX1 used for its reconstitution in BV173 sgPRDX1 cells. Highlighted cysteine codons (TGC or TGT) were changed to alanine ones (GCC) in order to generate indicated PRDX1 mutants.

3.2.5. Assessment of mRNA levels by qPCR in BV173 cell line and primary CML and Ph^+ B-ALL cells

For measurement of mRNA levels in BV173 with or without PRDX1, sgNTC or sgPRDX1 cells were seeded onto six well plates at 0.2mln/ml density and cultured for 24h with or without addition of 250nM IMAT to the culture medium. Prior to RNA isolation, cells were washed once with phosphate buffered saline (PBS) and pelleted by centrifugation. Primary

cells were freshly thawed prior to the analysis and from this point analyzed following the same procedure as BV173 cells.

Gene	Sequence
ATF_F	CCTAGGTCTCTTAGATGATTACC
ATF_R	CAAGTCGAACTCCTTCAAATC
CHOP_F	GAAGCGGATGGCTGAGAAA
CHOP_R	GTTGGAGAAGAGCTCCAAGAC
RAD50_F	CAAGGGACTGATGAGCAACTAA
RAD50_R	CCAGTTCACGATGACAGTCTAC
LIG4_F	GCCCGTGAATATGATTGCTATG
LIG4_R	TCAGGAGTCTGCTCGTTAGA
XRRC4_F	GAGACAGCGAATGCAAAGAAAT
XRRC4_R	CGTCTCAGGTAGTGAAGAATCAG
PAXIP1_F	ATGCTTGGAGAGTTCCCTTAAA
PAXIP1_R	TGGAAGAAGGCTGGACATTAG
BRCA1_F	GCTCTTCGCGTTGAAGAAGTA
BRCA1_R	CACACTTTGTGGAGACAGGTT
TXN1_F	TAAAGGGAGAGAGCAAGCAG
TXN1_R	CAGAGAGGGAATGAAAGAAAGG
TXN-R1_F	TCACCCCAGTTGCAATCC
TXN-R1_R	GGTTGGAACATTTTCATAGTCACA
PRDX1_F	CACTGACAAACATGGGGAAGT
PRDX1_R	TTTGCTCTTTTGGACATCAGG
RPL29_F	CAGCTCAGGCTCCCAAAC
RPL29_R	GCACCAGTCCTTCTGTCCTC

Table 5. List of primer pairs sequences used in qPCR. F and R stand for sense and antisense sequence, respectively.

The RNA was isolated using RNeasy kit (Qiagen, Hilden, Germany), using microcentrifuge columns and alcohol extraction. Concentration and purity of isolated RNA was assessed by NanoDrop 2000c spectrophotometer (Thermo Fisher Scientific). Next, 2µg of RNA was incubated with DNase (Sigma-Aldrich) and used for reverse transcription with Maxima First Strand cDNA Synthesis Kit (Thermo Fisher Scientific). The expression of target genes was measured in reference to RPL29 (ribosomal protein L29) by a fluorescence-based kinetic qPCR. qPCR reaction was performed utilizing LightCycler® 480 System (Roche) and intercalating fluorescent dye Fast SYBR Green Master Mix (Thermo Fisher Scientific). Sequences of the primers used for the reactions are listed in Table 5. mRNA expression levels were calculated by subtracting RPL29 reference gene's cycle threshold (Ct) from the target's Ctb (ΔCt) and the values are presented as $2^{-\Delta ct}$.

3.2.6. Assessment of changes in gene expression by RNAseq in IMAT-treated BV173 cells

Total RNA was alcohol extracted from the primary blast cells resuspended in Trizol (Invitrogen. RNA sequencing was performed using Illumina® Stranded mRNA Prep, Ligation (Illumina), indexed with IDT® for Illumina® RNA UD Indexes Set A (Illumina). The library was sequenced on a Next Seq 550 system (Illumina) using NextSeq® Reagent Kit v3 (150 cycles) with a TG NextSeq 500/550 High Output Flow Cell. FASTQ files were processed, and statistical analysis was performed with StrandNGS 3.3 Software (Strand Life Sciences Pvt. Ltd). Pathway analysis was done with GenePattern platform[210] and Gene Set Enrichment Analysis (GSEA, https://software.broadinstitute.org/gsea/)[211]. Data visualizations, heatmaps plotting and genes clustering were performed in MultiExperiment Viewer software (MeV, https://webmev.tm4.org/). All RNAseq experiments and analyses were performed in collaboration with dr A. Pastorczak and dr J. Madzio from the Department of Pediatrics, Oncology and Hematology, Medical University of Łódz.

3.2.7. Immunoblotting

Cells were lysed using lysis buffer (10% glycerol, 1.0% Triton X-100, 150mM NaCl, 5mM EDTA, 50mM Hepes, pH 7.4) supplemented with Complete Protease Inhibitor Cocktail (Roche) and Complete Phosphatase Inhibitor Cocktail (Roche). Total protein concentration in lysates were measured using Pierce BCA Protein Assay Kit (Thermo Fisher Scientific). 20µg of

whole-cell protein lysate was separated in 10% polyacrylamide gels and transferred to Protran nitrocellulose membranes (Schleicher and Schuell BioScience). Following protein transfer, membranes were blocked in 5% nonfat milk or BSA, incubated with primary antibodies followed by incubation with secondary HRP-linked antibodies. List of used antibodies can be found in Table 6. Signal was developed using SuperSignal Chemiluminescent Substrate (Thermo Fisher Scientific) or WesternBright Sirius HRP substrate (Advansta) and imaging was performed with ChemiDoc Imaging System (Bio-Rad Laboratories).

Antibody	Clone	Catalog no.	Manufacturer
BCL-W	31H4	2724	Cell Signaling
BIM	C34C5	2933	Cell Signaling
Caspase 3	polyclonal	9662	Cell Signaling
Caspase 9	polyclonal	9502	Cell Signaling
Cleaved PARP	D64E10	5625	Cell Signaling
PRDX1	polyclonal	HPA007730	Sigma-Aldrich
p-SAPK/JNK (Thr183/Tyr185)	polyclonal	9251	Cell Signaling
SAPK/JNK	polyclonal	9252	Cell Signaling
TXN1	C63C6	2429	Cell Signaling
α-tubulin	DM1A	CP06	Calbiochem
β-actin	AC-15	A3854	Sigma-Aldrich
γH2AX	20E3	9718	Cell Signaling

Table 6. List of antibodies used for immunobloting.

3.2.8. Assessment of cell viability by propidium iodide staining

Cells were seeded onto 24-well plate in 1ml of media in concentration 0.2mln/ml (K562, BV173) or 0.6mln/ml (all other used cell lines) and treated with indicated concentrations of compounds for 48h and stained with propidium iodide (PI) at a final

concentration of 1µg/ml. PI-negative cells were assessed by flow cytometry using FACSCanto II or LSRFortessa X-20 (BD Biosciences).

3.2.9. Assessment of PDX viability by propidium iodide staining

PDX cells were seeded onto 96-well U-bottom plates in SFEM-full medium. Final media volume per well was 200µl and the cells were maintained at the density 0.5mln/ml for 72h in the presence of indicated concentrations of compounds. Subsequently, cells were taken for cytometric analysis, and stained with PI at a final concentration of 1µg/ml. PI-negative cells were assessed by flow cytometry using FACSCanto II or LSRFortessa X-20 (BD Biosciences).

3.2.10. Clonogenic assay

BV173 sgNTC and sgPRDX1 cells were suspended at a density of $5x10^3$ in 200µl of RPMI medium (Gibco) supplemented with 10% FBS (HyClone) and placed in a sterile 5ml FACS tubes. Treated groups had IMAT added to media in a final concentration of 1000nM and were incubated for 2h in cell incubator with protection from light. Subsequently, 900µl of drug-free MethoCult™ H4434 Classic methylcellulose-based semi-liquid medium with recombinant cytokines for human cells (STEMCELL Technologies) was added to cells and cells were seeded in a final volume 1.1ml onto 35x10mm plates with grid pattern (Sarstedt). The plates with seeded cells were then placed in a closed container with PBS filled cuvette to prevent methylcellulose from drying and incubated in the cell incubator for 6 days. After the incubation, colonies consisting of at least 4 cells (CFUs – colony forming units) were counted inside 9x9 square on the plate and the results were the normalized to each group's control for each experiment separately.

3.2.11. Assessment of intracellular ROS levels

Staining for total intracellular ROS was performed using the permeable H2DCFDA dye (DCFDA) (Thermo Fisher Scientific). First, cells were suspended in PBS at density 1mln/ml and stained with DCFDA for 30min in the dark at 37°C in the cell incubator. Subsequently, cells were washed with PBS and resuspended in RPMI medium, supplemented with 10% FBS and 1% penicillin/streptomycin, at final density 0.2mln/ml, seeded onto 24-well plates in 1ml of media, and indicated concentrations of H_2O_2 and IMAT were added to corresponding wells.

At indicated timepoints of IMAT-treatment, cells were immediately taken for analysis on FACSCanto II (BD Biosciences).

For measurement of cytoplasmic and nuclear ROS levels, BV173 sgNTC and sgPRDX1 cells were seeded onto 24-well plate in 0.5ml of RPMI medium (Gibco) supplemented with 10% FBS (HyClone) at density 0.2mln/ml. Subsequently, IMAT was added to treated groups in final concentration 500nM and incubated in cell incubator. After indicated time of incubation with the drug (0.5h-16h), cytoplasmic or nuclear ROS were analyzed using either CellROX Green or CellROX DeepRed reagents (Thermo Fisher Scientific), respectively. Reagents were added to the cells in final concentration 5µM and incubated for another 30min at the incubator. Following the incubation, cells were washed twice with PBS, resuspended in 200µl of PBS and analyzed on FACSCanto II (BD Biosciences). Mean fluorescence of the unstained control was subtracted from the mean fluorescence of stained samples and it was then normalized to each group's control for each experiment separately.

3.2.12. Assessment of 8-OH-DG levels in cell medium

BV173 sgNTC and sgPRDX1 cells were seeded onto 24-well plate in 1ml of RPMI medium (Gibco) supplemented with 10% FBS (HyClone) at a density 0.2mln/ml and IMAT was added to treated groups in a final concentration 500nM. After 24h incubation with the drug in the cell incubator, 150µl of media from each well was taken, centrifuged at 1000g for 15min, and 100µl of cleared supernatant was taken for further analysis. Assay was performed using 8-Hydroxy-2-desoxyguanosine (8-OHDG) ELISA kit (MyBioSource). Samples absorbance was measured at 450nm wavelength on microplate reader (ASYS UVM 340; Biochrom) and 8-OHDG concentration was calculated with use of curve generated by using standards attached to the kit.

3.2.13. Assessment of H2AX activation

BV173 sgNTC and sgPRDX1 cells were seeded onto 24-well plate in 1ml of RPMI medium (Gibco) supplemented with 10% FBS (HyClone) at density 0.2mln/ml and IMAT was added to treated groups in final concentration 250nM or 500nM. After 24h of incubation in the cell incubator, activation of H2AX was assessed by Muse® H2A.X Activation Dual

Detection Kit (Luminex) following manufacturer's protocol. In short, cells after treatment were washed with PBS and fixed for 5min in fixation buffer on ice. After fixation, cells were washed with PBS again and permeabilized in permeabilization buffer for 5min on ice. Subsequently, 5µl of anti-Histone H2A.X/PECy5 was added to 90µl of fixed and permeabilized cells and cells were stained for 30min at RT, protected from light. Next, cells were washed with PBS once again, resuspended in assay buffer and taken for analysis in Muse Cell Analyzer (Merck).

3.2.14. Assessment of DSBs levels by TUNEL assay

BV173 sgNTC and sgPRDX1 cells were seeded onto 24-well plate in 1ml of RPMI medium (Gibco) supplemented with 10% FBS (HyClone) at density 0.2mln/ml and IMAT was added to treated groups in final concentration 250nM or 500nM. After 24h of incubation in the cell incubator, amount of DNA breaks was assessed by APO-BrdU™ TUNEL Assay Kit (ThermoFisher Scientific) in accordance with manufacturer's protocol. In short, cells after treatment were washed with PBS and fixed in 1% paraformaldehyde on ice for 15min. After fixation, cells were washed with PBS and permeabilized in 70% ethanol for 30min on ice. After permeabilization, cells were incubated with master mix, containing terminal deoxynucleotidyl transferase and BrdUTP, for 1h at the cell incubator. Subsequently, cells were washed with PBS and stained with anti-BrdU antibody for 30min at RT in dark. Next, cells were stained with propidium iodide, and taken for analysis on FACSCanto II or LSRFortessa X-20 (BD Biosciences).

3.2.15. Statistical analysis

Data visualization and statistical analysis were performed using the R programming language. All statistical tests were preceded by testing for outliers, normality of residuals distribution and homogeneity of variances, as those conditions must be met before using parametric tests. For data that passed those tests, 2-way ANOVA or pairwise t-test with Bonferroni correction were used. ANOVA tests were calculated with White-adjustment to exclude the effect of variable errors in the regression models. Statistical significance for data sets that didn't pass tests for normality was calculated using non-parametric Mann-Whitney test.

All statistical analysis was performed in consultation and collaboration with dr Maksymilian Bielecki from the Department of Psychology, SWPS University of Social Sciences and Humanities, Warsaw.

4. Results

4.1. Evaluation of the efficacy of IMAT in combination with thioredoxin system inhibition

Gene	logFC	*p*	Signif.
HMOX1	1.03	0.0329	*
SOD2	0.62	0.0110	*
PRDX3	0.37	0.0734	
GSS	0.31	0.0301	*
TXN-R1	0.27	0.1560	
PRDX1	0.21	0.3990	
GSTM4	0.19	0.1060	
TXN1	0.16	0.2110	
PRDX2	-0.12	0.2460	
PRDX4	-0.23	0.1050	
GPX4	-0.23	0.1510	
GPX1	-0.23	0.0504	
PRDX6	-0.35	0.0167	*
GSTA3	-0.44	0.0087	**
TXNIP	-1.08	0.0372	*
MGST3	-1.27	0.0010	**
GSTA4	-2.11	0.0002	***

Table 7. Metaanalysis of chosen gene expression changes upon BCR-ABL1 induction in pre-B cell line. Presented in the table are selected genes related to two main antioxidant systems: GSH and TXN. Genes were sorted according to their logFC value, from highest to lowest. Data extracted from publicly available dataset (GSE75058)[212].

As discussed previously, BCR-ABL1 activity disturbs the cell's redox homeostasis[89]. Moreover, Kesarwani and colleagues performed a comparative analysis of gene expression after induction of BCR-ABL1 in pre B cells (GSE75058)[212]. The analysis of this dataset revealed a tendency of GSH-related genes to be downregulated (i.e. *GSTA4, MGST3, GPX1, GPX4*) and

the TXN1 system genes (*TXN1, TXN-R1, PRDX1*) to be upregulated upon BCR-ABL1 expression (Table 7).

Although differences in the levels of some genes weren't statistically significant, a consistent expression pattern could be observed. This data allowed a formulation of a hypothesis that the TXN system may play a supporting role in Ph^+ leukemias. These observations, together with the fact that the TXN system inhibition triggers apoptosis of B-ALL cells and synergizes with some treatments of B malignancies[73,74], led to the investigation of the efficacy of TKIs, drugs that are the key component of Ph+ leukemia treatment, in combination with the TXN system inhibitors (AUR and ADE).

4.1.1. Lymphoid Ph^+ cell lines

The cytotoxic effects of two TKIs (IMAT and DASA) in combination with either AUR (Fig. 3) or ADE (Fig. 4) were tested in BV173 and SUP-B15 lymphoid Ph^+ cell lines, and synergy scores were calculated for each combination. AUR and ADE EC_{20} and EC_{50} were chosen based on previously reported results for BV173 and SUP-B15 cell lines[74], while concentrations of TKIs up to EC_{20} were tested, as their higher concentrations, weren't much more effective in those cells. Synergy scores higher than 10 indicate synergy, and the higher the score, the stronger the synergistic effect.

Both AUR and ADE alone exerted a significant cytotoxic effect on both cell lines. Moreover, 1µM AUR potentiated the effects of both IMAT and DASA in both cell lines, while 0.5µM AUR synergized with TKIs only in SUP-B15 cells. ADE showed a higher synergistic effect in BV173 cells in comparison to AUR, while in SUP-B15, the effects were comparable.

These observations indicate the role of the TXN system in lymphoid Ph^+ cells maintenance and their response to TKIs, making the TXN system elements in those cells an interesting object of further research.

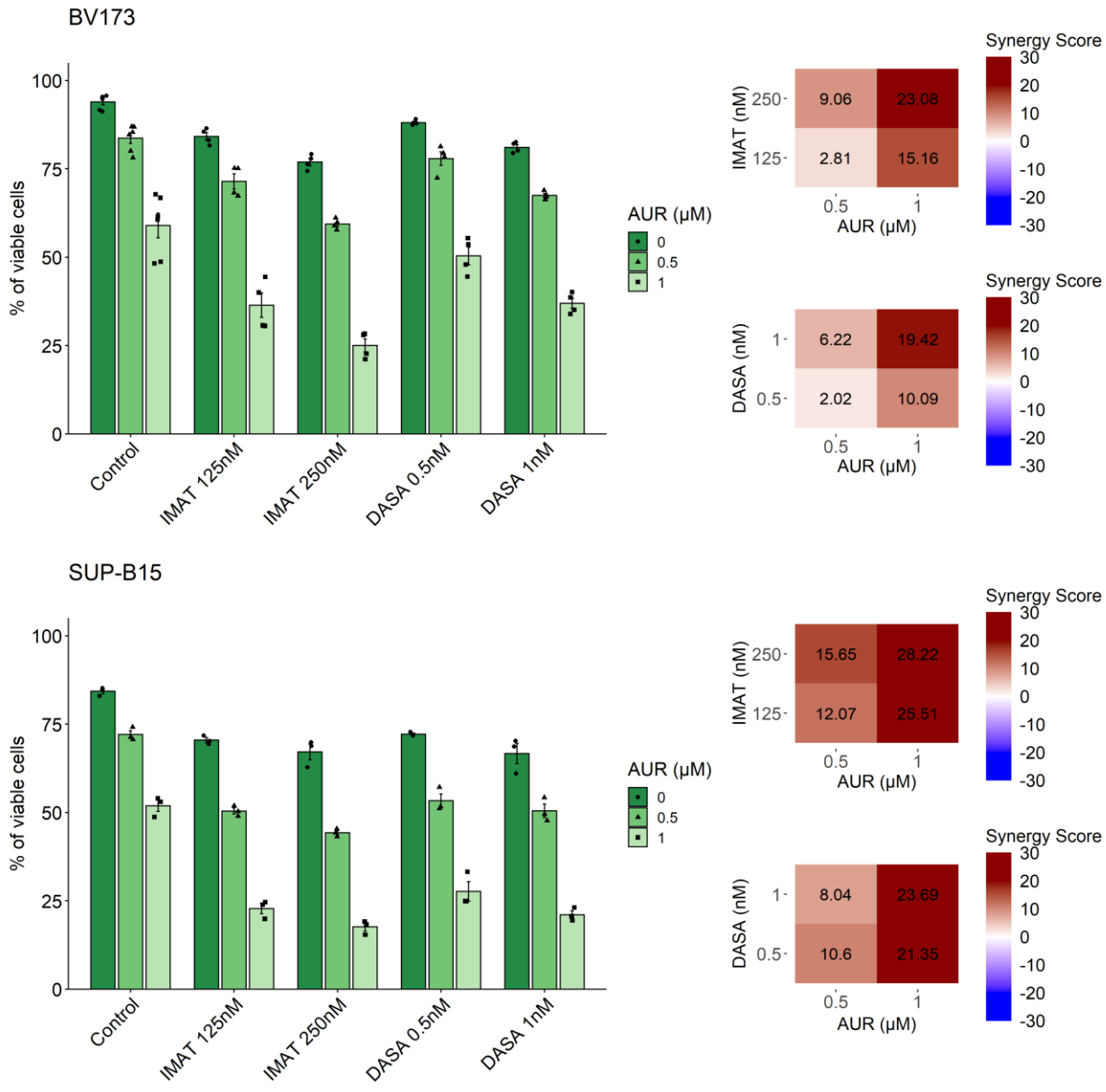

Fig 3. Efficacy of the combination of AUR with IMAT or DASA in Ph⁺ lymphoid cell lines. BV173 (n=4-6) and SUP-B15 (n=2-3) Ph⁺ lymphoid cell lines were treated with IMAT or DASA in combination with AUR for 48h and viability was assessed by the exclusion of dead cells in flow cytometry using PI staining. The synergistic effect was calculated with the SynergyFinder R package[213]. Synergy scores: lower than -10 – antagonism, between -10 and 10 – additive effect, higher than 10 - synergy. Means ± SD are presented.

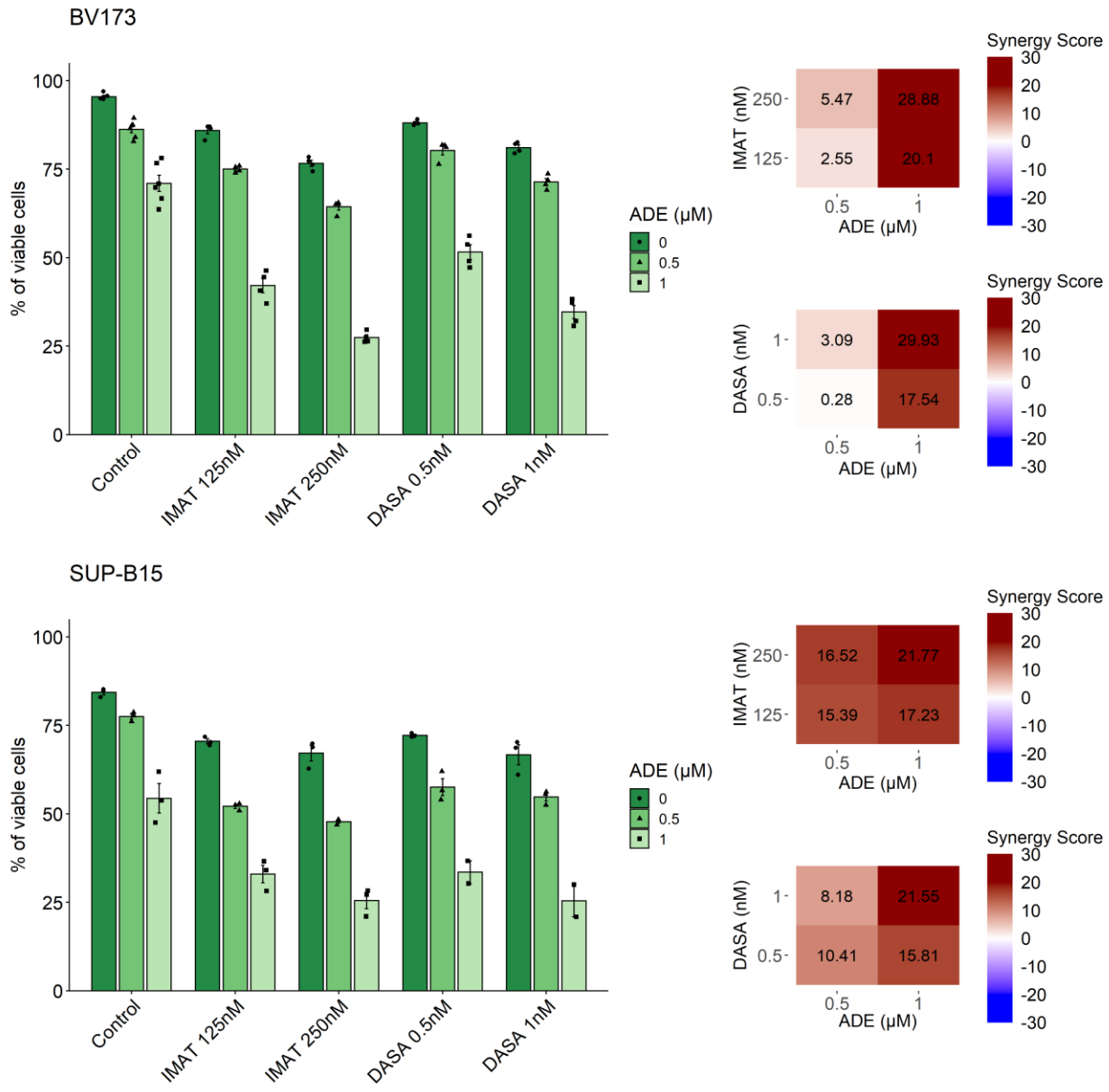

Fig 4. Efficacy of the combination of ADE with IMAT or DASA in Ph⁺ lymphoid cell lines. BV173 (n=4-6) and SUP-B15 (n=2-3) Ph⁺ lymphoid cell lines were treated with IMAT or DASA in combination with ADE for 48h and viability was assessed by the exclusion of dead cells in flow cytometry using PI staining. The synergistic effect was calculated with the SynergyFinder R package[213]. Synergy scores: lower than -10 – antagonism, between -10 and 10 – additive effect, higher than 10 - synergy. Means ± SD are presented.

4.1.2. Myeloid Ph⁺ cell lines

To check if similar synergistic interaction between TKIs and TXN system inhibitors occurs also in Ph+ myeloid cells, corresponding tests with adjusted TKIs doses were performed for K562, LAMA-84, and MEG-A2 CML cell lines (Fig. 5 and 6).

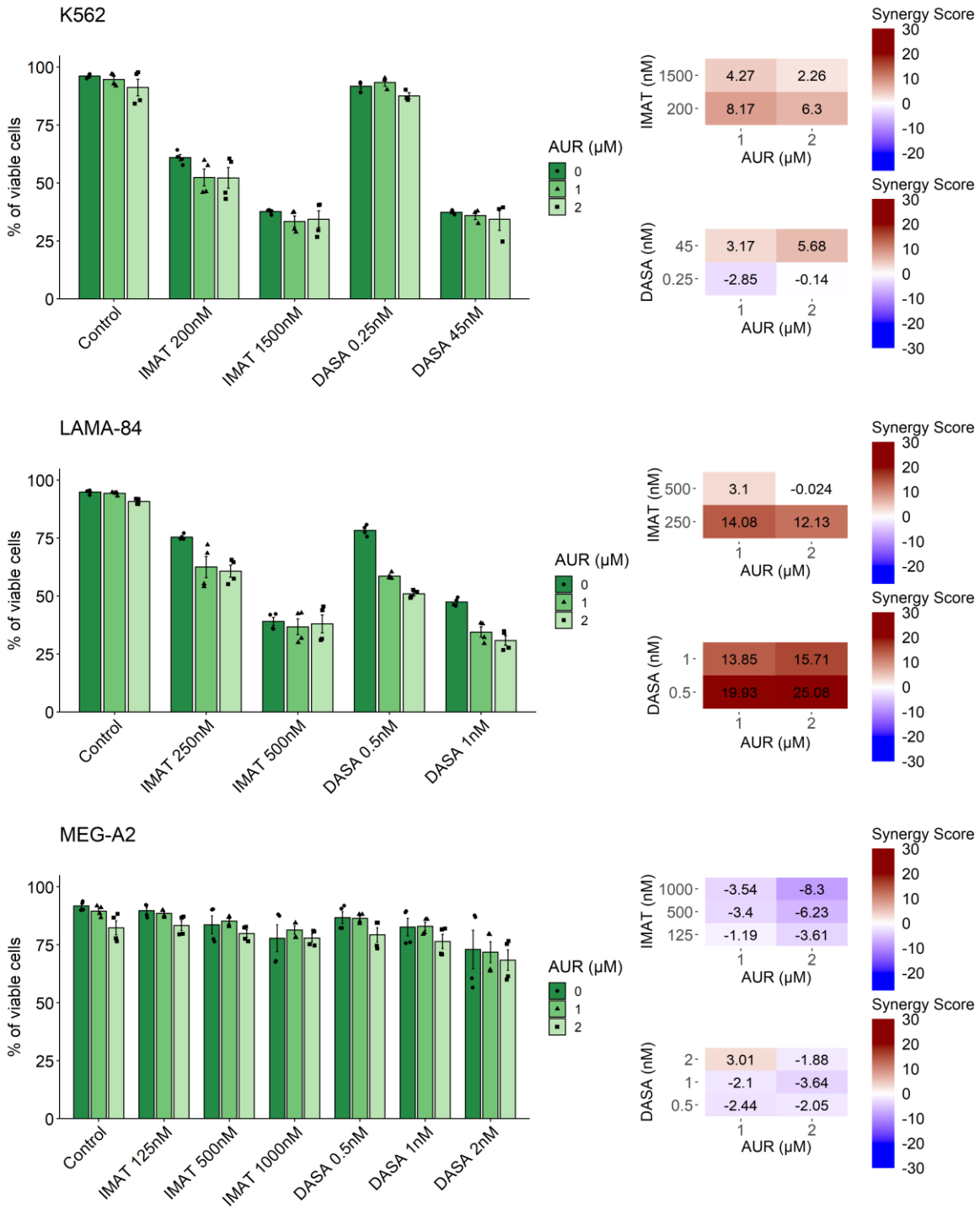

Fig 5. Efficacy of AUR with TKIs combination in CML cell lines. K562, LAMA-84, and MEG-A2 CML cell lines (n=4 for all cell lines) were treated with IMAT or DASA in combination with AUR for 48h, and viability was assessed by the exclusion of dead cells in flow cytometry using PI staining. T The synergistic effect was calculated with the SynergyFinder R package[213]. Synergy scores: lower than -10 – antagonism, between -10 and 10 – additive effect, higher than 10 - synergy. Means ± SD are presented.he synergistic effect was assessed with the SynergyFinder R package[213]. Means ± SD are presented.

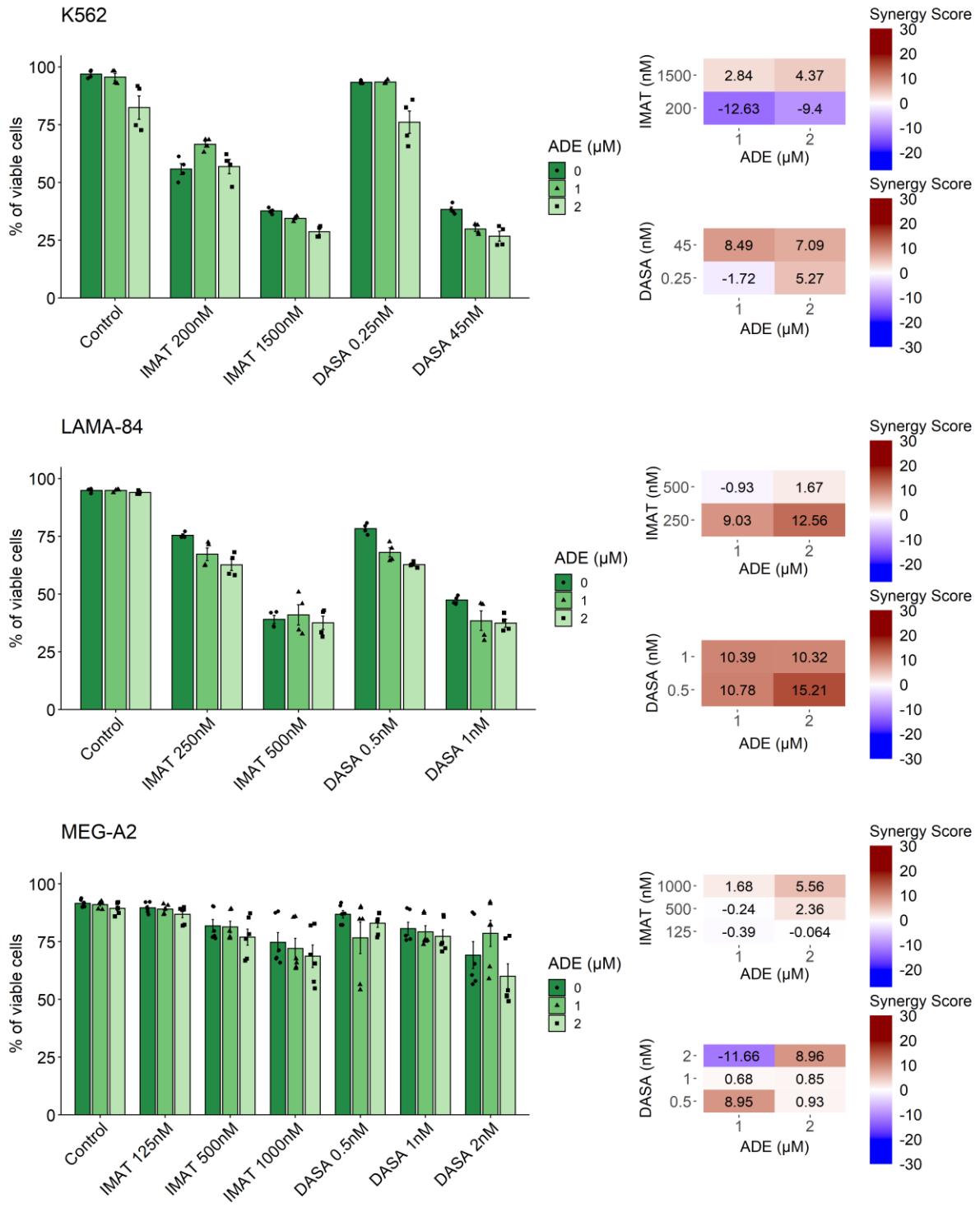

Fig 6. Efficacy of ADE with TKIs combination in CML cell lines. K562 (n=4), LAMA-84 (n=4), and MEG-A2 (n=6) CML cell lines were treated with IMAT or DASA in combination with ADE for 48h and viability was assessed by the exclusion of dead cells in flow cytometry using PI staining. The synergistic effect was calculated with the SynergyFinder R package[213]. Synergy scores: lower than -10 – antagonism, between -10 and 10 – additive effect, higher than 10 - synergy. Means ± SD are presented.

Two of them, K562 and LAMA-84, were sensitive to both TKIs, while MEG-A2 cells were resistant to IMAT and DASA in the examined doses. Moreover, all tested myeloid cell lines were insensitive to AUR and ADE in monotherapy, even if the drugs were used in higher doses than in the previous experiment with lymphoid cell lines. Any noticeable synergistic effects of combining TXN system inhibitors with TKIs were observed exclusively in LAMA-84 cells. Though the synergy scores for DASA in combination with either AUR or ADE exceeded 10, the overall enhancement of TKIs cytotoxicity by the addition of the TXN system inhibitors was lower than in lymphoid cells.

These results suggest that the TXN system does not play such a prominent role in CML cells' viability and sensitivity to TKIs treatment as in the case of lymphoid Ph^+ cells.

4.2. Identification of the lymphoid-specific role of PRDX1 in Ph+ leukemias

4.2.1. Evaluation of the levels of the TXN system antioxidant enzymes in Ph^+ leukemias

To further investigate the role of the TXN system components in Ph^+ leukemic cells, protein levels of PRDX1 and TXN1 have been assessed in CML and Ph^+ B-ALL cell lines by immunoblotting (Fig. 7).

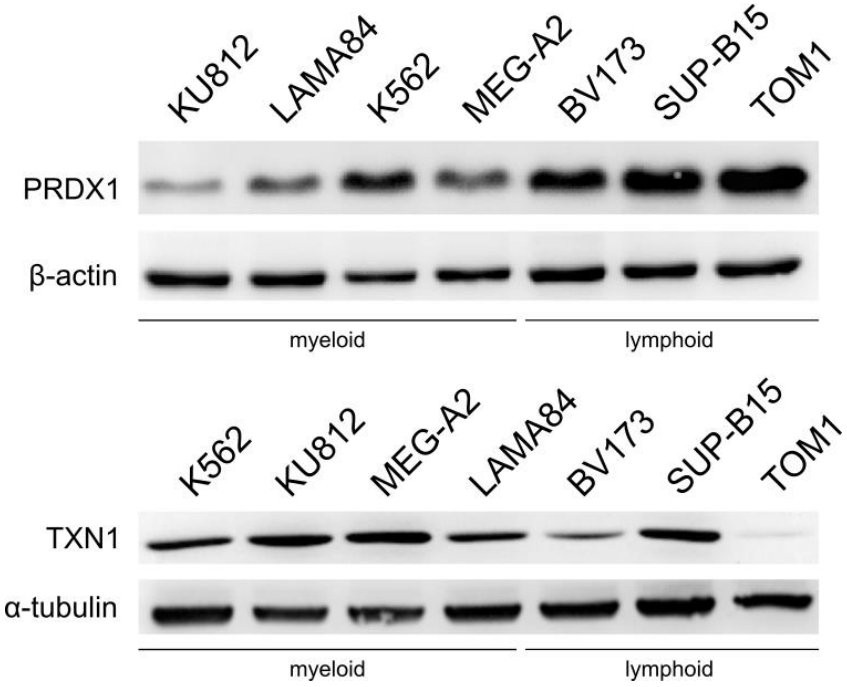

Fig. 7. PRDX1 and TXN1 protein levels in Ph^+ cell lines. Protein levels were assessed by immunoblotting. PRDX1 – peroxiredoxin 1, TXN1 – thioredoxin 1.

Ph⁺ lymphoid cell lines BV173, SUP-B15, and TOM1 exhibited higher PRDX1 levels in whole-cell lysates in comparison to CML cells. TXN1 expression pattern, on the other hand, wasn't consistent among Ph⁺ B-ALL samples. Next, the levels of mRNA encoding PRDX1, TXN1, and TXN-R1 in primary leukemic cells isolated from the bone marrow of patients suffering from myeloid (CML CP and CML lyBP) and lymphoid (CML lyBP and Ph⁺ B-ALL) Ph⁺ leukemia were measured by qPCR (Fig. 8). Relative mRNA expression of TXN1 and TXN-R1 turned out to be downregulated in lymphoid samples in comparison to myeloid ones, while only PRDX1 was significantly upregulated in lymphoid cells. This result led to the hypothesis that in Ph⁺ lymphoid leukemia cells, PRDX1 is a key element of the TXN system, playing an important role in their survival and sensitivity to TKIs treatment.

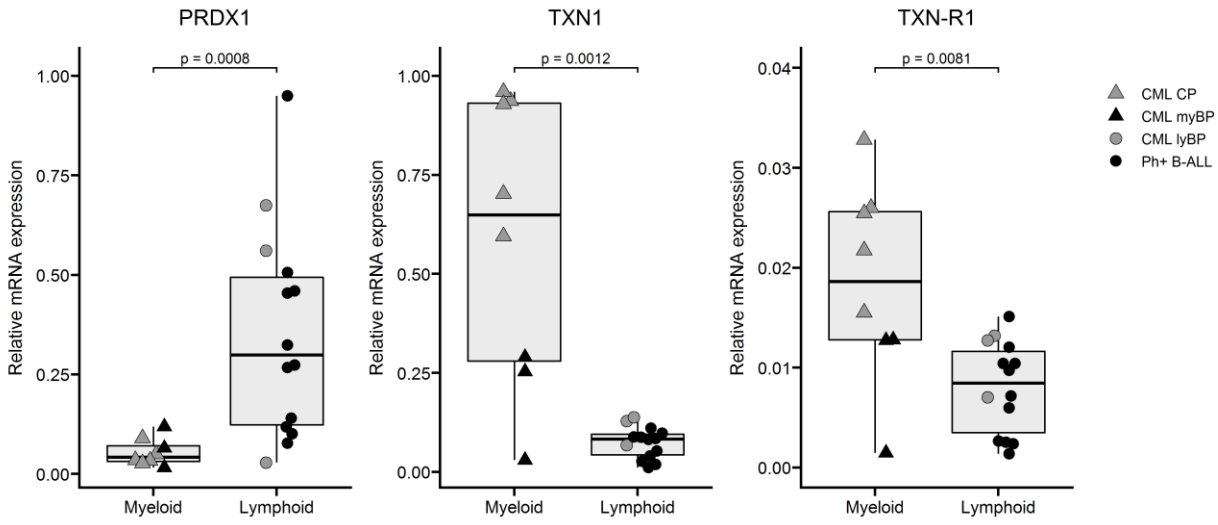

Fig 8. mRNA levels of the TXN system elements in lymphoid and myeloid Ph⁺ primary cells. Relative PRDX1 mRNA levels in primary cells isolated from the bone marrow of leukemic patients: CML CP – chronic myeloid leukemia (CML) in chronic phase (n=5), CML myBP – CML in myeloid blast phase (n=3), CML lyBP – CML in lymphoid blast phase (n=3), Ph+ B-ALL – Philadelphia positive B cell acute lymphoblastic leukemia (n=11). cDNA was obtained by reverse transcription of the whole RNA isolated from primary leukemic cells. Fluorescence was measured using SybrGreen and relative expression was calculated using the RPL29 gene as a reference. Medians ± confidence intervals are presented. Statistical significance was evaluated using the Mann-Whitney test. Experiment performed in collaboration with dr Joanna Madzio from Department of Pediatrics, Oncology and Hematology, Medical University of Łódź.

4.2.2. The effect of PRDX1 silencing on Ph+ cells growth and sensitivity to TKIs

To assess the role of PRDX1 in Ph^+ leukemias, CRISPR-Cas9-mediated genomic knockouts of PRDX1 in myeloid (K562) and lymphoid (BV173) Ph^+ cells have been obtained. The knockouts were generated by a lentiviral transduction of target cells with a vector expressing Cas9 endonuclease and a guide RNA (gRNA), either non-targeting (sgNTC) or complementary to *PRDX1* gene (sgPRDX1). A simplified summary of this genetic modification is presented in Figure 9A. After selection with PURO, PRDX1 knockout was confirmed on the protein level by immunoblotting (Fig. 9B).

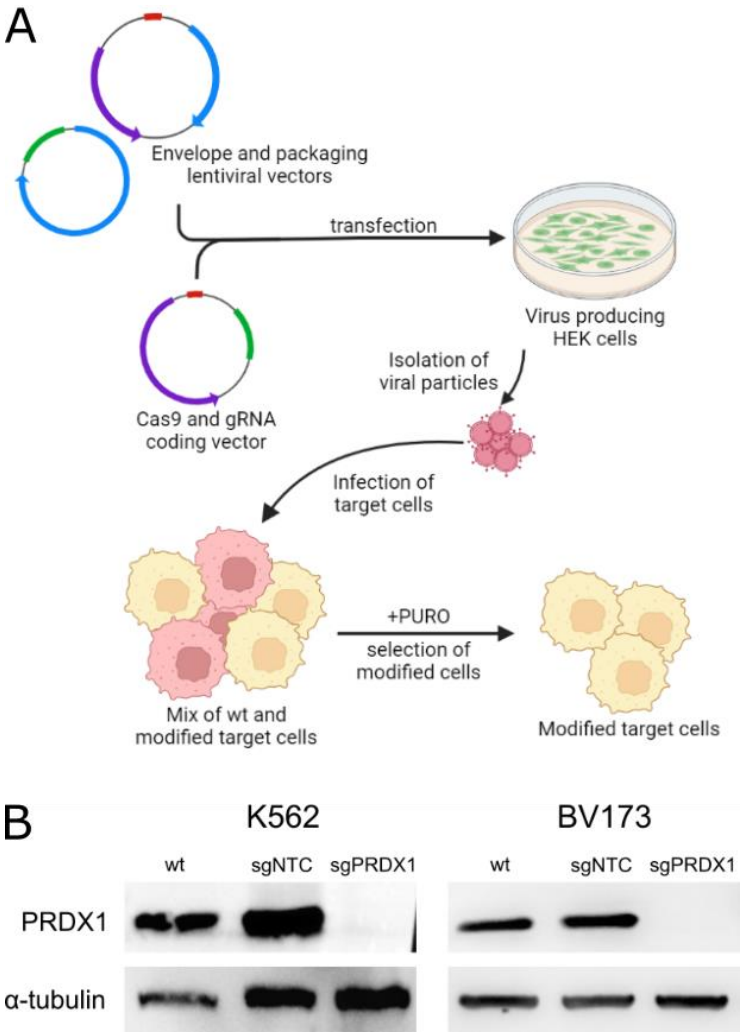

Fig. 9. Generation of K562 and BV173 cell lines with PRDX1 genomic knockouts. A. An illustrative representation of CRISPR-Cas9 genomic modification of target cells. PURO – puromycin. B. Confirmation of the PRDX1 knockout (sgPRDX1 cells) in K562 and BV173 cells by immunoblotting. Parental (wt) and non-targeting control gRNA-modified cells (sgNTC) are shown as reference for the PRDX1 base level.

Next, the numbers of viable sgPRDX1 and control (sgNTC) cells were assessed by counting in the light microscope, with Trypan Blue exclusion, in a 72h time-course (Fig. 10). While the numbers of cells at times of counting were unaffected by PRDX1 knockout in K562 cells, in BV173 the PRDX1 knockout significantly reduced the numbers of viable cells, with the effect increasing over time. As PRDX1 main function in the cell is the removal of H_2O_2, the additional groups of BV173 cells were cultured in the presence of ROS scavengers (sodium pyruvate and catalase). The addition of scavengers restored the growth of sgPRDX1 cells to the levels of control sgNTC cells, showing that the observed PRDX1 knockout effect in BV173 cells was dependent on PRDX1 catalytic function.

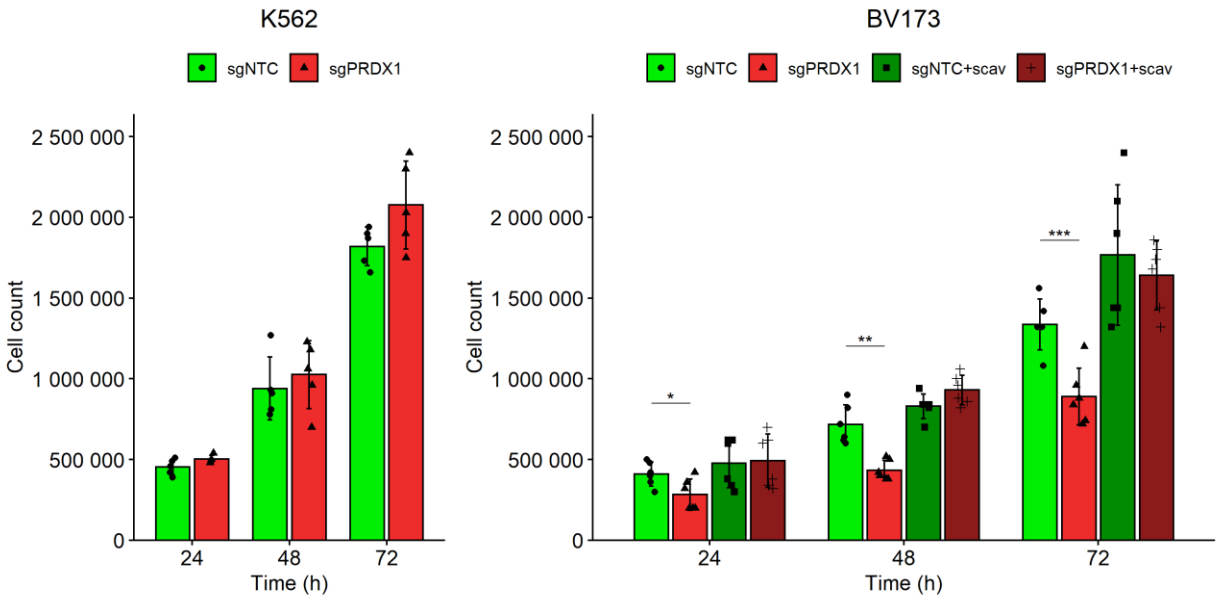

Fig. 10. Impact of PRDX1 knockout on the growth of K562 and BV173 cell lines. The number of live K562 (n=5) and B173 (n=6) cells was assessed by Trypan Blue exclusion in the light microscope. Cells were seeded in 1ml of the medium at a density of 0.2mln/ml (200ths cells/well) and 10µl of cells were taken for counting from each well at indicated timepoints. Two BV173 groups had ROS scavengers (scav) added to the media at the start of the experiment: 50µg/ml catalase, and 1mM sodium pyruvate. Means ± SD are presented. Statistical significance was estimated within specific timepoints by a pairwise t-test with Bonferroni correction, with comparisons between cells without or with scavengers separately. * $p<0.05$, ** $p<0.01$, ***$p<0.001$, non-significant comparisons not shown on graph.

As the PRDX1 knockout slowed down the growth of BV173 cells, the next step was to assess the sensitivity of sgPRDX1 cells to TKIs treatment. First, the effectiveness of IMAT was tested in K562 and BV173 sgNTC cells and the corresponding PRDX1 knockouts (Fig. 11).

PRDX1 knockout substantially sensitized BV173 cells to IMAT, while in K562 cells the effect was smaller.

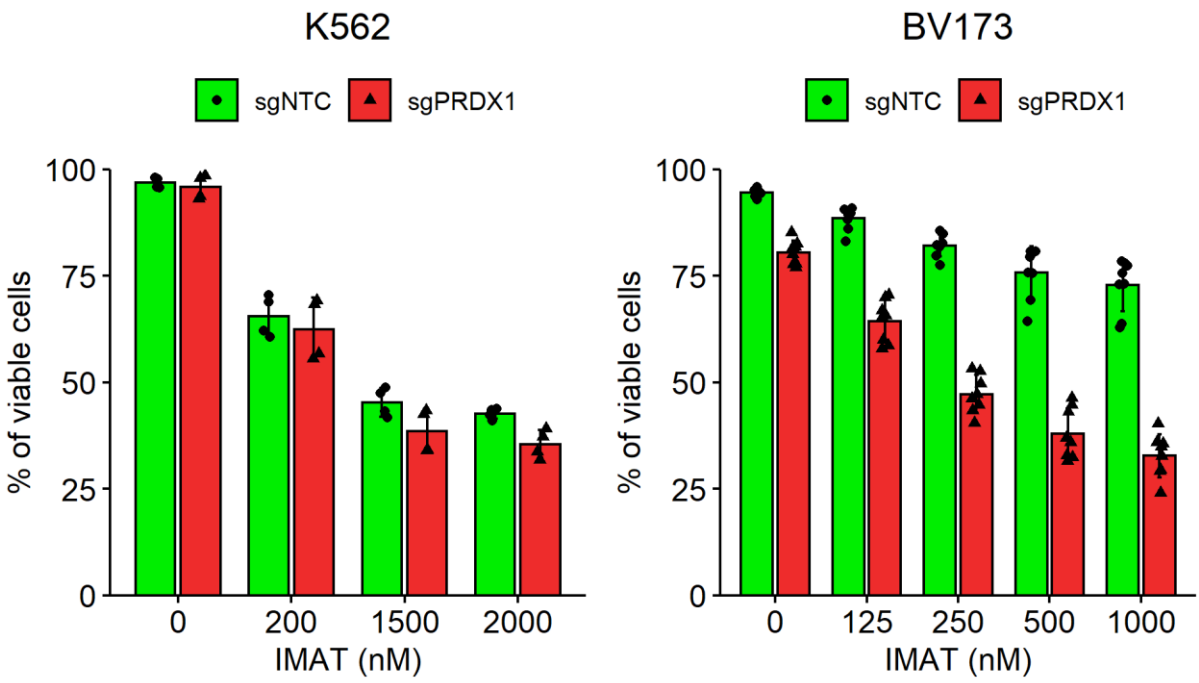

Effect	DFn	DFd	*F*	η_G^2	*p*	Signif.
IMAT	3	24	675.90	0.98	< .001	***
group	1	24	7.07	0.28	.014	*
IMAT:group	3	24	1.95	0.11	.149	

Effect	DFn	DFd	*F*	η_G^2	*p*	Signif.
IMAT	4	70	231.84	0.90	< .001	***
group	1	70	788.79	0.93	< .001	***
IMAT:group	4	70	38.36	0.57	< .001	***

Fig. 11. Effects of PRDX1 knockout on the sensitivity of K562 and BV173 cell lines to IMAT treatment. K562 (n=4) and BV173 (n=8) cells' viability was assessed after 48h treatment with indicated concentrations of IMAT by the PI exclusion of dead cells in flow cytometry. Means ± SD are presented. Statistical differences between groups were assessed by a White-adjusted 2-way ANOVA: *p<0.05, ***p<0.001.

The effectiveness of DASA in sgPRDX1 cells was also investigated (Fig. 12). Differences between sgPRDX1 and control groups in K562 cells were negligible. BV173 control cells, in opposition to K562, were largely resistant to DASA even at 160nM (approximate C_{max} in patients' serum[214]), with less than 20% of the cells killed. Importantly, in BV173 cells, PRDX1 knockout caused immense sensitization to the treatment even at the 20nM concentration of the drug. Moreover, PRDX1 knockout alone decreased untreated BV173 cells viability by approx. 15-20%. The observed sensitization to treatment wasn't just an additive effect, as the differences in viability between groups with rising TKIs concentrations were significantly

different, as assessed by the significance of the 2-way ANOVA interaction factor (Anova tables in Fig. 11 and Fig.12). The augmentation of TKIs effect by PRDX1 knockout specifically in Ph^+ B-ALL but not CML cells further suggests the lineage-specific role of this protein.

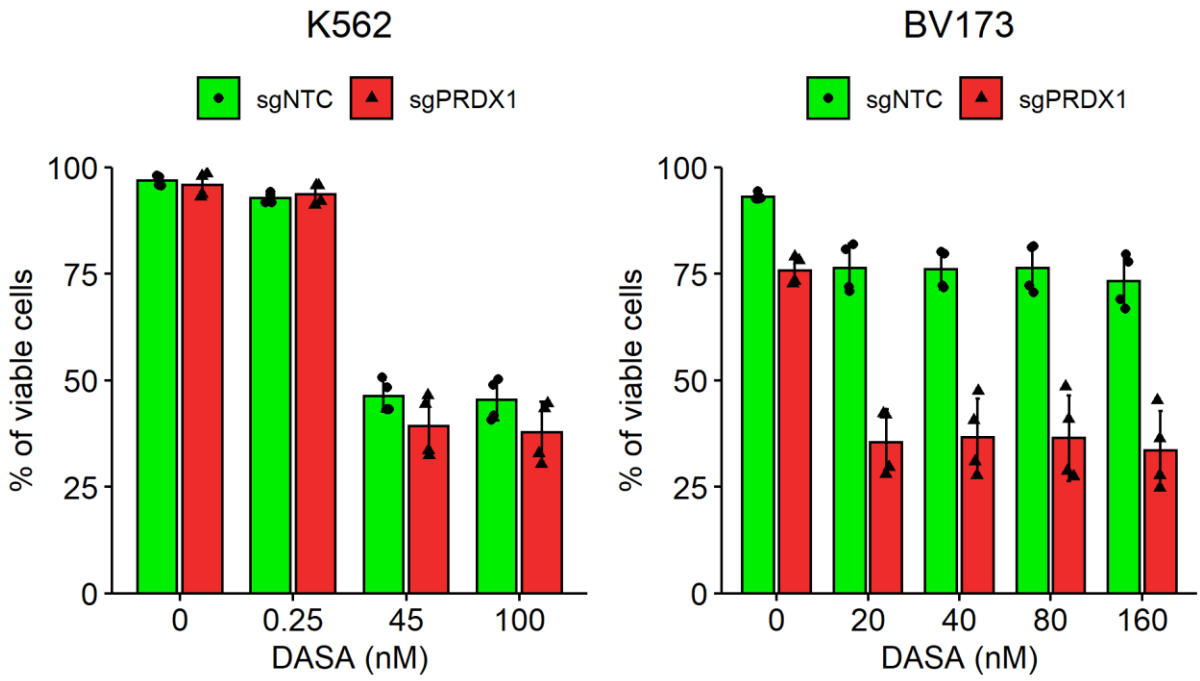

Effect	DFn	DFd	*F*	η_G^2	*p*	Signif.
DASA	3	24	279.70	0.98	< .001	***
group	1	24	4.18	0.19	.052	
DASA:group	3	24	1.61	0.19	.213	

Effect	DFn	DFd	*F*	η_G^2	*p*	Signif.
DASA	4	30	64.90	0.79	< .001	***
group	1	30	201.92	0.90	< .001	***
DASA:group	4	30	10.03	0.37	< .001	***

Fig. 12. Effects of PRDX1 knockout on the sensitivity of K562 and BV173 cell lines to DASA treatment. Cell viability (n=4) was assessed after 48h treatment with indicated concentrations of DASA by the PI exclusion of dead cells in flow cytometry. Means ± SD are presented. Statistical differences between groups were assessed by a White-adjusted 2-way ANOVA: ***p<0.001.

To test the effects of PRDX1 knockout on the proliferation and viability of IMAT-treated cells in a longer time, control and sgPRDX1 BV173 cells were treated with 1000nM IMAT for 2h and taken for clonogenic assay. After six days of incubation, the number of CFUs was assessed (Fig. 13).

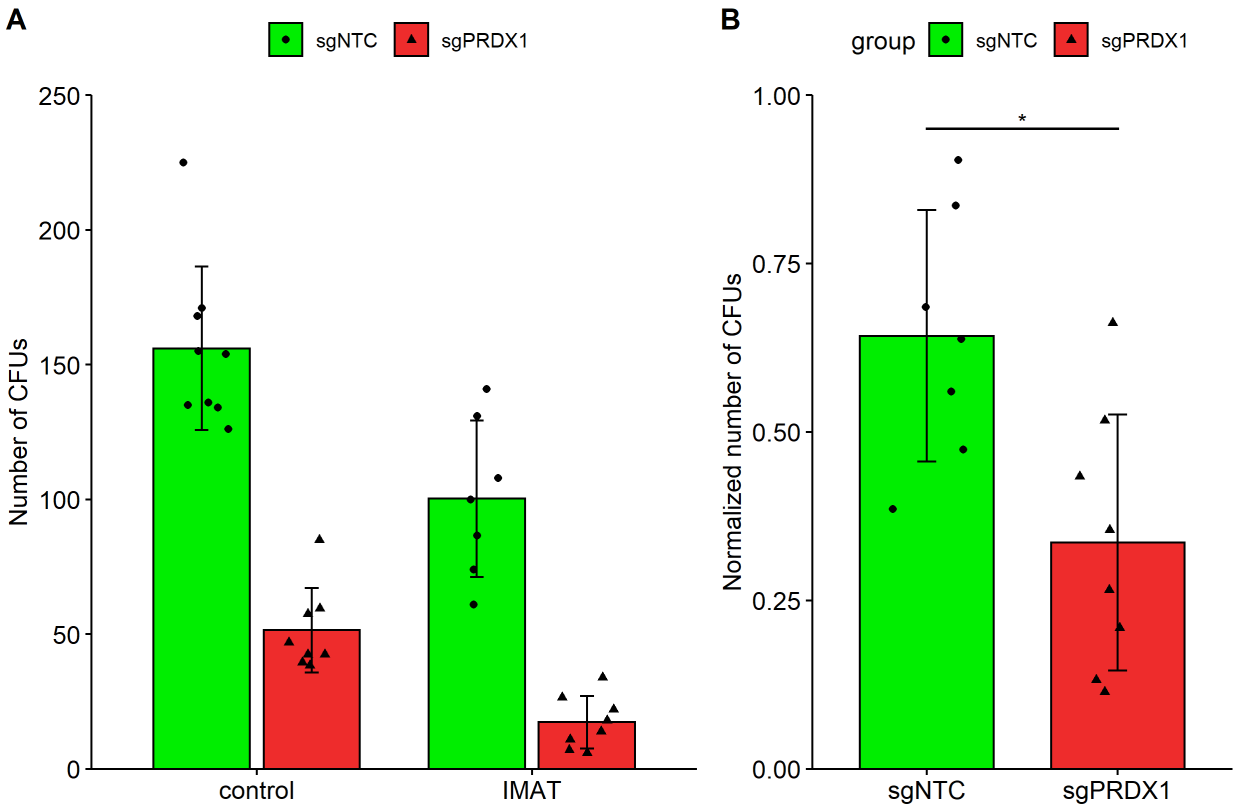

Fig. 13. Effects of PRDX1 knockout on the clonogenic potential of BV173 cells treated with IMAT. BV173 cells (n=7) were pretreated with 1µM IMAT for 2h before seeding on plates after 5.5 times dilution with methylcellulose semi-liquid media without a drug. After 6 days of incubation, colonies consisting of at least 4 cells (CFUs, colony-forming units) were counted. A. Absolute CFUs number of untreated and IMAT-treated cells. Due to very high differences between groups clearly visible, statistical significance wasn't tested. Means ± SD are presented B. Normalized CFUs number of IMAT-treated cells. Results were normalized to each group's average CFUs in the untreated group. Means normalized to controls ± SD are presented. Statistical significance was estimated by a Mann-Whitney test: *p<0.05.

The absolute CFU number was much lower in both control and IMAT-treated sgPRDX1 groups compared to sgNTC cells. To properly compare the IMAT effect on clonogenic potential between groups, CFU counts were normalized to exclude effect of basal CFU number difference in control sgNTC and sgPRDX1 cells. The normalized number of CFUs in treated BV173 sgPRDX1 cells was significantly lower, with approximately two times fewer CFUs than in the sgNTC group, showing that even relatively short IMAT treatment exhibits a persistent effect on sgPRDX1 cells growth and viability for a longer period.

4.2.3. Evaluation of the PRDX1 knockout's effects on apoptosis induction in BV173 cells incubated with IMAT

The changes in apoptosis-related signaling were assessed in IMAT-treated BV173 cells (Fig. 14).

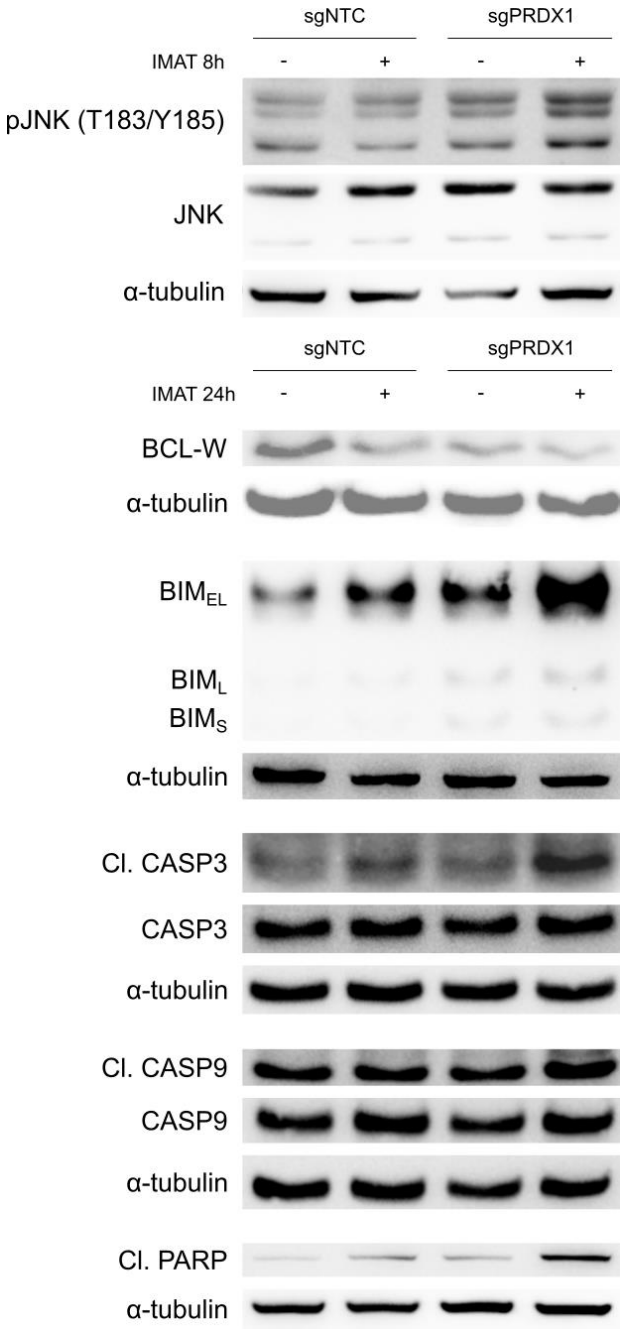

Fig. 14. Changes in the protein levels and activation of apoptosis-related proteins in sgPRDX1 BV173 cells incubated with IMAT. Before lysates gathering, cells were treated with 250nM IMAT for either 8h or 24h. Protein levels were assessed by immunoblotting.

First, overactivation of JNK was observed in untreated sgPRDX1 cells in comparison to control cells, which was further elevated after 8h-treatment with IMAT, indicating higher stress levels in sgPRDX1 cells. Another two proteins that were affected by PRDX1 knockout were two apoptotic regulators, BCL-W and BIM. Anti-apoptotic BCL-W was downregulated upon PRDX1 knockout. In contrast, all isoforms of pro-apoptotic BIM were upregulated in untreated sgPRDX1 cells and further increased after incubation of the cells with IMAT. Moreover, increased amounts of cleaved PARP, caspases 3, and 9 were found in the IMAT-treated sgPRDX1 cells. Overall, PRDX1 knockout potentiated activation of JNK, decreased anti-apoptotic protein BCL-W, increased proapoptotic BIM, and enhanced induction of intrinsic apoptosis. These results show that PRDX1 protects those cells from stress factors and apoptosis in the resting state and after treatment with IMAT.

4.3. The PRDX1 silencing's impact on genome-wide mRNA expression in Ph⁺ lymphoid cells upon IMAT treatment

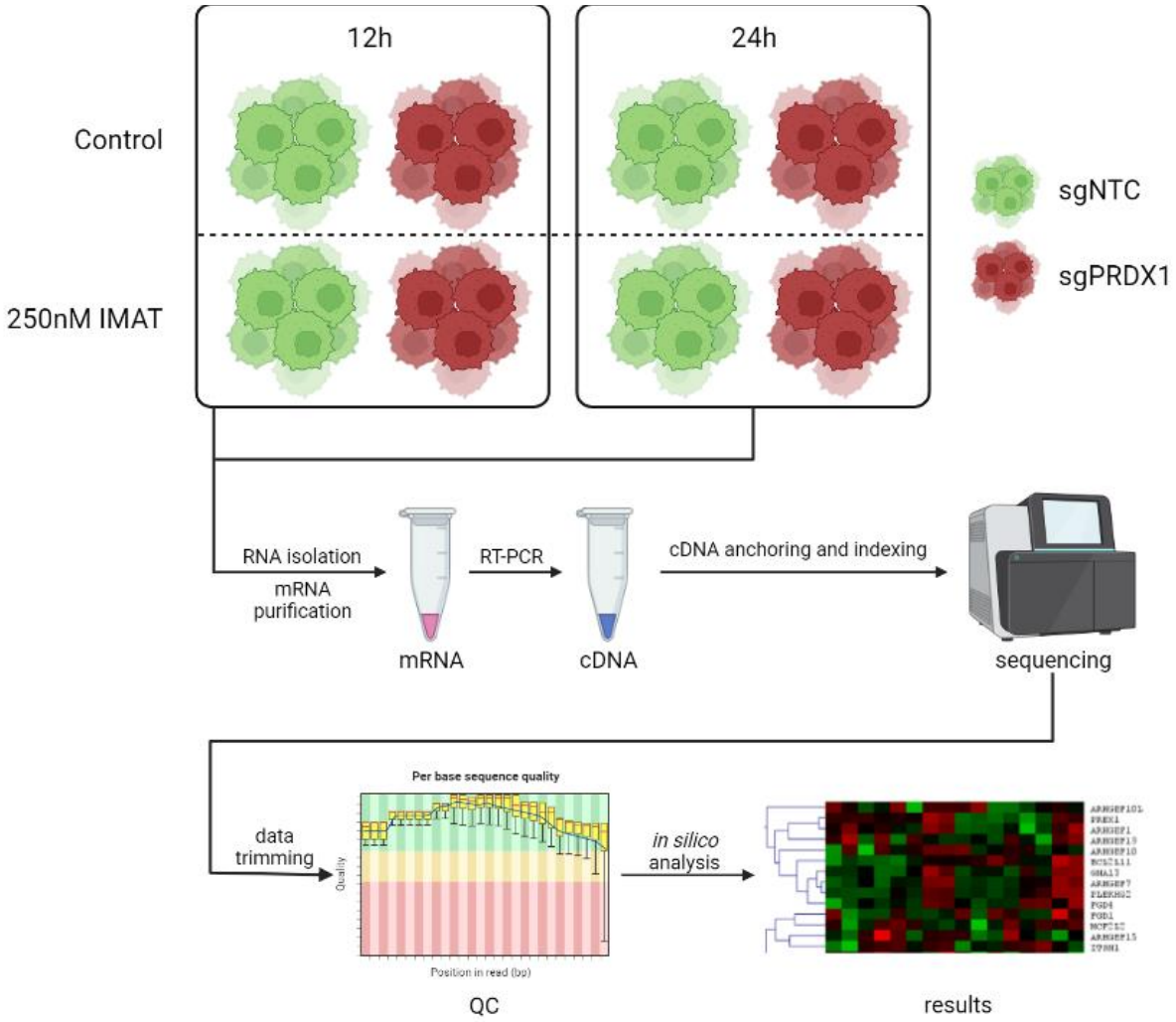

Fig. 15. Design of the RNAseq experiment of BV173 cells upon treatment with IMAT. A simplified scheme of the experiment setup and steps.

To further study the genome-wide changes in mRNA levels upon PRDX1 knockout, RNAseq of either untreated or IMAT-treated BV173 sgNTC and sgPRDX1 cells was performed. A diagram of the experimental layout is presented in Figure 15. The raw data have been trimmed to dispose of faulty or nonreliable reads and the quality control has been performed. Overall data quality was very high, with over 98% of aligned reads, consistent average read lengths, and approx. 90% of reads aligned to protein coding genes in all samples (Fig. 16A). Also, the 3D principal component analysis (PCA) scores of sample replicates were similar to each other, showing consistency in the obtained data (Fig. 16B).

A

Sample	Total no. of reads	Aligned reads	Uniquely matched reads	Average read length	Reads aligned to genome	Protein coding genes
sgNTC ctrl 12h	49 534 476	98.4%	95.2%	57	7 882 572	92.1%
sgNTC ctrl 12h	45 711 146	98.5%	95.4%	57	7 237 891	93.4%
sgNTC ctrl 24h	39 090 704	98.5%	95.4%	58	5 502 835	92.8%
sgNTC ctrl 24h	61 310 044	98.4%	95.3%	57	9 605 036	92.4%
sgNTC + IMAT 12h	49 832 082	98.3%	94.8%	57	9 118 581	91.5%
sgNTC + IMAT 12h	43 169 482	98.2%	94.6%	57	7 536 182	91.5%
sgNTC + IMAT 24h	46 819 544	98.2%	94.1%	57	8 154 257	87.3%
sgNTC + IMAT 24h	41 944 810	98.0%	94.2%	57	7 888 869	89.4%
sgPRDX1 ctrl 12h	50 131 870	98.4%	95.3%	57	8 149 490	92.9%
sgPRDX1 ctrl 12h	47 439 676	98.5%	95.4%	58	7 482 251	93.5%
sgPRDX1 ctrl 24h	49 941 012	98.0%	94.2%	57	8 566 535	89.0%
sgPRDX1 ctrl 24h	44 910 510	98.2%	94.7%	57	7 618 033	91.1%
sgPRDX1 + IMAT 12h	47 397 696	98.3%	95.0%	57	8 396 135	91.9%
sgPRDX1 + IMAT 12h	43 360 964	98.2%	94.9%	57	8 055 162	92.4%
sgPRDX1 + IMAT 24h	47 164 472	98.4%	94.9%	58	7 918 225	91.5%
sgPRDX1 + IMAT 24h	53 940 014	98.4%	95.0%	57	9 120 383	91.8%

B

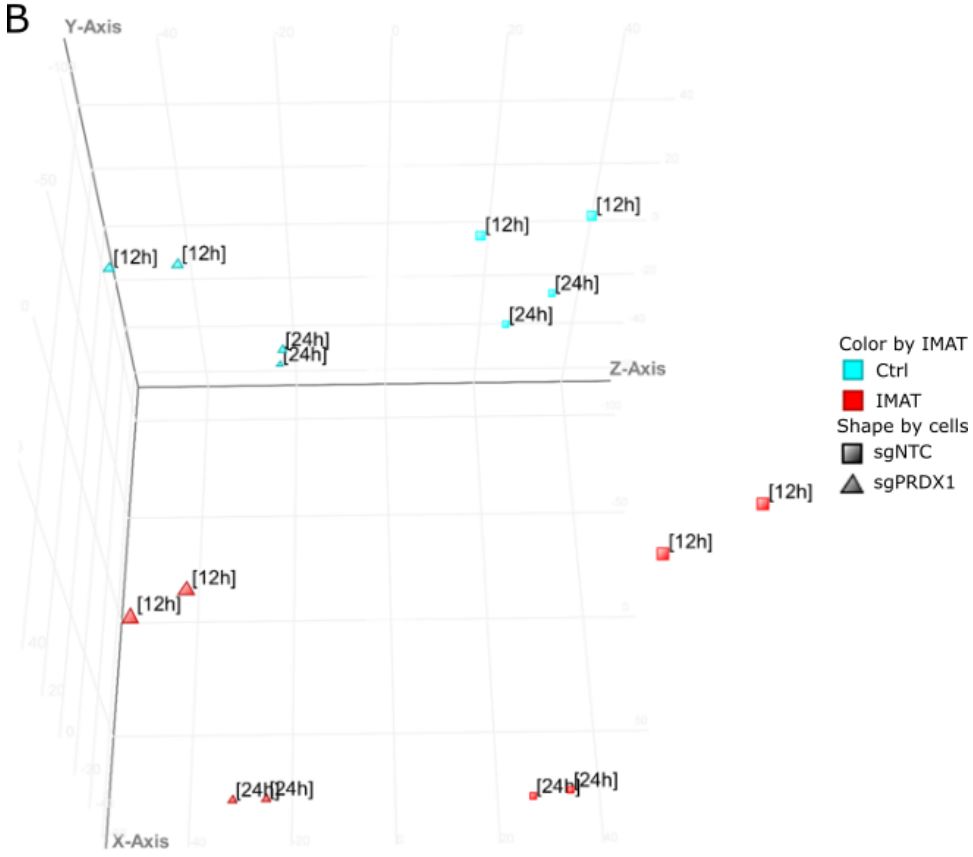

Fig. 16. Quality controls of the whole-exome sequencing of BV173 cells upon treatment with IMAT. A. Quality control of the obtained RNAseq data. B. 3D principal component analysis (PCA) scores of RNAseq results. Experiment and analysis were performed in collaboration with dr A. Pastorczak and dr J. Madzio from Department of Pediatrics, Oncology and Hematology, Medical University of Łódź.

4.3.1. Assessment of changes in gene expression caused by PRDX1 silencing 1

A list of the most differentially expressed mRNA transcripts upon PRDX1 knockout (absolute fold change > 2) was generated (Table 8), and most of the reported ones were downregulated (42 out of 58). Also, a subset of 10 transcripts exhibiting similar expression patterns to PRDX1 was identified (Table 8). Cancer-relevant functions of genes dysregulated upon PRDX1 knockout in BV173 cells are summarized in Table 9 and briefly discussed below.

Several genes which are downregulated in cells with PRDX1 knockout may be involved in the observed phenotype of BV173 sgPRDX1 cells. *Bone Morphogenetic Protein Receptor Type 1A* (***BMPR1A***) overexpression was identified as a poor prognostic factor in acute myeloid leukemia (AML) patients and its involvement in the maintenance and increase of stem-like features in AML cell line Kasumi-1 was shown[215]. *Myeloid leukemia factor 1* (***MLF1***), even though not very well studied in lymphoid malignancies, has been proposed as a regulator of RUNX1[216], a protein involved in hematopoiesis and oncogenesis, overactivated by t(12;21) translocation in B-ALL[217,218]. *CAS1 domain containing 1* (***CASD1***) encodes an enzyme responsible for 9-O-acetylation in ALL cells, contributing to cell survival and drug resistance[219]. *Disabled homolog 2* (***DAB2***) has been considered to be a tumor suppressor for a while[220]. However, recent findings suggest its role in metastasis in some cancer types[221,222], though its molecular mechanism of action, especially in leukemia, is poorly understood. *KH RNA Binding Domain Containing, Signal Transduction Associated 3* (***KHDRBS3***) has been identified as a factor increasing stemness of breast cancer cells[223]. Other genes from this subset have an unknown function or have not been studied in the leukemic or malignant setting.

Rank	Gene	FC	p adj.	Rank	Gene	FC	p adj.
1	**ANXA5**	**-35.90**	**2.18e-04**	30	RIN3	-2.53	4.31e-02
2	**BMPR1A**	**-29.30**	**4.57e-03**	31	AARSD1	-2.47	4.40e-03
3	**MLF1**	**-25.00**	**7.85e-04**	32	KCTD12	-2.47	9.47e-03
4	SKAP2	-20.30	2.59e-02	33	PTGES3L-AARSD1	-2.46	4.40e-03
5	PRDX1	-19.80	8.35e-07	34	APOC4-APOC2	-2.40	4.41e-02
6	**C17orf112**	**-19.00**	**3.16e-03**	35	PCDHGC3	-2.40	4.92e-02
7	**CASD1**	**-17.60**	**1.69e-03**	**36**	**KHDRBS3**	**-2.39**	**1.23e-02**
8	FSTL5	-15.10	4.29e-03	37	PLEK	-2.37	1.23e-02
9	**DAB2**	**-11.40**	**3.39e-02**	38	SEP8	-2.35	4.90e-02
10	**LOC100506465**	**-10.60**	**1.23e-02**	39	IL2RG	-2.32	1.22e-03
11	SAMHD1	-10.20	3.40e-03	40	ATP8B4	-2.21	7.27e-04
12	SPARC	-8.39	4.97e-02	41	CYBB	-2.20	1.32e-02
13	KLRC4	-7.40	1.75e-02	**42**	**ZNF28**	**-2.19**	**1.80e-03**
14	MRS2	-6.25	2.56e-02	43	LRRC26	2.05	7.02e-03
15	PLXDC2	-5.91	2.77e-02	44	DENND5B	2.09	1.23e-02
16	**HTATIP2**	**-5.50**	**3.48e-03**	45	TMEM254	2.10	1.29e-02
17	TPRG1	-4.61	2.25e-02	46	BHLHB9	2.13	2.45e-02
18	KLRC3	-4.30	8.87e-03	47	PRKAR2B	2.14	2.07e-02
19	LIX1	-3.91	4.97e-02	48	PRICKLE2-AS1	2.18	2.62e-02
20	TSTD1	-3.71	4.57e-03	49	ABHD4	2.18	3.04e-02
21	ZNF613	-3.37	8.83e-03	50	MRS2P2	2.24	1.61e-02
22	IRF8	-3.16	9.12e-06	51	PPM1H	2.27	2.25e-02
23	CUZD1	-3.11	2.94e-02	52	KRBA1	2.31	4.64e-02
24	FAM24B-CUZD1	-3.05	8.41e-03	53	SRCIN1	2.41	4.67e-02
25	**DHX57**	**-2.80**	**1.69e-03**	54	S100A7A	2.54	1.41e-02
26	LOC101927215	-2.70	4.30e-02	55	PLCB1	2.70	2.65e-02
27	FAM24B	-2.61	1.29e-02	56	GRID1	2.83	8.70e-03
28	PRAME	-2.59	2.56e-02	57	PLXNA1	2.87	1.29e-02
29	H19	-2.58	4.08e-02	58	SMIM10	10.80	3.42e-02

Table 8. Differentially expressed genes in sgPRDX1 BV173 cells. A. List of genes which expression was the most significantly affected by PRDX1 knockout (absolute FC > 2). Raw reads were quantified using the trimmed mean of the m-values algorithm and expressions fold change was calculated in comparison to the control (sgNTC) group. Genes are ranked according to their fold change, from most downregulated to most upregulated. Genes with similar expression pattern to PRDX1 were highlighted in bold, as measured by Pearson distance. P-value was assessed by moderated T-test with Benjamini-Hochberg correction. FC – fold change, p adj. – adjusted p value. Experiment and analysis were performed in collaboration with dr A. Pastorczak and dr J. Madzio from Department of Pediatrics, Oncology and Hematology, Medical University of Łódź.

Function	Gene	Model
DNA integrity maintenance	↓ *SAMHD1*	Kidney[224]
Drug resistance	↓ *CASD1*	ALL[219]
	↓ *SPARC*	CML[225]
Metastasis	↓ *DAB2*	PC[221], BlaC[222]
Oncogenesis	↓ *MLF1*	AML[216]
Proliferation stimulation	↓ *IRF8*	AML[226]
	↓ *PRAME*	CML[227]
	↓ *APOC4-APOC2*	AML[228,229]
Stemness support	↓ *KHDRBS3*	BC[223]
	↓ *CYBB*	CML[230]
	↓ *BMPR1A*	AML[215]
Survival promotion	↓ *ANXA5*	B-ALL[231,232]
	↓ *H19*	APML[233]
Tumor suppressor	↑ *LRRC26*	BC[234]
	↑ *SRCIN1*	NB[235]
Oncodriver	↑ *PLCB1*	HCC[236]
	↑ *PRKAR2B*	PC[237,238]

Table. 9. Known cancer-relevant functions of genes dysregulated upon PRDX1 knockout in BV173 cells - summary. Arrows next to gene names indicate whether the gene was up- or downregulated in sgPRDX1 BV173 cells. AML – acute lymphoblastic leukemia, APML – acute promyeloblastic leukemia, B-ALL – B cell acute lymphoblastic leukemia, BlaC – bladder cancer, BC – breast cancer, CML – chronic myeloid leukemia, HCC - hepatocellular carcinoma, NB – neuroblastoma, PC – prostate cancer.

Among other transcripts downregulated in sgPRDX1 cells, the most relevant seem to be *annexin A5* (***ANXA5***)**,** *SAM and HD domain containing deoxynucleoside triphosphate* (***SAMHD1***)**,** *secreted protein acidic and cysteine rich* (***SPARC***)*, interferon regulatory factor 8* (***IRF8***)*,* ***H19****, preferentially expressed antigen of melanoma* (***PRAME***)*, apolipoprotein C-IV-apolipoprotein C-II* (***APOC4-APOC2***)*, pleckstrin* (***PLEK***)*,* and *cytochrome B-245 beta chain* (***CYBB***)**.** The most downregulated gene, ***ANXA5****,* (over 35-fold downregulation)*,* encodes

annexin V protein. It promotes a function of protein kinase C λ (PKCλ), [231], which has been shown to play an important role in the transformation, maintenance, and survival of Ph^+ B-ALL cells. Deletion of PKCλ decreased proliferative potential and increased apoptosis more prominently in Ph^+ lymphoid as compared to myeloid cells.[232] ***SAMHD1*** product is involved in replicative stress response by promotion of degradation of DNA stalled at replication forks[224]. ***SPARC*** encodes a glycoprotein whose role in cancer is controversial, as in some malignancies it is downregulated (i.e. ovarian, colorectal, or AML with *MLL* translocation) while in others its overexpression was correlated to adverse outcome (i.e. breast cancer, melanoma or cytogenetically normal AML)[239,240]. However, the most compelling SPARC role was reported for CML, where its overexpression correlated with IMAT resistance[225]. ***IRF8*** product, interferon-regulatory factor 8 (IRF8), has been shown to act as a tumor suppressor in AML[241,242], although results published by Zhendong et al. suggest that IRF8 supports AML cells proliferation[226]. ***H19***, encoding long non-coding RNA, overexpression in AML has been reported to predict unfavorable outcome and its silencing in HL60 promyeloblastic leukemia cell line caused increased apoptosis and slowed proliferation rate[233]. ***PRAME*** has been shown to play important role in K562 cells' cell cycle progression and proliferation[227]. APOC2 (product of ***APOC4-APOC2***) upregulation was observed in several cancers[243], and it is reported to be linked to AML cells' proliferation and survival[228,229]. ***PLEK*** transcript, a binding partner of PKC, was found to be hypomethylated in several childhood acute lymphoblastic leukemias[244]. Upregulation of NOX2, encoded by the ***CYBB*** gene, has been identified as a marker of adverse prognosis in AML[245], and its inhibition prolonged survival of mice bearing K-RAS-induced myeloproliferative disease[246]. It was also shown to be crucial for the self-renewal of leukemia stem cells in murine xenograft human myeloid disease model[230]. Some of the other downregulated genes or their products in BV173 sgPRDX1 cells have been shown to be up- (*CUB and zona pellucida like domains 1* [***CUZD1***][247], *limb and CNS expressed 1* [***LIX1***][248], *tumor protein p63 regulated 1* [***TPRG1***][249]) or downregulated (*protocadherin gamma subfamily C, 3* [***PCDHGC3***][250]) in several cancer types, although their significance is not completely understood, especially in leukemia.

Out of the transcripts upregulated in BV173 cells with PRDX1 knockout, some were identified as tumor suppressors (*leucine rich repeat containing 26* [***LRRC26***][234]*, SRC kinase signaling inhibitor 1* [***SRCIN1***][235]) and some have been found to be upregulated and/or acting as oncodrivers (*phospholipase C beta 1* [***PLCB1***][236]*, protein kinase CAMP-dependent type II regulatory subunit beta* [***PRKAR2B***][237,238]) in several cancer types, although their role in hematological cells and malignancies is not well known.

4.3.2. Investigation of changes in signaling pathways between IMAT-treated PRDX1-deficient and control cells

To visualize pathway enrichment changes between the IMAT-treated BV173 sgPRDX1 and control cells in a functional manner, clustering of differentially activated pathways has been performed (Fig. 17 and Fig. 18). The clusters have been formed based on the convergence of genes contained in dysregulated pathways and cluster names have been assigned manually depending on the contained pathways and genes, utilizing a knowledge-based approach.

The most conspicuous observation at the 12h time point of IMAT treatment is the downregulation of many pathways linked to cell metabolism and proliferation in the PRDX1-deficient cells in comparison to sgNTC cells (Fig. 17A). A disruption of oxidative phosphorylation and metabolic pathways was discovered, indicating that sgPRDX1 cells enter an energy crisis upon IMAT treatment. Translation regulation and transcription clusters contain pathways related to the initiation of transcription and translation, ribosome activity, and genes encoding RNA polymerases and ribosomal proteins. Downregulation of these pathways most likely causes deregulation of gene expression and protein synthesis, causing attenuation of metabolic processes and cell proliferation. Also, cytokine signaling is downregulated. This is mainly related to the interleukin 2 (IL-2) family and interferons pathways. Lower expression levels of IL2 family elements may cause partial inactivation of several proteins critical for malignant B cells, such as STAT5[251], and cause decreased proliferation and viability[252]. Activation of DNA repair pathways suggests the accumulation of DNA damage. Upregulation of PI3K-related signaling was also identified. PI3K signaling is overactivated in Ph^+ leukemias and contributes to increased proliferation and drug

resistance[253,254], but as discussed before, uncontrolled PI3K activity can lead to ROS accumulation[86] and negative selection of malignant B cells[55], possibly explaining the impact of the observed PI3K-upregulation in sgPRDX1 cells on their apoptotic phenotype. Interestingly, upregulation of cell division can be observed, although with impaired transcription and translation it very likely deepens cell crisis through protein depletion.

A

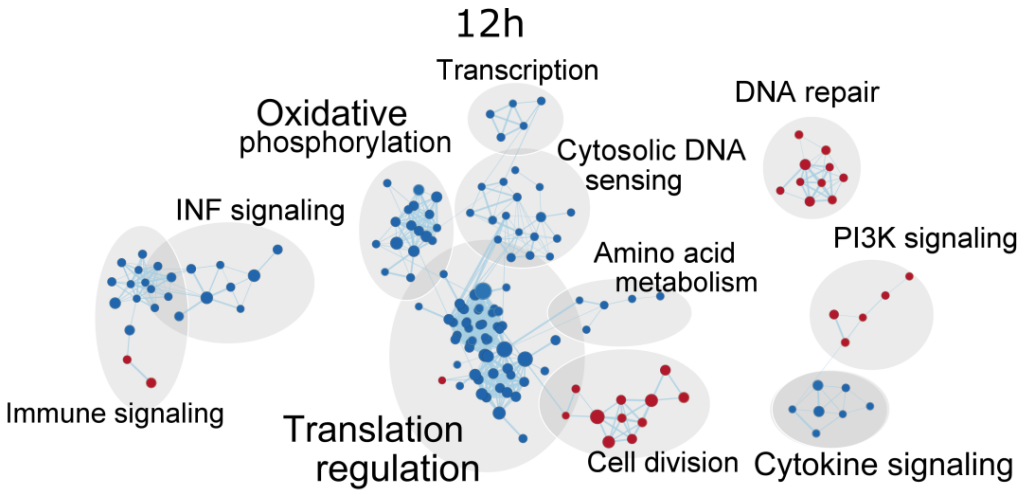

B

Pathway	Size	ES	NES	Nom p-val	FDR q-val	Rank at max
REACTOME AMINO ACID TRANSPORT ACROSS THE PLASMA MEMBRANE	22.00	0.74	2.15	0.00	0.01	1,337.00
HALLMARK MITOTIC SPINDLE	190.00	0.44	1.92	0.00	0.08	2,968.00
WP PHOTODYNAMIC THERAPYINDUCED NFE2L2 NRF2 SURVIVAL SIGNALING	20.00	0.67	1.90	0.00	0.09	1,734.00
REACTOME ASSEMBLY AND CELL SURFACE PRESENTATION OF NMDA RECEPTORS	28.00	0.57	1.81	0.01	0.15	2,438.00
REACTOME CREB1 PHOSPHORYLATION THROUGH NMDA RECEPTOR MEDIATED ACTIVATION OF RAS SIGNALING	22.00	0.61	1.79	0.00	0.17	2,438.00
REACTOME NEUREXINS AND NEUROLIGINS	34.00	0.55	1.78	0.00	0.18	2,438.00
WP GENES INVOLVED IN MALE INFERTILITY	90.00	0.44	1.75	0.00	0.22	1,443.00

Fig. 17. Changes in signaling pathways caused by PRDX1 knockout in BV173 cells upon 12h IMAT treatment. A. Functional clustering of IMAT-induced pathways significantly upregulated (red) or downregulated (blue) upon PRDX1 knockdown in BV173 cells. The pathways were identified by gene set enrichment analysis (GSEA) of differentially expressed genes in sgPRDX1 and sgNTC cells after 12h of treatment. Each node represents a different pathway. Node size corresponds to gene set size. The thickness of lines between nodes depicts the number of convergent genes between two gene sets. B. List of significantly enriched pathways ($p<0.05$), that didn't fit any of the clusters. ES – enrichment score, NES – normalized enrichment score, Nom p-val – nominal p value, FDR q-val – false discovery rate q value. Experiment and analysis were performed in collaboration with dr A. Pastorczak and dr J. Madzio from Department of Pediatrics, Oncology and Hematology, Medical University of Łódź.

A

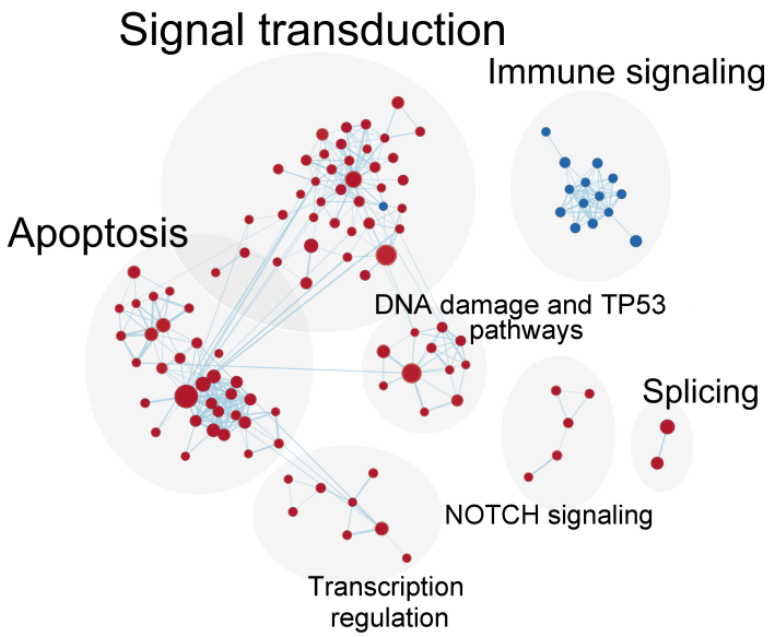

B

Pathway	Size	ES	NES	Nom p-val	FDR q-val	Rank at max
REACTOME INTERCONVERSION OF NUCLEOTIDE DI AND TRIPHOSPHATES	26.00	0.56	1.63	0.02	0.22	1,516.00
WP OXIDATIVE STRESS	25.00	0.57	1.63	0.01	0.23	934.00
REACTOME HEME SIGNALING	41.00	0.51	1.63	0.00	0.23	2,526.00
REACTOME INITIATION OF NUCLEAR ENVELOPE NE REFORMATION	19.00	0.62	1.63	0.01	0.24	576.00
WP PATHWAYS REGULATING HIPPO SIGNALING	71.00	0.47	1.65	0.00	0.23	2,200.00
WP P53 TRANSCRIPTIONAL GENE NETWORK	55.00	0.50	1.65	0.00	0.25	1,441.00
PID ILK PATHWAY	43.00	0.52	1.67	0.01	0.22	2,164.00
WP PHOTODYNAMIC THERAPYINDUCED NFE2L2 NRF2 SURVIVAL SIGNALING	20.00	0.62	1.67	0.01	0.22	1,290.00
PID TAP63 PATHWAY	39.00	0.53	1.68	0.01	0.23	393.00
WP 1Q211 COPY NUMBER VARIATION SYNDROME	20.00	0.61	1.69	0.01	0.21	1,830.00
PID AJDISS 2PATHWAY	36.00	0.55	1.73	0.01	0.16	2,648.00
REACTOME DEACTIVATION OF THE BETA CATENIN TRANSACTIVATING COMPLEX	36.00	0.57	1.74	0.00	0.16	2,952.00
WP PRIMARY FOCAL SEGMENTAL GLOMERULOSCLEROSIS FSGS	52.00	0.54	1.76	0.00	0.13	3,373.00
WP RETT SYNDROME CAUSING GENES	35.00	0.61	1.83	0.00	0.10	2,084.00
WP NRF2ARE REGULATION	19.00	0.69	1.83	0.00	0.13	1,471.00
REACTOME DOWNREGULATION OF SMAD2 3 SMAD4 TRANSCRIPTIONAL ACTIVITY	23.00	0.64	1.85	0.00	0.13	4,324.00
WP PHOTODYNAMIC THERAPYINDUCED UNFOLDED PROTEIN RESPONSE	24.00	0.69	1.94	0.00	0.06	1,164.00

Fig. 18. Changes in signaling pathways caused by PRDX1 knockout in BV173 cells upon 24h IMAT treatment. A. Functional clustering of IMAT-induced pathways significantly upregulated (red) or downregulated (blue) upon PRDX1 knockdown in BV173 cells. The pathways were identified by gene set enrichment analysis (GSEA) of differentially expressed genes in sgPRDX1 and sgNTC cells after 12h of treatment. Each node represents a different pathway. Node size corresponds to gene set size. The thickness of lines between nodes depicts the number of convergent genes between two gene sets. B. List of significantly enriched pathways ($p<0.05$), that didn't fit any of the clusters. ES – enrichment score, NES – normalized enrichment score, Nom p-val – nominal p value, FDR q-val – false discovery rate q value. Experiment and analysis were performed in collaboration with dr A. Pastorczak and dr J. Madzio from Department of Pediatrics, Oncology and Hematology, Medical University of Łódź.

Several significantly upregulated pathways that didn't fit into any of the clusters were also uncovered (Fig. 17B), among them the unfolded protein response (UPR) pathway and the NRF2-related oxidative stress signaling. This is in line with the discovery of significant UPR activation upon TXN system inhibition in B-ALL[74] and the fact that its prolonged overactivation leads to activation of apoptotic signaling[255].

The most prominent changes in signaling induced by 24h IMAT treatment upon PRDX1 knockout were the upregulation of apoptotic signal transduction and apoptosis-related pathways, as well as activation of p53 and DNA damage response signaling (Fig. 18A). These changes most likely result from the prior ongoing energy and metabolic crisis and accumulation of DNA damage, causing elevated apoptosis. Among the unclustered gene sets (Fig. 18B), two related to UPR have been identified again, suggesting persistent ER stress. Also, pathways connected to ROS accumulation and oxidative stress were uncovered, which is expected due to PRDX1 catalytic function in the cell.

Additionally, at both time points, downregulation of immune response signaling pathways, linked to cytosolic DNA sensing and cytokine signaling was observed. These pathways include genes involved in antigen presentation (i.e. *human leukocyte antigen B* [*HLA-B*], *HLA-DR beta 5* [*HLA-DRB*]), interleukin and interferons response (i.e. *integrin subunit beta 2* [*ITGB2*]*, IL10, IL15*), and control of several immune-related transcription factors (i.e. *class II major histocompatibility complex transactivator* [*CIITA*]*, nuclear factor kappa B subunit 1* [*NFKB1*]). Although this is an interesting and previously undescribed effect of PRDX1 knockout, the sole *in vitro* studies performed in this study do not allow for the proper interpretation of the immune-related changes.

4.4. Examination of ER stress and oxidative stress in PRDX1-deficient and proficient Ph+ lymphoid cells subjected to IMAT

4.4.1. Assessment of ER stress upregulation in PRDX1-deficient cells

As RNAseq revealed persistent ER stress and ROS-induced UPR activation in BV173 sgPRDX1 cells in comparison to control cells, it emerged as a possible cause of upregulated apoptosis in PRDX1-deficient cells upon IMAT treatment. To test this hypothesis, the levels of *activating transcription factor 4* (*ATF4*) and C*/EBP homologous protein* (*CHOP*) mRNA were

measured by qPCR (Fig. 19). Both of those genes are activated in ER stress conditions and often serve as ER stress and UPR markers[256,257]. Cells were subjected to the same conditions as the ones analyzed in RNAseq. The analysis showed an increase in both genes' mRNA levels upon PRDX1 knockout, which is in line with the previous reports[74], however, IMAT treatment caused their downregulation (Fig. 19A). The same results were shown in RNAseq (Fig. 19B).

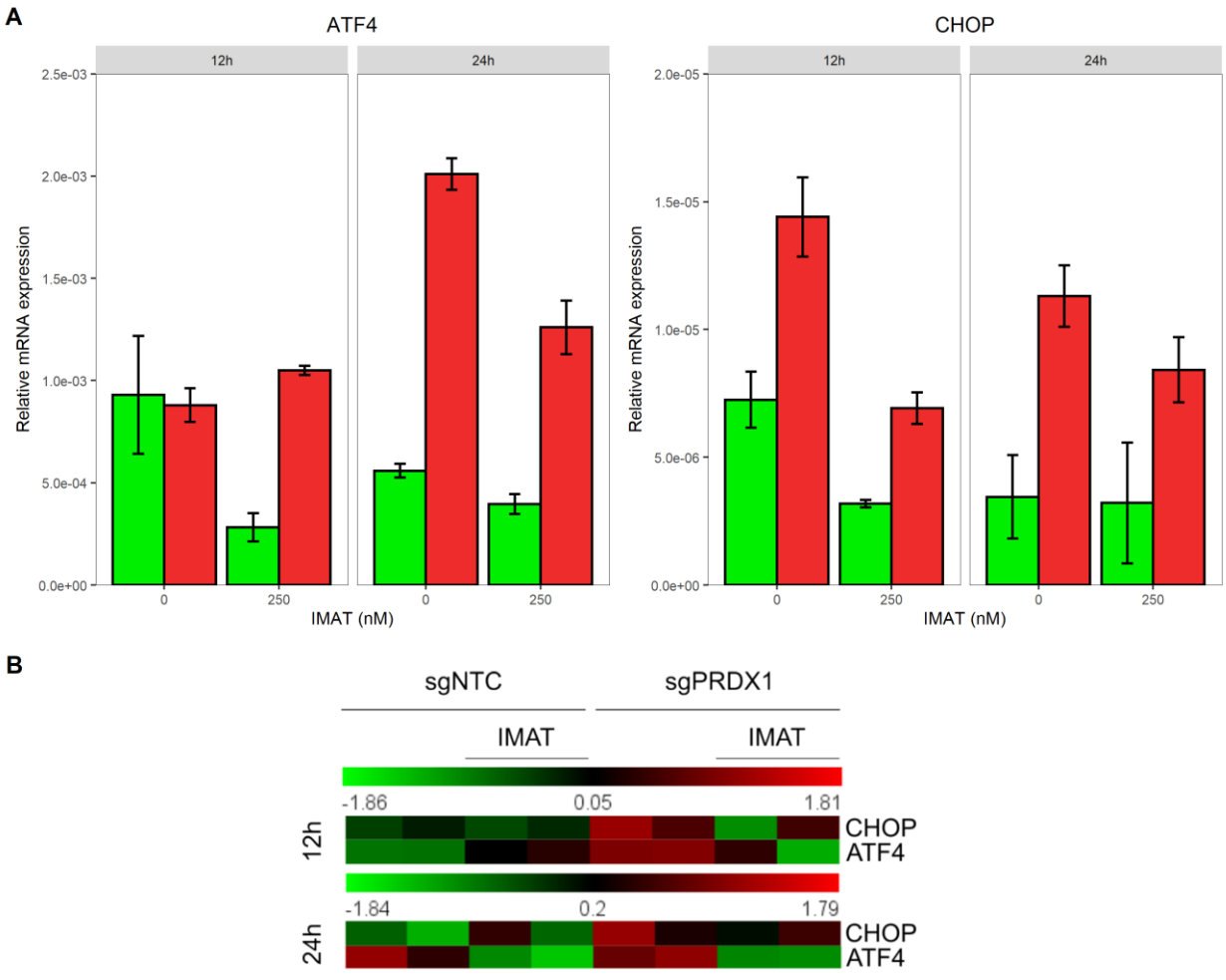

Fig. 19. mRNA levels of genes related to ER stress upon PRDX1 knockout. BV173 sgNTC and sgPRDX1 cells were incubated for 12h or 24h with IMAT, followed by RNA isolation and RT-qPCR. A. Relative *CHOP* and *ATF4* mRNA levels in BV173 cells were measured using SybrGreen and RPL29 gene as a reference in two technical repeats. Means + SD are presented. B. Heatmap of *ATF4* and *CHOP* expression in BV173 cells, obtained from RNAseq data and generated by GSEA analysis. Heatmaps represent row Z scores.

4.4.2. Measurement of cytoplasmic and nuclear levels of ROS in IMAT-treated cells

As PRDX1 canonical function is the removal of H_2O_2 and thus, maintenance of redox homeostasis[258], the impact of its knockdown on BV173 cell's ability to metabolize exogenous H_2O_2 and intracellular ROS levels upon IMAT treatment was studied.

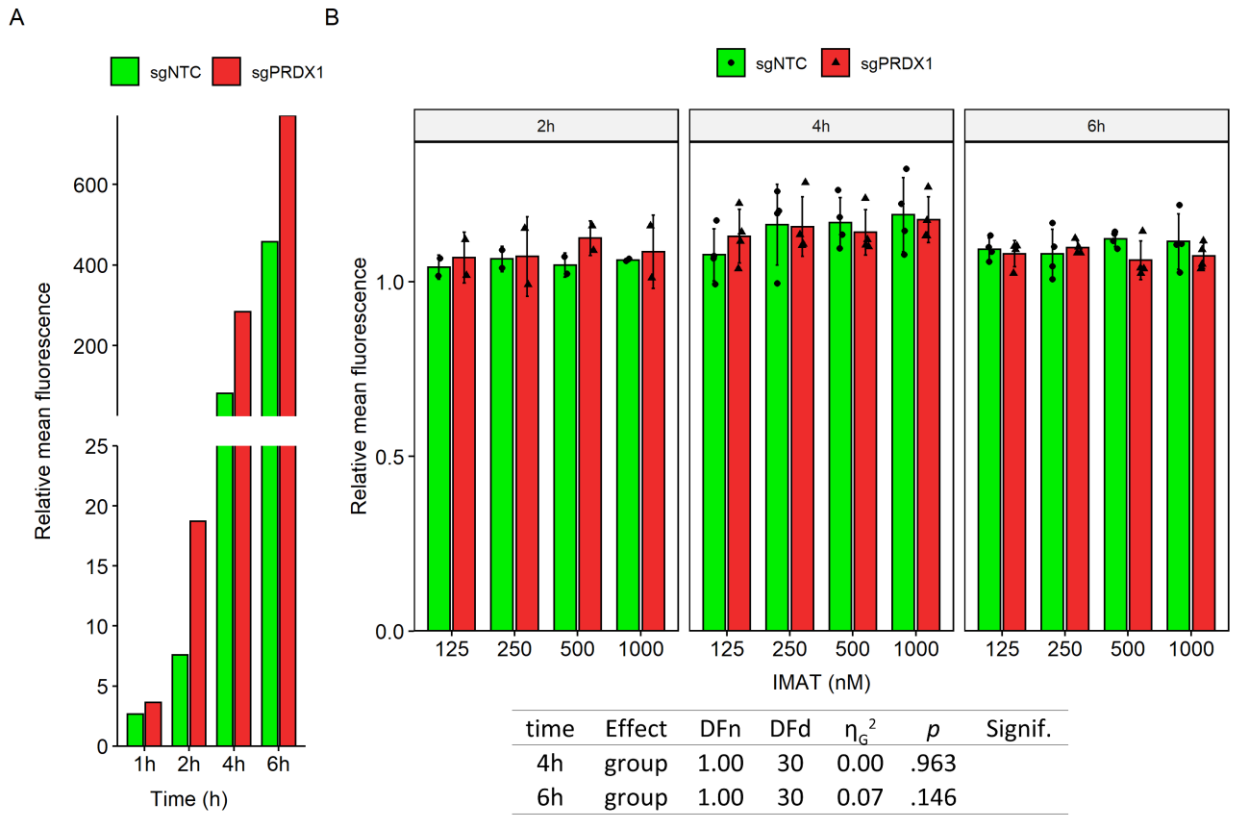

time	Effect	DFn	DFd	η_G^2	*p*	Signif.
4h	group	1.00	30	0.00	.963	
6h	group	1.00	30	0.07	.146	

Fig. 20. Intracellular ROS levels measured by CM-H2-DCFDA in BV173 cells. BV173 cells were stained with 10µM DCFDA and subsequently incubated with 50µM H_2O_2 (panel A; n=1) or IMAT (panel B; n=2-4) for indicated times. Intracellular ROS levels were assessed by measurement of DCFDA fluorescence in flow cytometry. Means +- SD are presented. Differences between sgNTC and sgPRDX1 cells were assessed by a White-adjusted two-way ANOVA for each timepoint separately with disregard to IMAT concentration and a test for 2h timepoint wasn't performed due to low n.

First, an experiment aiming to evaluate the ability to metabolize exogenously added H_2O_2 by PRDX1-proficient and -deficient cells was performed. In this experiment, the accumulation of intracellular ROS upon treatment of the cells with H_2O_2 was investigated with the DCFDA assay (Fig. 20A). As expected, BV173 sgPRDX1 cells accumulated higher levels of ROS over the time upon H_2O_2 addition to cell media in comparison to control cells. Next, the ROS levels in cells incubated with various concentrations of IMAT were measured (Fig. 20B).

IMAT didn't affect ROS levels in any of the tested cell lines. Moreover, no differences in ROS levels in any of the IMAT concentrations or treatment time points were observed between control and sgPRDX1 cells.

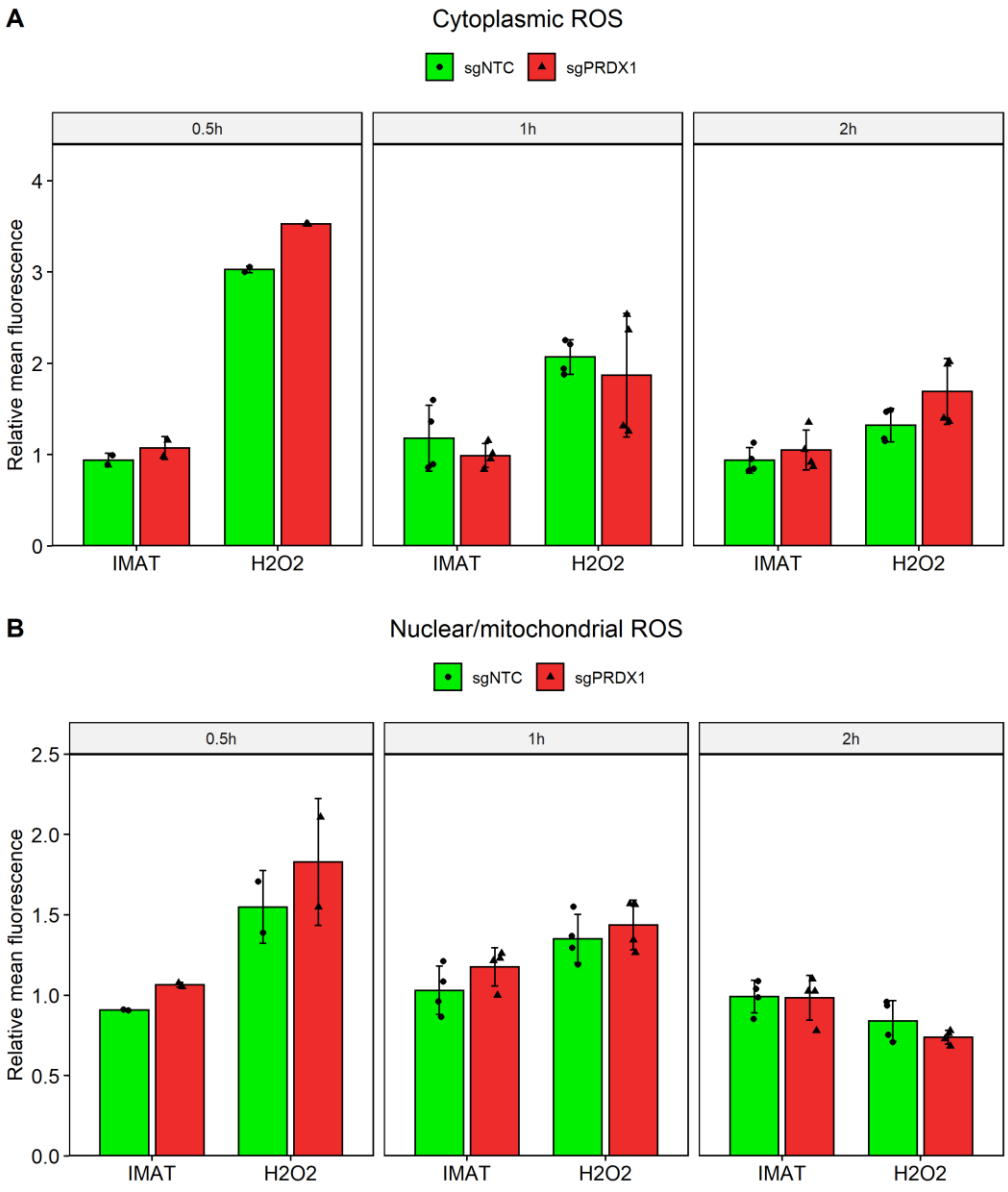

Fig. 21. The effect of PRDX1 knockout on nuclear and cytoplasmic levels of ROS in IMAT-treated BV173 cells. The cells were treated with either 500nM IMAT or 200µM H_2O_2 for indicated times, stained with either a cytoplasmic (CellROX™ Green, panel A; n=2-4) or a nuclear (CellROX™ Deep Red, panel B; n=2-4) dye, and analyzed in flow cytometry. Mean fluorescence was normalized to each timepoint's control group separately, independently for each experiment. Means ± SD are presented. Statistical significance for each group was estimated by a pairwise t-test with Bonferroni correction, with comparisons between sgNTC and sgPRDX1 for each timepoint and condition separately. A test for 0.5h timepoint wasn't performed due to low n. Non-significant comparisons are not shown on the graph.

To further investigate the impact of PRDX1 knockout on ROS levels in specific cellular compartments, the assessment of cytoplasmic (Fig. 21A) and nuclear (Fig. 21B) ROS levels was performed, using compartment-specific dyes. Cells were treated with IMAT or H_2O_2 and the fluorescence was measured at 0.5h, 1h and 2h timepoints. No statistically significant differences were found at the 1h and 2h timepoints. Results from 0.5h timepoint weren't statistically tested due to low biological repeats number, although a mild ROS levels increase in sgPRDX1 cells cytoplasm could be observed after 0.5h treatment with H_2O_2.

4.4.3. Assessment of OxS markers released to culture media in IMAT-treated cells

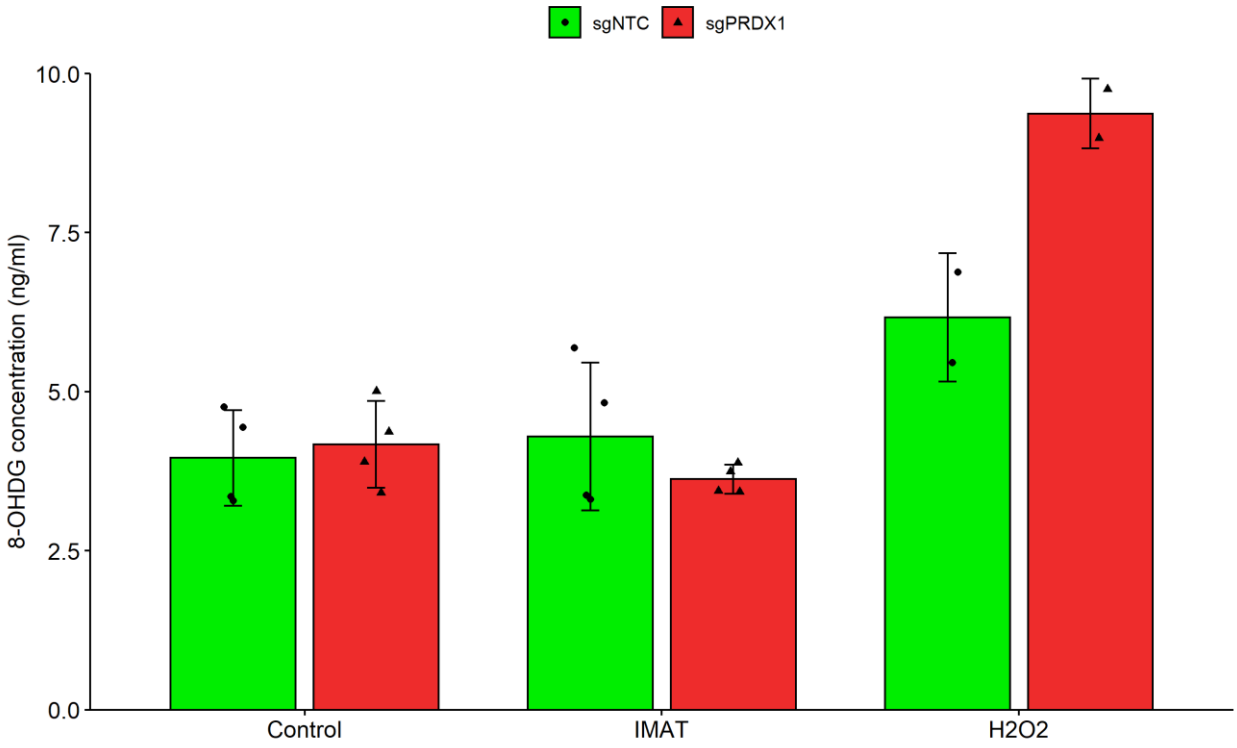

Fig. 22. The levels of 8-OHDG in cell culture media collected from sgPRDX1 and control (shNTC) BV173 cells incubated with IMAT. BV173 cells (n=2-4) were treated with either 500nM IMAT for 24h or 10mM H_2O_2 for 2h. Media was collected from each well, centrifuged and supernatants were used for the assay. 8-hydroxy-2'-deoxyguanosine (8-OHDG) concentration was assessed with an ELISA kit purchased from MyBioSource following the manufacturer's protocol. Means ± SD are presented. Statistical significance was estimated by a pairwise t-test with Bonferroni correction for each condition separately. A test for group treated with H_2O_2 wasn't performed due to low n. Non-significant comparisons are not shown on the graph.

As an increase in ROS level could be transient and hence undetectable by the previously chosen timepoints and assays, accumulation of a DNA oxidation product, 8-hydroxy-2'-deoxyguanosine (8-OHdG), in the cell medium was measured after 24h-IMAT

treatment (Fig. 22). No differences were found between IMAT-treated PRDX1-deficient and proficient cells. An observable effect, but due to small groups not statistically tested, was detected between groups treated with H_2O_2.

Taken together those results suggest that triggering the ER-stress isn't the major mechanisms responsible for higher IMAT-induced apoptosis induction in PRDX1-deficient cells. Even though higher activation of ER stress-mediated UPR upon PRDX1 knockout can be observed, its elements downregulation by IMAT treatment discouraged further investigation of UPR in this context. Despite this, more in-depth studies would be needed to fully exclude this mechanism's role in the sensitivity of PRDX1-deficient cells to IMAT.

Moreover, the lack of identified signs of IMAT-induced ROS accumulation in sgPRDX1 cells, including direct and indirect approaches, suggests that OxS does not significantly influence PRDX1-deficient sensitivity to IMAT. As this was surprising, keeping in mind the PRDX1 function in the cell, OxS was further investigated with other approaches.

4.5. Evaluation of the role of PRDX1's catalytic function in Ph+ lymphoid cells' sensitivity to IMAT

4.5.1. Impact of the reconstitution of WT PRDX1 and its mutated variants on Ph+ lymphoid cells' sensitivity to IMAT

To evaluate whether PRDX1 catalytic activity is crucial for BV173 cells' sensitivity to TKIs treatment, reconstitution of WT PRDX1 and its point-mutated variants was performed. In the PRDX1 coding sequence, one of three cysteines have been mutated to alanines. Two of them, Cys52 and Cys173, are known to be required for forming disulfide bonds essential for homodimer formation required for PRDX1's catalytic activity. The third Cys83 function isn't fully elucidated, although it is hypothesized to play a role in the formation of chaperone-like PRDX1 decamers[259,260] (Fig. 23).

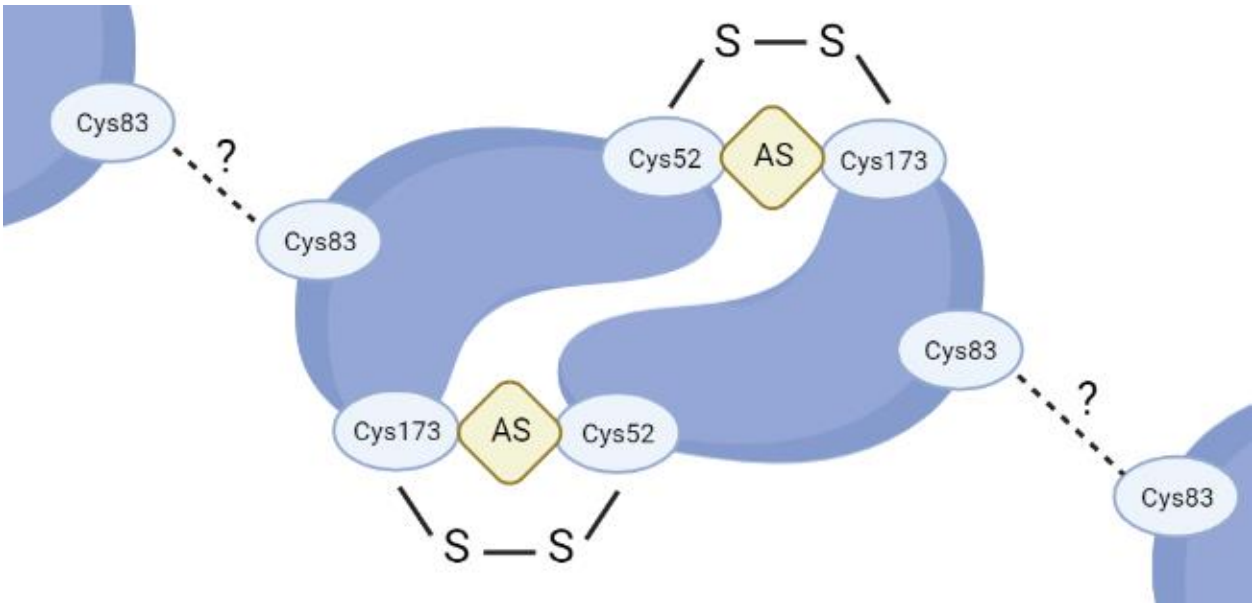

Fig. 23. PRDX1 functional dimer and the role of cysteine residues. Illustration presenting oxidized PRDX1 dimer after the catalytic cycle (post H_2O_2 reduction)[114]. Cys52 and Cys173 are required for PRDX1 catalytic function and PRDX1 dimerization, and Cys83 is hypothesized to play a role in oligomerization, although there is no direct evidence for its significance in this process[259,260]. AS – active site.

BV173 sgPRDX1 cells were modified with a vector containing either WT PRDX1 or its catalytically active (C83A) or inactive (C52A and C173A) variants. PRDX1 protein expression was evaluated by immunoblotting (Fig. 24A). A slight shift of the reconstituted PRDX1 bands results from the presence of the T2A linker in the overexpressed proteins. Sensitivity to IMAT of BV173 sgPRDX1 cells with PRDX1 reconstitution was assessed after 48h incubation with the drug (Fig. 24B). Restoration of both catalytically active variants substantially reversed the PRDX1 knockout effect on cells' viability, both in untreated and treated groups, while restoration of inactivated PRDX1 did marginally improve the cell viability.

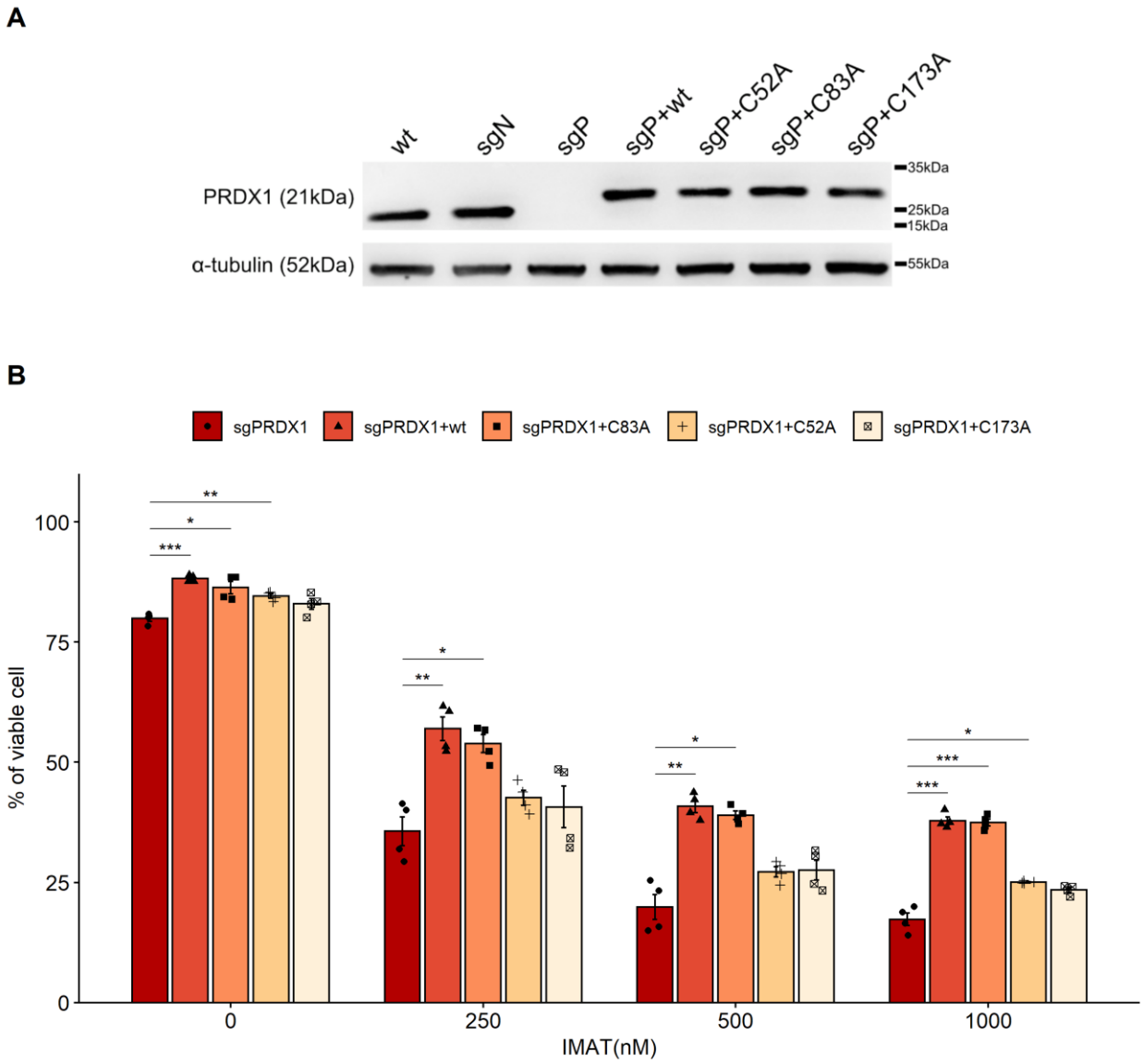

Fig. 24. The reconstitution of wild-type (wt) PRDX1 or its Cys-mutated variants in BV173 sgPRDX1 cells and their influence on the cells' sensitivity to IMAT. BV173 sgPRDX1 cells were genetically modified with a vector encoding either wt PRDX1 or its variants with selected Cys to Ala substitutions (C52A, C83A, C173A). A. Confirmation of PRDX1 reconstitution in sgPRDX1 BV173 cells by immunoblotting. B. Cell viability was assessed after 48h treatment with indicated concentrations of IMAT by PI exclusion of dead cells in flow cytometry (n=4). Means ± SD are presented. Statistical significance was estimated by a pairwise t-test with Bonferroni correction in comparison to sgPRDX1 cells, for each IMAT concentration separately. * p<0.05, ** p<0.01, ***p<0.001, non-significant comparisons not shown on the graph.

4.5.2. Effects of ROS scavengers on the sensitivity to IMAT

To fully elucidate the impact of ROS on BV173 sgPRDX1 cells' sensitivity to IMAT, ROS scavengers, sodium pyruvate and catalase, were used to remove ROS from cells in the 48h IMAT treatment assay (Fig. 25). ROS removal caused noticeable viability improvement of sgPRDX1 cells, but slightly better survival in groups treated with higher IMAT concentration was also observed for sgNTC cells.

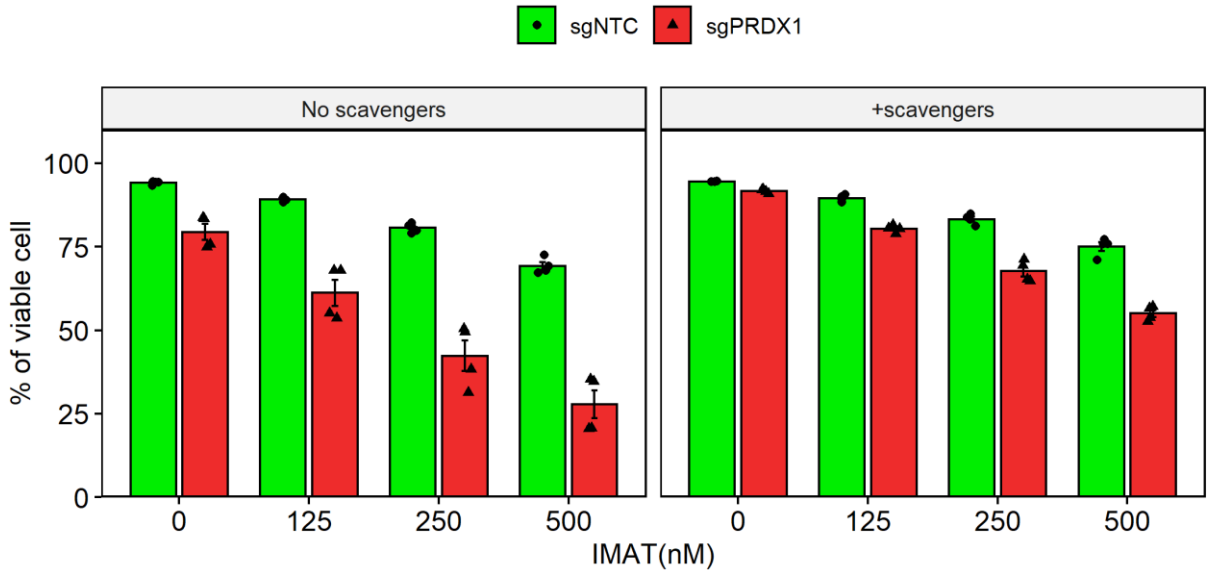

Effect	DFn	DFd	*F*	η_G^2	*p*	Signif.
imat	3	24	70.21	0.90	< .001	***
group	1	24	182.52	0.91	< .001	***
imat:group	3	24	10.42	0.54	< .001	***

Effect	DFn	DFd	*F*	η_G^2	*p*	Signif.
imat	3	24	423.56	0.98	< .001	***
group	1	24	254.50	0.93	< .001	***
imat:group	3	24	47.49	0.81	< .001	***

Fig. 25. Effect of ROS scavengers on IMAT cytotoxicity in BV173 cells. Cell viability (n=4) was assessed after 48h treatment with indicated concentrations of IMAT by PI exclusion of nonviable cells in flow cytometry. Two BV173 groups had ROS scavengers (scav) added to the media at the start of the experiment: 50µg/ml catalase, and 1mM sodium pyruvate (right panel). Means ± SD are presented. Statistical differences between groups were assessed by a White-adjusted 2-way ANOVA, with comparisons between groups without or with scavengers separately: ***p<0.001.

Even though elevated levels of ROS weren't detected in sgPRDX1 cells in previous experiments, significant improvement of cells viability (both untreated and subjected to IMAT) upon either catalytically active PRDX1 reconstitution or addition of scavengers indicates that PRDX1 catalytic activity plays an important role in cells survival and sensitivity

to IMAT. This could be explained by limited sensitivity of previously used assays as well as a possible narrow and/or transient localization of ROS accumulation, making it extremely hard to detect using the utilized techniques, although there is no data to fully support this hypothesis.

4.6. Investigation of the effect of PRDX1 knockout on DNA damage induction in Ph+ lymphoid cells

4.6.1. Measurement of DSBs levels and DDR-related genes expression in IMAT-treated PRDX1-proficient and -deficient cells

Because RNAseq of IMAT-treated BV173 sgPRDX1 cells revealed upregulation of pathways related to DNA damage and repair, PRDX1 role in the maintenance of DNA integrity was investigated. To measure the amount of DSBs in BV173 cells upon IMAT treatment, levels of γH2AX DSB marker have been assessed. It was measured using anti-γH2AX-specific antibodies, with two methods: flow cytometry (Fig. 26A) and immunoblotting (Fig. 26B). The cytometric approach showed an increase in the accumulation of γH2AX in untreated sgPRDX1 compared to control cells, and this effect increased upon IMAT treatment in a dose-dependent manner. As ROS scavengers reversed PRDX1 knockout effects in BV173 cell's growth, their influence on DNA damage markers was also tested. The addition of scavengers caused a lowering of γH2AX levels in sgPRDX1 cells, with restoration to control level in untreated cells. In contrast, the level of γH2AX upon IMAT treatment was still higher in PRDX1 knockout cells even in the presence of ROS scavengers. This observation was independent of IMAT dose, as indicated by the insignificant IMAT-group interaction factor in the 2-way ANOVA analysis. The results obtained with flow cytometry were confirmed with immunoblotting (Fig. 26B), where significantly higher levels of γH2AX in sgPRDX1 cells treated with IMAT were observed, regardless of scavengers' presence.

A

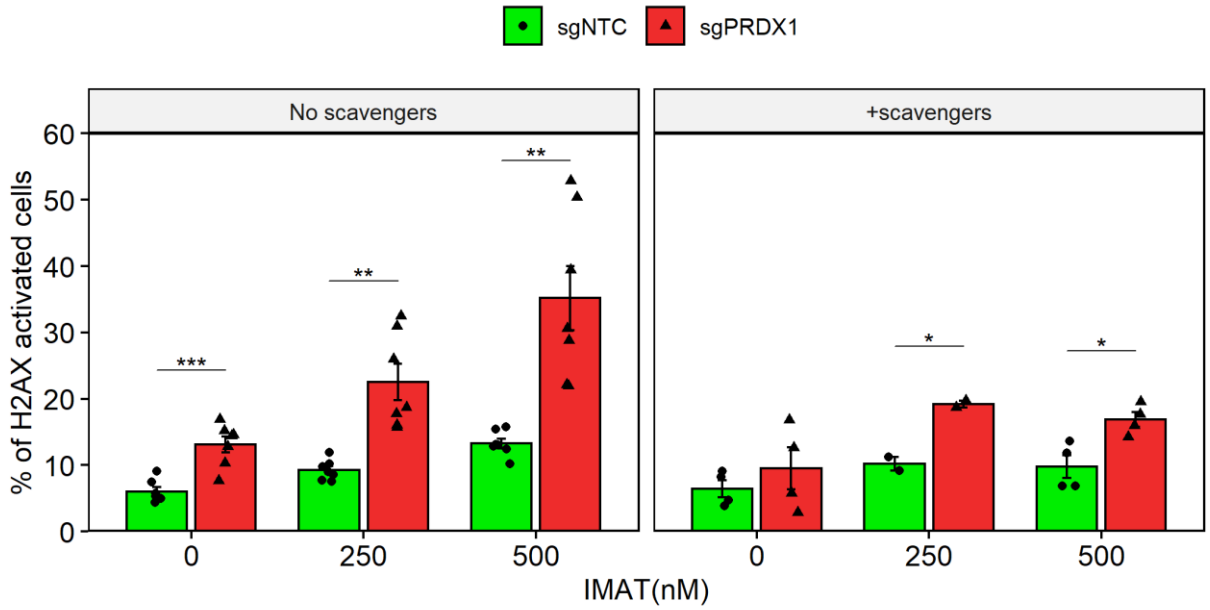

Effect	DFn	DFd	*F*	η_G^2	*p*	Signif.
imat	1	38	30.39	0.52	< .001	***
group	1	38	14.98	0.12	< .001	***
imat:group	1	38	7.78	0.21	.008	**

Effect	DFn	DFd	*F*	η_G^2	*p*	Signif.
imat	1	16	5.41	0.31	.033	*
group	1	16	1.13	0.11	.304	
imat:group	1	16	0.78	0.06	.392	

B

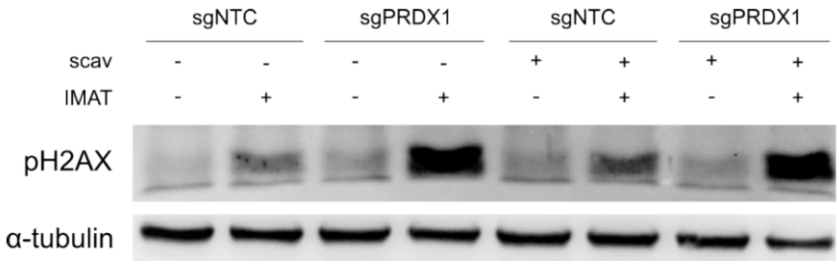

Fig. 26. Effects of PRDX1 knockout on H2AX activation in BV173 cells upon IMAT treatment. Before the assays, BV173 cells were treated with indicated concentrations of IMAT for 24h, with or without the addition of ROS scavengers (50µg/ml catalase, 1mM sodium pyruvate) to cell media. A. Levels of H2AX activation measured using Histone H2A.X Dual Detection Kit (n=4-6). Cells were fixed, permeabilized, and stained according to the manufacturer's protocol and analyzed on MUSE Cell Analyzer, with discrimination of dead cells. Statistical significance was estimated by a White-adjusted 2-way ANOVA (tables below graph) and pairwise t-test with Bonferroni correction (on the graph). Means ± SD are presented. B. Assessment of H2AX activation in BV173 cells by immunoblotting, following 24h treatment with 250nM IMAT, using an antibody specific to p-H2AX. Means ± SD are presented. * p<0.05, ** p<0.01, ***p<0.001, non-significant comparisons not shown on graphs.

A more direct assessment of DSB was also performed utilizing the TUNEL assay (Fig. 27). It is based on the enzymatic addition of BrdUTP nucleotide specifically to the DSBs and its detection with fluorochrome-conjugated antibodies using flow cytometry. It has confirmed previous observations that the levels of DSBs are higher in sgPRDX1 cells. This

effect was dependent on IMAT concentration, as confirmed by a statistically significant IMAT-group interaction factor in the 2-way ANOVA analysis. Also, the addition of scavengers reversed this effect only partially.

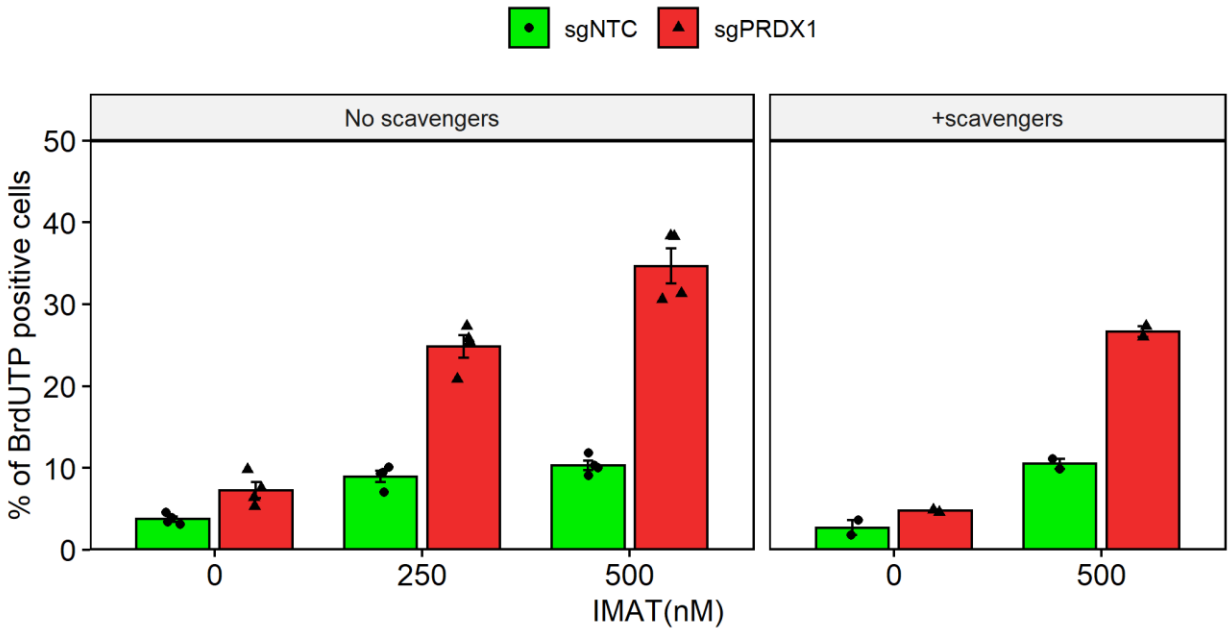

Effect	DFn	DFd	*F*	η_G^2	*p*	Signif.
imat	1	20	131.22	0.88	< .001	***
group	1	20	8.17	0.22	.010	*
imat:group	1	20	49.44	0.74	< .001	***

Fig. 27. The effects of PRDX1 knockout on the levels of DNA double-strand breaks in BV173 cells upon IMAT treatment assessed by TUNEL. Before the assays, BV173 cells were treated with indicated concentrations of IMAT for 24h, with or without the addition of ROS scavengers (50µg/ml catalase, 1mM sodium pyruvate) to cell media. Cells were stained following the manufacturer's protocol and analyzed in flow cytometry (n=2-4). Means ± SD are presented. Statistical significance was estimated by a White-adjusted 2-way ANOVA. Groups with scavengers weren't statistically tested due to low n. * p<0.05, ** p<0.01, ***p<0.001.

As RNAseq analysis revealed upregulation of DDR-related pathways upon IMAT treatment in PRDX1-deficient cells, expression of chosen DDR-related genes (*RAD50, LIG4, XRCC4, PAXIP1* and *BRCA1*) was additionally measured by qPCR in BV173 cells (Fig. 28). *RAD50* is required for forming the MRN complex[261], *LIG4, XRCC4* and *PAXIP1* are important for cNHEJ pathway[262,263], and *BRCA1* is indispensable for HR activity[264]. While the expression of *RAD50, XRCC4* and *PAXIP1* was elevated by PRDX1 knockout alone, 24h IMAT treatment caused

upregulation of all genes in comparison to control, most prominently pronounced in case of *RAD50* and *LIG4*.

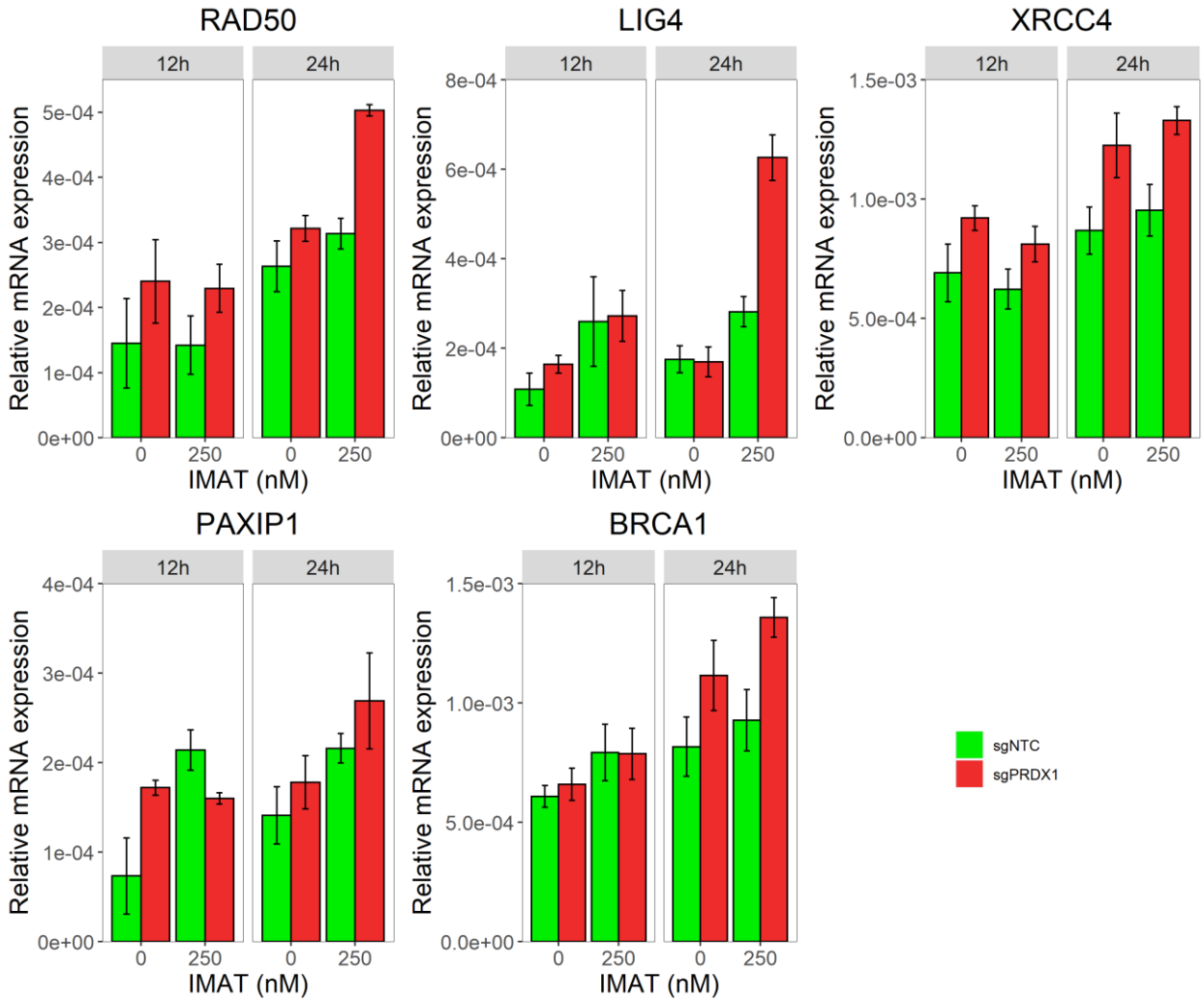

Fig. 28. mRNA levels of genes related to DDR. BV173 sgNTC and sgPRDX1 cells were incubated for 12h or 24h with IMAT, followed by RNA isolation and RT-qPCR. A. Relative mRNA levels in BV173 cells were measured using SybrGreen and RPL29 gene as a reference in two technical repeats. Means + SD are presented.

Taken together, those results clearly show that PRDX1 knockout in BV173 cells causes accumulation of DNA damage, even though RNAseq and qPCR showed the upregulation of DNA damage-related pathways and genes. This indicates that DDR upregulation in PRDX1-deficient cells isn't sufficient to counteract the accumulation of DSB. This uncovers DNA repair as a potential vulnerability in BV173 sgPRDX1 cells, warranting further investigations.

4.6.2. Efficacy of DNA repair inhibitors in PRDX1 knockout lymphoid and myeloid cells

Previous results revealed the upregulation of DNA damage repair elements upon PRDX1 knockout in BV173 cells, including induction of genes related to HR (*BRCA1*) and NHEJ (*LIG4, POLL*) with concomitant accumulation of DNA damage. This indicates the role of PRDX1 in the maintenance of genomic integrity, leading to the hypothesis that PRDX1-deficient cells might be more sensitive to inhibition of DNA repair. To test this, the effectiveness of two NHEJi, NEDI and OLAP was tested in BV173 cells (Fig. 29).

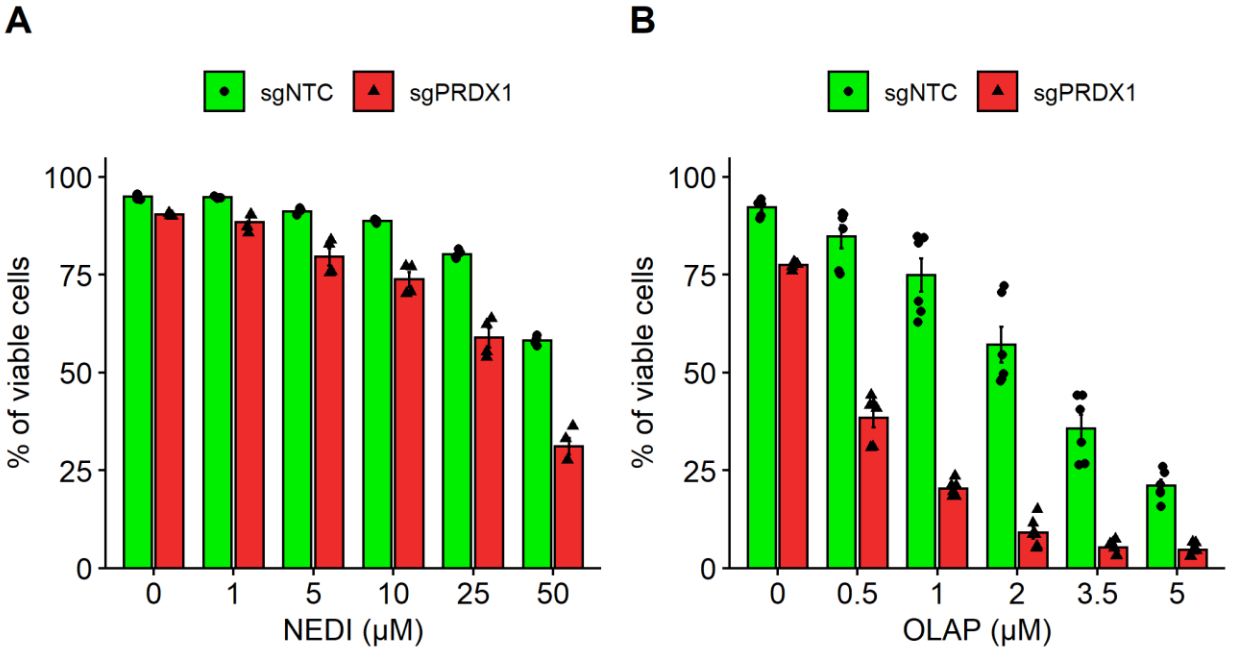

Effect	DFn	DFd	*F*	η_G^2	*p*	Signif.
conc	1	44	1,132.38	0.97	< .001	***
group	1	44	54.71	0.51	< .001	***
conc:group	1	44	58.93	0.63	< .001	***

Effect	DFn	DFd	*F*	η_G^2	*p*	Signif.
conc	1	68	200.45	0.76	< .001	***
group	1	68	51.45	0.53	< .001	***
conc:group	1	68	3.01	0.04	.087	

Fig. 29. Sensitivity of BV173 cells with PRDX1 knockout to NHEJi. BV173 cells viability was assessed after 48h treatment with indicated concentrations of NEDI (panel A; n=4) or OLAP (panel B; n=6) by PI exclusion of dead cells in flow cytometry. Means ± SD are presented. Statistical differences between groups were assessed by a White-adjusted 2-way ANOVA: ***p<0.001.

NEDI inhibits DNA-PKs, therefore blocking cNHEJ, while OLAP is a PARP1 inhibitor, thus blocking altNHEJ. Due to NEDI low cytotoxic effect at the C_{max} (~10μM[201]), concentrations up to 50μM were tested (Fig. 29A). PRDX1 knockout cells exhibited significantly higher sensitivity

to NEDI, especially in its higher tested concentrations. OLAP, on the other hand, effectively killed control cells at much lower concentrations, with only 25% viable sgNTC cells at 1/2 C_{max} (Fig. 29B). Even though OLAP was cytotoxic to control cells, PRDX1 knockout caused a much higher sensitivity to the treatment.

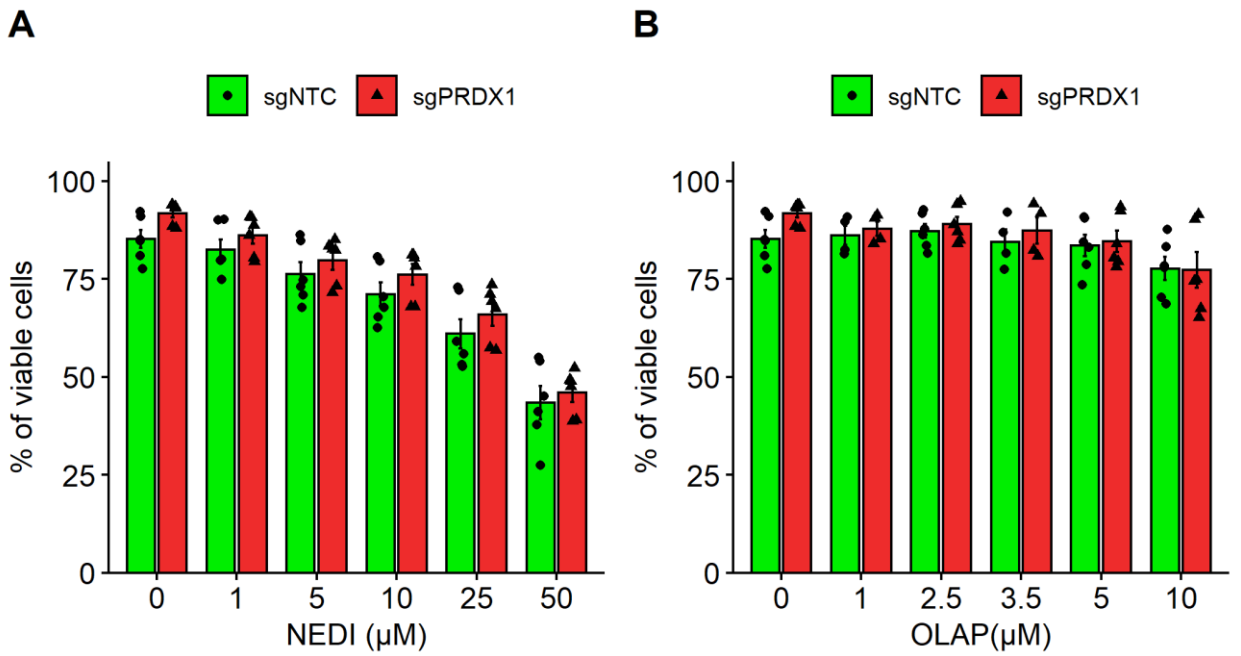

Effect	DFn	DFd	*F*	η_G^2	*p*	Signif.
conc	1	68	226.17	0.82	< .001	***
group	1	68	6.09	0.07	.016	*
conc:group	1	68	0.14	0.00	.713	

Effect	DFn	DFd	*F*	η_G^2	*p*	Signif.
conc	1	60	13.32	0.30	.001	***
group	1	60	4.41	0.06	.040	*
conc:group	1	60	0.73	0.02	.395	

Fig. 30. Sensitivity of K562 cells with PRDX1 knockout to NHEJi. K562 cells viability was assessed after 48h treatment with indicated concentrations of NEDI (panel A; n=6) or OLAP (panel B; n=5) by PI exclusion of nonviable cells in flow cytometry. Means ± SD are presented. Statistical differences between groups were assessed by a White-adjusted 2-way ANOVA: *p<0.05, ***p<0.001.

To check whether the observed effects are specific to lymphoid lineage, the same assay was performed in K562 cells (Fig. 30). Surprisingly, PRDX1 knockout in those cells slightly improved their viability in untreated and treated groups. Even though this observation is statistically significant, the size of the effect was small and almost negligible.

The observed impact of PRDX1 knockout in BV173, but not K562 cells, on sensitivity to NHEJi suggests that PRDX1 plays a much more prominent role in NHEJ maintenance in lymphoid BV173 cells than their myeloid K562 counterpart.

4.6.3. Efficacy of DNA repair inhibitors and IMAT combinations in lymphoid and myeloid cells

Potentiation of NHEJ inhibition effect by PRDX1 knockout in BV173 cells led to a conclusion that inhibition of NHEJ could potentiate the cytotoxicity of the combination of the TXN system inhibitors with TKIs . But first, TKIs and NHEJi interaction had to be tested, to exclude possibility of antagonistic effects.

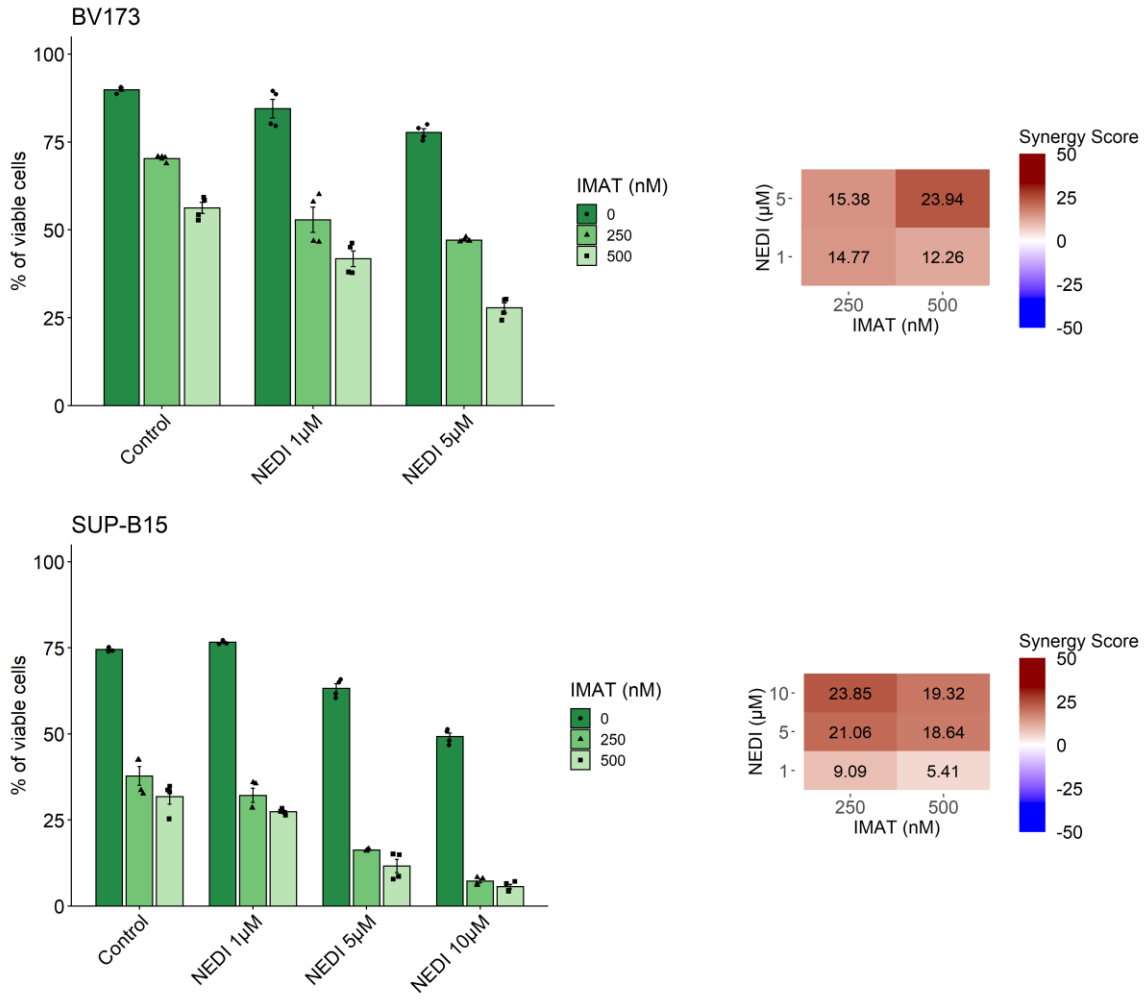

Fig. 31. Cytotoxic effects and synergy assessment of IMAT and NEDI combination in Ph+ lymphoid cells. BV173 and SUP-B15 Ph^+ lymhoid cell lines were treated with IMAT in combination with NEDI (n=4). Cells were incubated with drugs for 48h, and the viability was assessed by the exclusion of dead cells in flow cytometry using PI staining. The synergistic effect was calculated with the SynergyFinder R package[213]. Synergy scores: lower than -10 – antagonism, between -10 and 10 – additive effect, higher than 10 - synergy. Means ± SD are presented.

Therfore, the efficacy of the combination of IMAT and NHEJi in Ph⁺ lymphoid cell lines was tested. Both BV173 and SUP-B15 cells scored similarly in synergy assessment of NEDI and IMAT (Fig. 31), but OLAP potentiated IMAT treatment more in BV173 cells (Fig. 32). This shows a potential for combining NHEJi with IMAT for the treatment of Ph⁺ B-ALL.

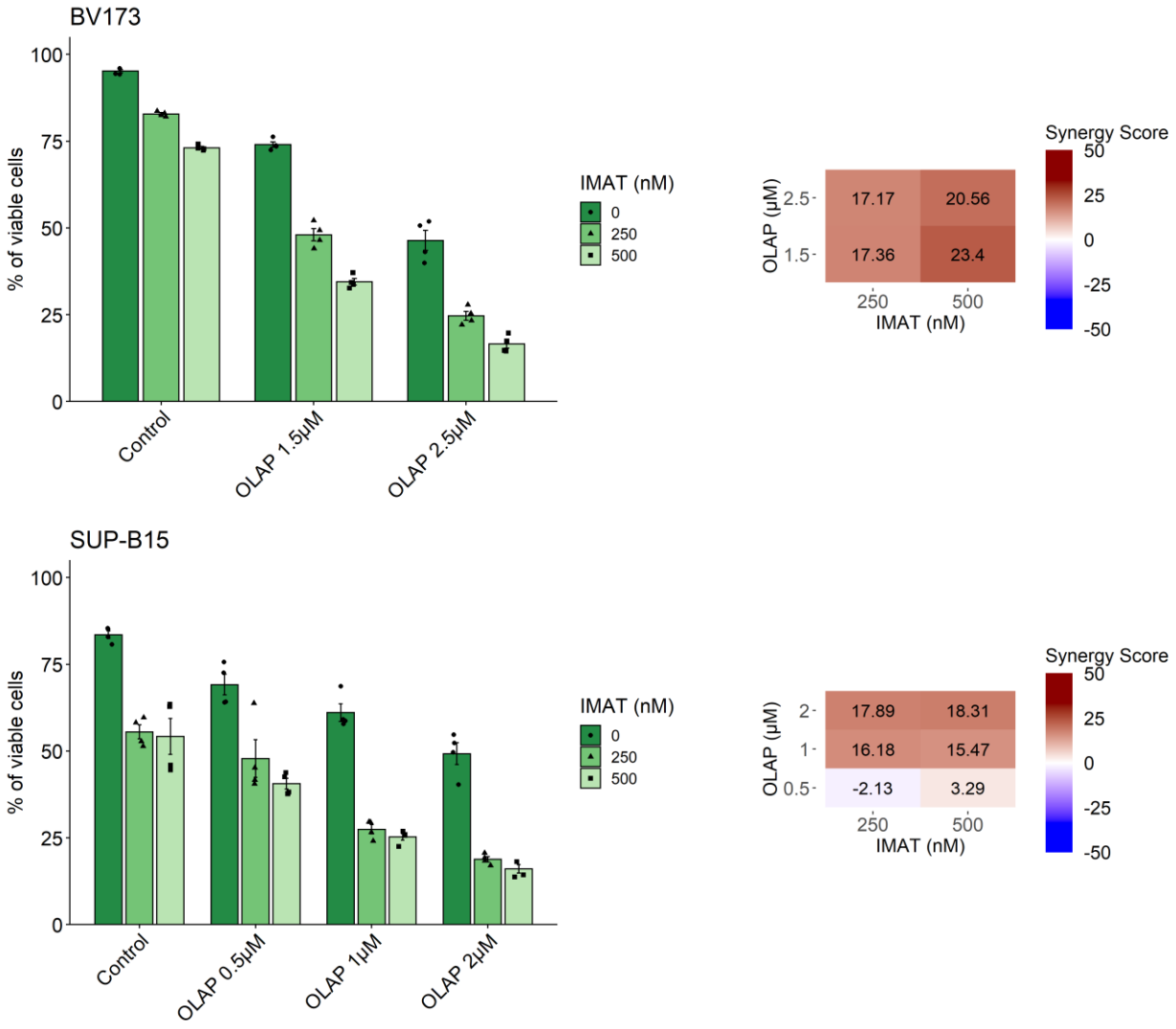

Fig. 32. Cytotoxic effects and synergy assessment of IMAT and OLAP combination in Ph+ lymphoid cells. BV173 and SUP-B15 Ph⁺ lymphoid cell lines were treated with IMAT in combination with OLAP (n=4). Cells were incubated with drugs for 48h, and the viability was assessed by the exclusion of dead cells in flow cytometry using PI staining. The synergistic effect was calculated with the SynergyFinder R package[213]. Synergy scores: lower than -10 – antagonism, between -10 and 10 – additive effect, higher than 10 - synergy. Means ± SD are presented.

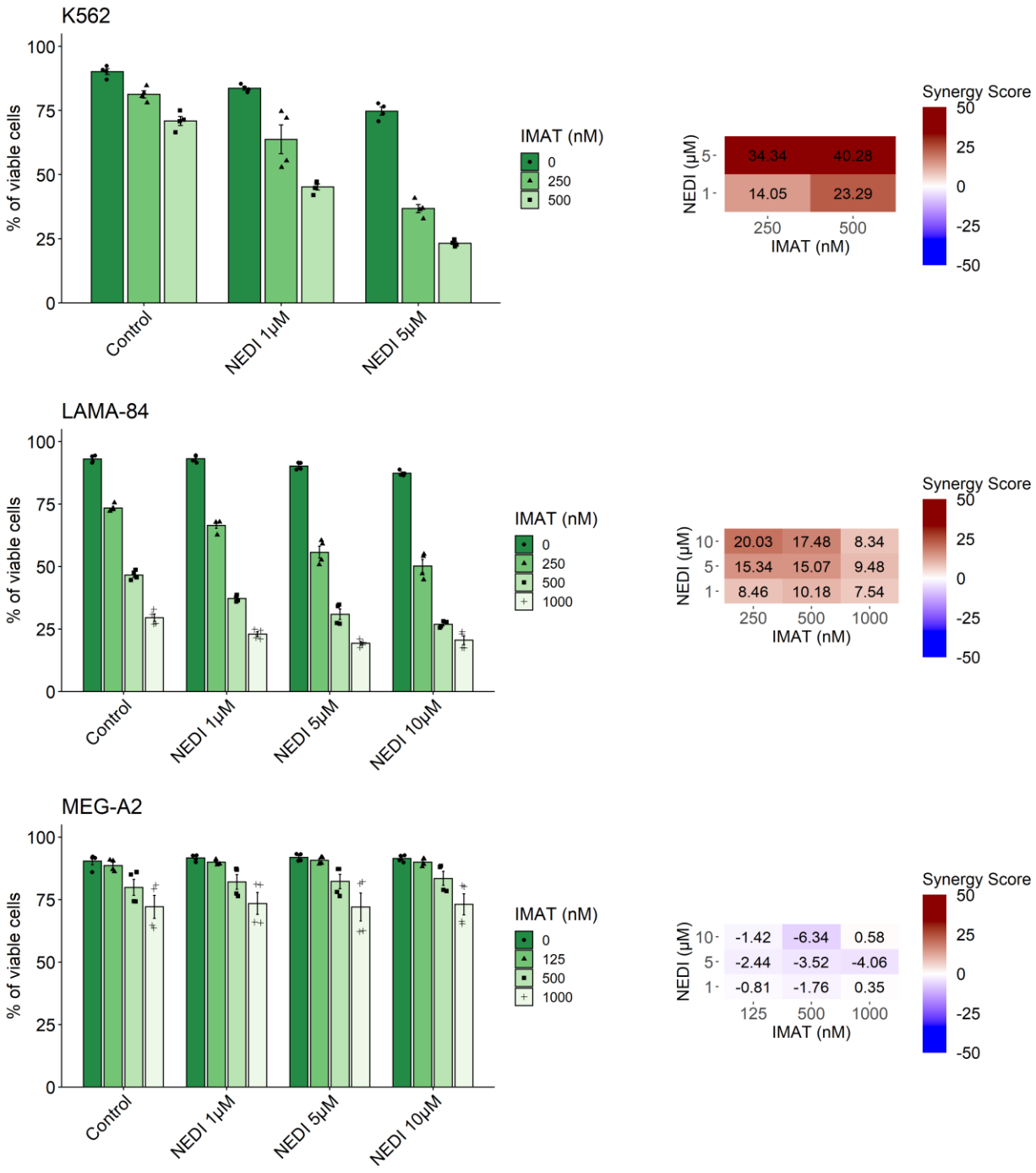

Fig. 33. Cytotoxic effects and synergy assessment of IMAT and NEDI combination in CML cells. K562, LAMA-84, and MEG-A2 CML cell lines were treated with IMAT in combination with NEDI (n=4). Cells were incubated with drugs for 48h, and viability was assessed by the exclusion of dead cells in flow cytometry using PI staining. The synergistic effect was calculated with the SynergyFinder R package[213]. Synergy scores: lower than -10 – antagonism, between -10 and 10 – additive effect, higher than 10 - synergy. Means ± SD are presented.

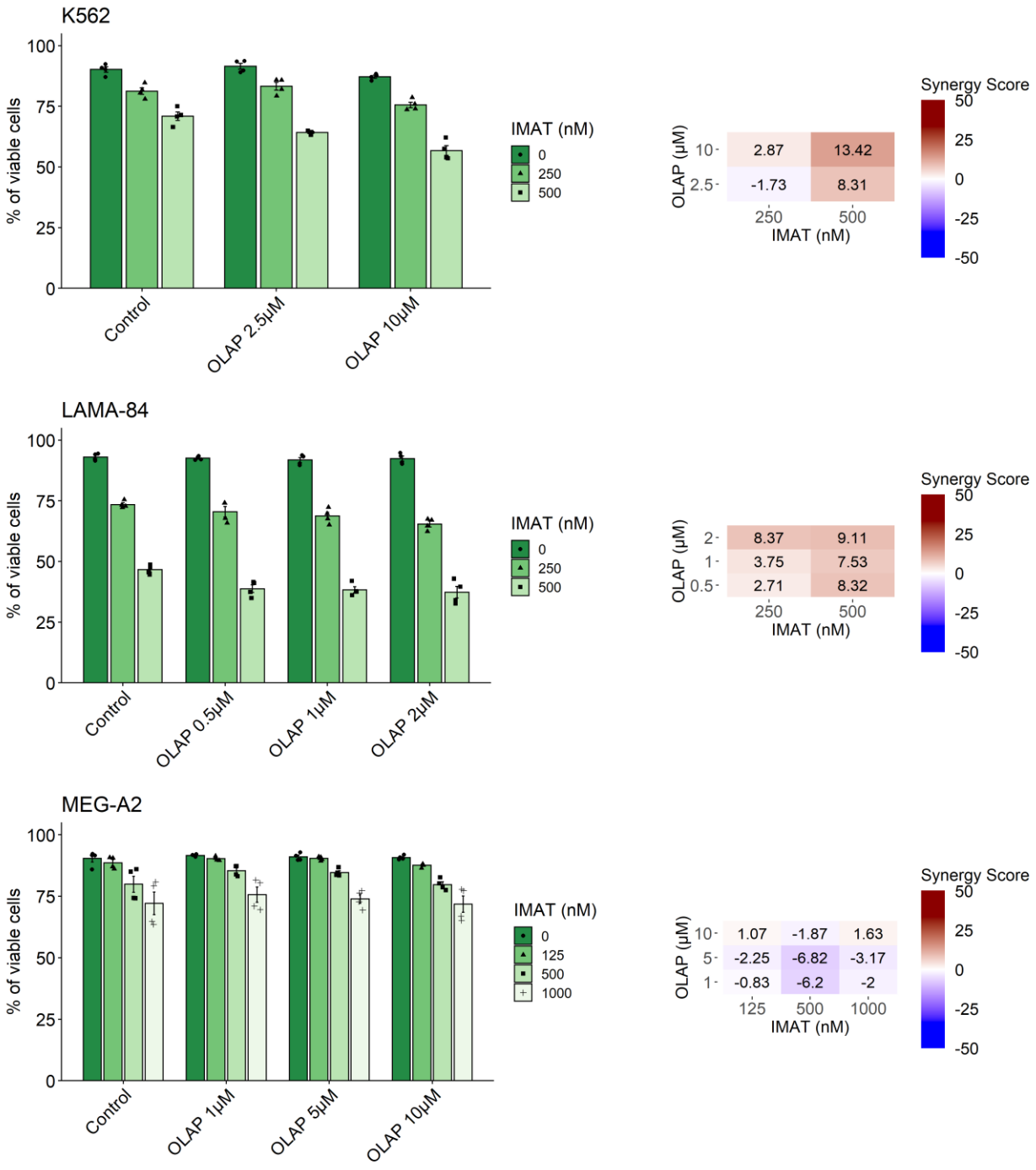

Fig. 34. Cytotoxic effects and synergy assessment of IMAT and OLAP combination in CML cells. K562, LAMA-84, and MEG-A2 CMLS cell lines were treated with IMAT in combination with OLAP (n=4). Cells were incubated with drugs for 48h, and viability was assessed by the exclusion of dead cells in flow cytometry using PI staining. The synergistic effect was calculated with the SynergyFinder R package[213]. Synergy scores: lower than -10 – antagonism, between -10 and 10 – additive effect, higher than 10 - synergy. Means ± SD are presented.

The same assays have been performed in myeloid cells to test the lineage-specificity of those observations. NEDI showed a strong synergistic effect in all tested IMAT concentrations in K562 cells, and a significant synergy was achieved in higher doses of drugs in LAMA-84 cells, while MEG-A2 cells were insensitive to the combination (Fig. 33). OLAP, on the other hand, did not synergize with IMAT, except for a weak interaction in the highest concentrations in K562 cells (Fig. 34).

Those observations suggest that NEDI or OLAP addition to IMAT might be highly beneficial in the lymphoid Ph^+ leukemias. As for myeloid Ph^+ cells, NEDI combination with IMAT might also be favorable in some cases, although inconsistency of the results between cell lines indicate that this effect could vary between cases. Moreover, OLAP didn't significantly potentiate IMAT effects in tested myeloid Ph^+ cell lines, indicating that this approach may have a limited potential.

4.6.4. Comparison of IMAT and NHEJi efficacy in Ph+ lymphoid and myeloid cells with PRDX1 knockout

Previous experiments showed that both PRDX1 knockout and NHEJi seem to sensitize Ph^+ lymphoid cells to IMAT treatment, and PRDX1 knockout alone upregulates pathways related to DNA damage response and repair. This suggests that additional inhibition of DNA repair might further potentiate cell death in PRDX1-deficient cells. The impact of PRDX1 knockout on combination treatment has been tested in BV173 cells (Fig. 35). Knockout of PRDX1 greatly potentiated both combinations' effects, although much greater cytotoxicity was achieved for IMAT and OLAP combination, with almost all cells dead in higher combinations. The same treatment was applied to K562 cells to check whether the observed response is specific to lymphoid cells only. PRDX1 knockout in K562 cells slightly sensitized them to NEDI and IMAT combination, while it did not exert beneficial effects on OLAP and IMAT treatment (Fig. 36).

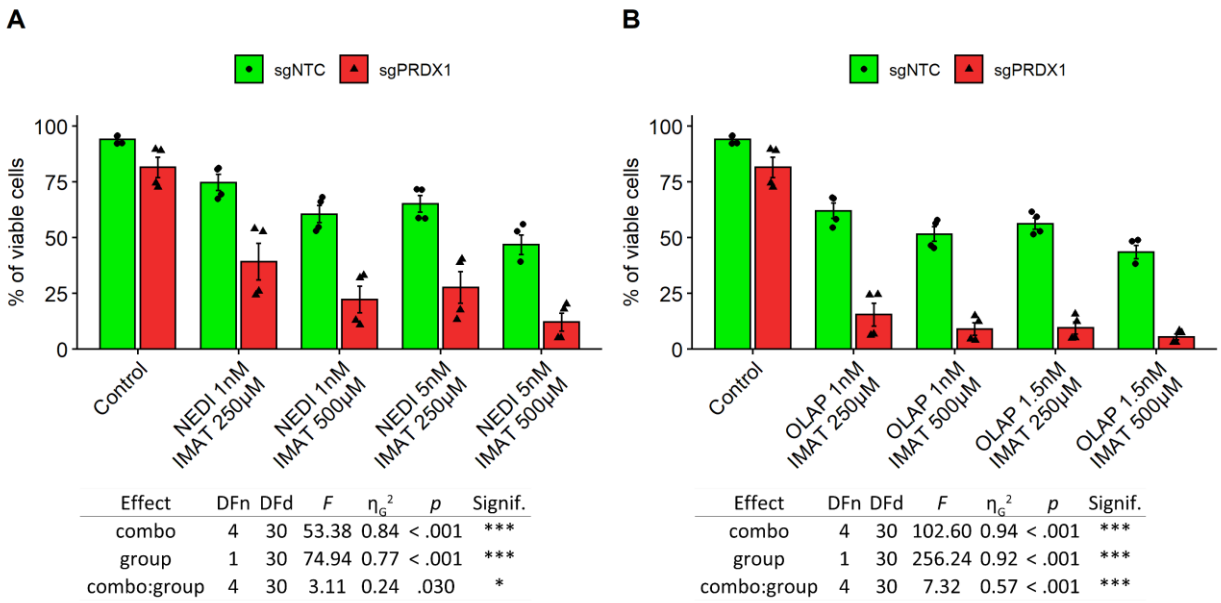

Effect	DFn	DFd	*F*	η_G^2	*p*	Signif.
combo	4	30	53.38	0.84	< .001	***
group	1	30	74.94	0.77	< .001	***
combo:group	4	30	3.11	0.24	.030	*

Effect	DFn	DFd	*F*	η_G^2	*p*	Signif.
combo	4	30	102.60	0.94	< .001	***
group	1	30	256.24	0.92	< .001	***
combo:group	4	30	7.32	0.57	< .001	***

Fig. 35. Cytotoxic effects and synergy assessment of IMAT and NHEJi combination in sgPRDX1 lymphoid cells. BV173 cells' viability was assessed after 48h treatment with indicated concentrations of IMAT in combination with either NEDI (panel A, n=4) or OLAP (panel B, n=4) by PI exclusion of dead cells in flow cytometry. Means ± SD are presented. Statistical differences between groups were assessed by a White-adjusted 2-way ANOVA: *p<0.05, ***p<0.001.

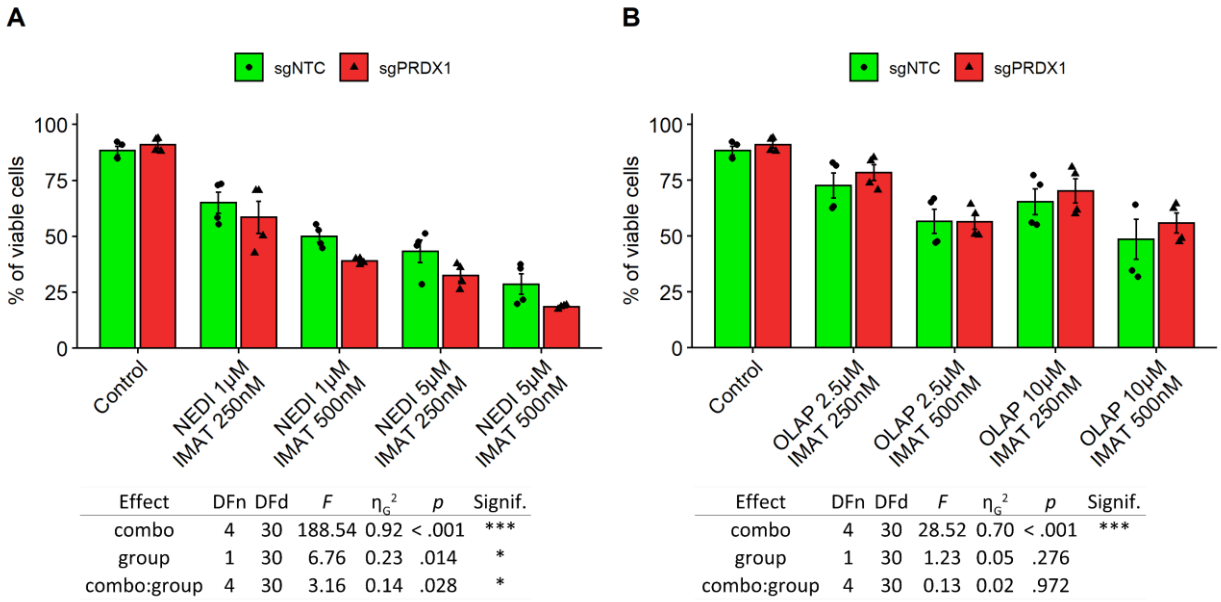

Effect	DFn	DFd	*F*	η_G^2	*p*	Signif.
combo	4	30	188.54	0.92	< .001	***
group	1	30	6.76	0.23	.014	*
combo:group	4	30	3.16	0.14	.028	*

Effect	DFn	DFd	*F*	η_G^2	*p*	Signif.
combo	4	30	28.52	0.70	< .001	***
group	1	30	1.23	0.05	.276	
combo:group	4	30	0.13	0.02	.972	

Fig. 36. Cytotoxic effects and synergy assessment of IMAT and NHEJi combination in sgPRDX1 myeloid cells. K562 cells' viability was assessed after 48h treatment with indicated concentrations of IMAT in combination with either NEDI (panel A, n=4) or OLAP (panel B, n=4) by PI exclusion of dead cells in flow cytometry. Statistical differences between groups were assessed by a White-adjusted 2-way ANOVA: *p<0.05, ***p<0.001.

Those results showed that the inhibition of PRDX1 by genomic knockout potentiated NHEJi and TKIs effect, both in monotherapy and in combination with each other. This fact encouraged development of triple combination assay, using TKIs, NHEJi and AUR in lymphoid Ph^+ cells. As tested myeloid Ph^+ cell lines were insensitive to AUR in high concentrations and PRDX1 knockout did not potentiate their response to separate combination elements, only lymphoid cell lines were tested further.

4.7. Assessment of the efficacy of triple combination comprising AUR, NHEJi, and TKIs in lymphoid Ph+ cells

Previous results led to the hypothesis, that parallel inhibition of BCR-ABL1, NHEJ and TXN system might have beneficial effects in lymphoid Ph^+ leukemias. To test it, two lymphoid Ph^+ cell lines BV173 and SUP-B15, and several patient-derived PDXs were used. Inhibition of BCR-ABL1 was achieved by using either IMAT or DASA, TXN system was targeted with AUR, while cNHEJ or altNHEJ were blocked with either NEDI or OLAP, respectively.

4.7.1. Lymphoid Ph+ cell lines

The efficacy of triple combinations of AUR, NHEJi and TKIs were evaluated in Ph^+ lymphoid cell lines. Firstly, a triple combination of AUR, IMAT, and NEDI was performed. Very strong enhancement of the cytotoxic effects of IMAT and NEDI combinations by the addition of relatively low AUR concentrations was noticeable in BV173 cells, while a weaker but significant impact of AUR addition was observed in SUP-B15 cells (Fig. 37). A combination of IMAT, AUR, and OLAP was also tested (Fig. 38). Again, a significant effect of AUR addition to IMAT and OLAP combinations was uncovered for both cell lines, although overall viability was higher for BV173 as well as SUP-B15 cells than in combinations with NEDI.

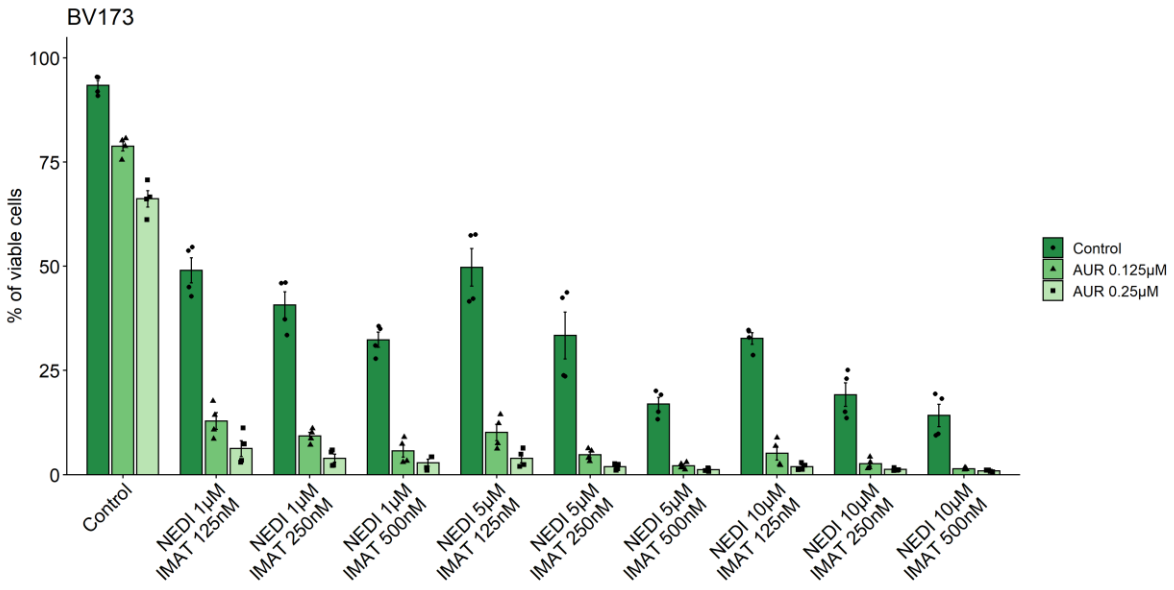

Effect	DFn	DFd	*F*	η_G^2	*p*	Signif.
Conc.	9	90	501.54	0.97	< .001	***
AUR	2	90	303.43	0.93	< .001	***
Conc.:AUR	18	90	8.53	0.65	< .001	***

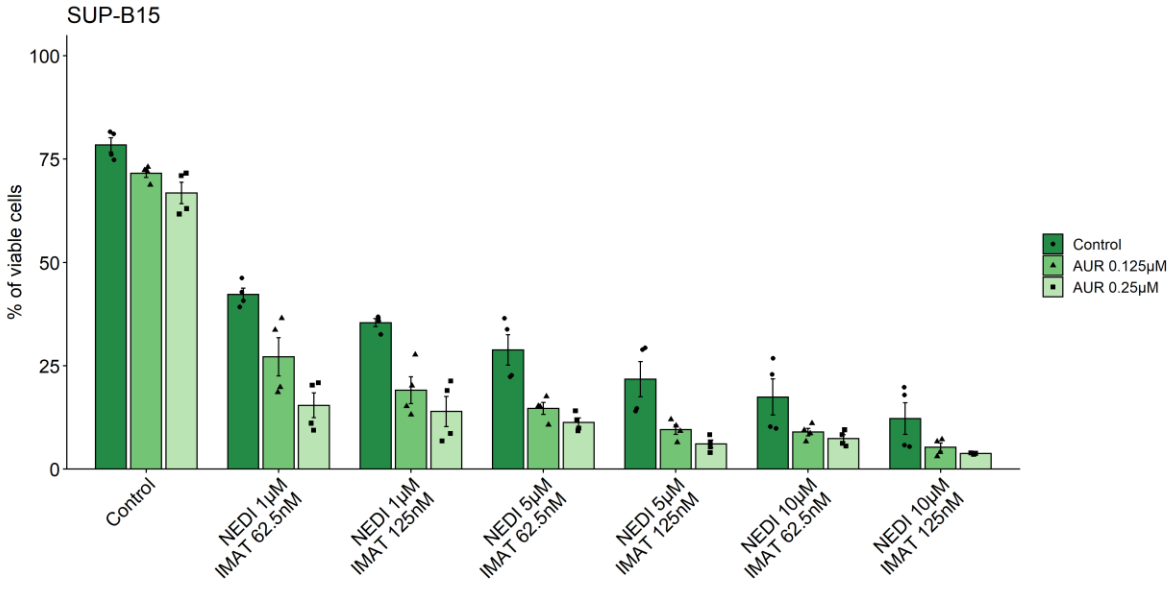

Effect	DFn	DFd	*F*	η_G^2	*p*	Signif.
Conc.	6	63	273.98	0.95	< .001	***
AUR	2	63	45.10	0.69	< .001	***
Conc.:AUR	12	63	1.93	0.25	.047	*

Fig. 37. Triple combination of AUR, IMAT, and NEDI in lymphoid Ph⁺ cell lines. BV173 (n=4) and SUP-B15 (n=4) cells' viability was assessed after 48h treatment with indicated concentrations of drugs combinations in the absence or presence of AUR by PI exclusion of dead cells in flow cytometry. Statistical differences between groups without distinction between AUR concentrations were assessed by a White-adjusted 2-way ANOVA: *p<0.05, ***p<0.001.

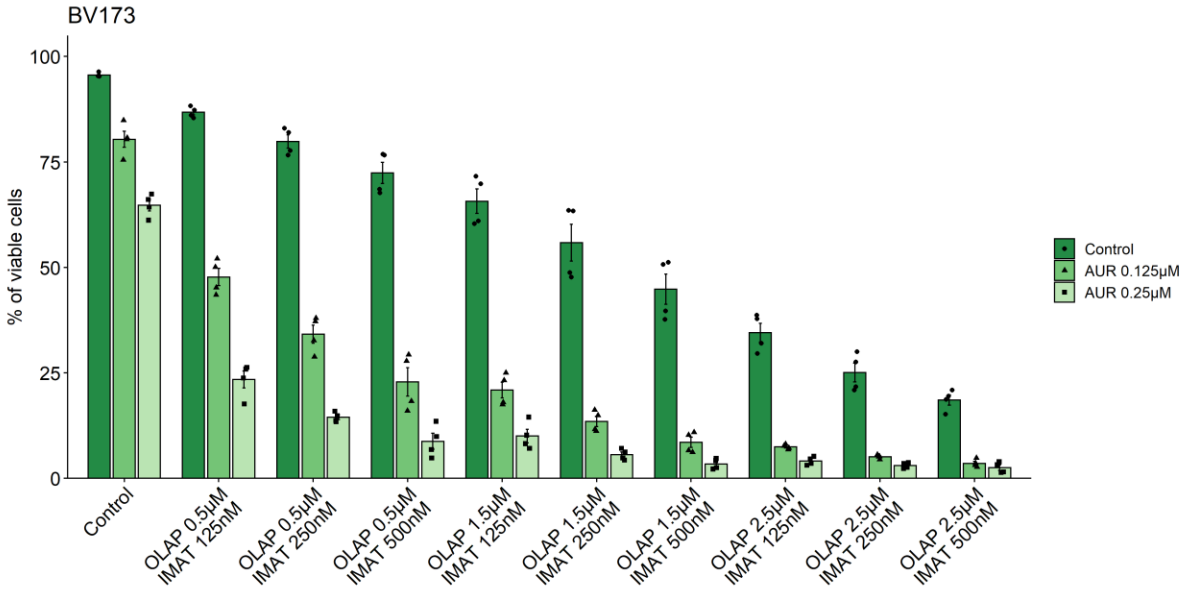

Effect	DFn	DFd	*F*	η_G^2	*p*	Signif.
Conc.	9	90	656.92	0.98	< .001	***
AUR	2	90	969.96	0.97	< .001	***
Conc.:AUR	18	90	42.05	0.84	< .001	***

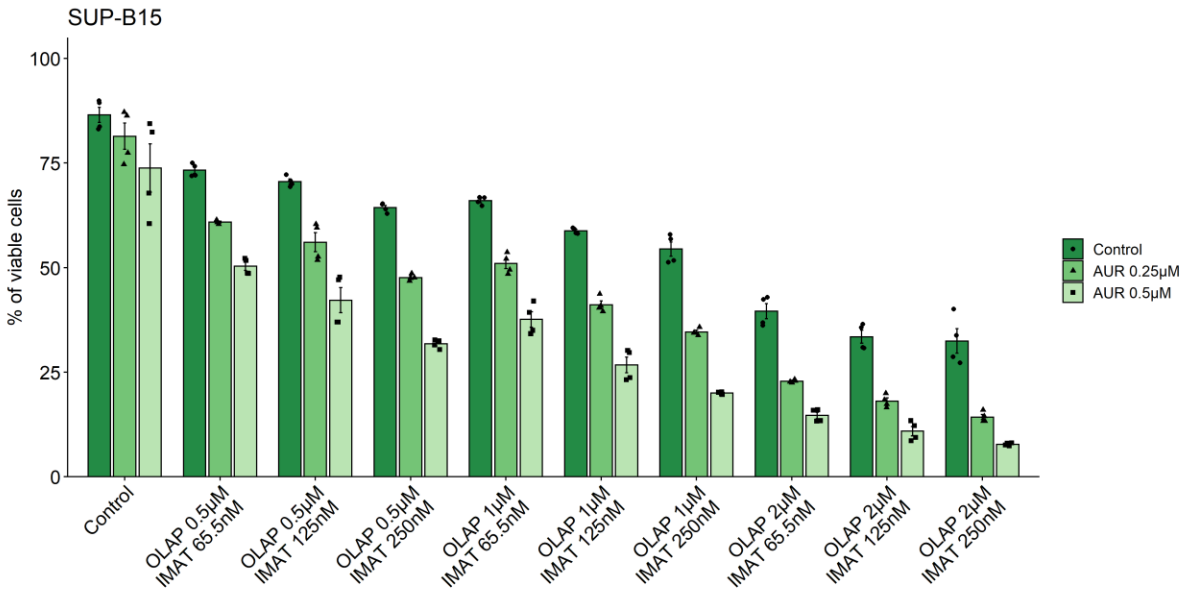

Effect	DFn	DFd	*F*	η_G^2	*p*	Signif.
Conc.	9	90	433.13	0.97	< .001	***
AUR	2	90	412.28	0.93	< .001	***
Conc.:AUR	18	90	10.22	0.43	< .001	***

Fig. 38. Triple combination of AUR, IMAT, and OLAP in lymphoid Ph$^+$ cell lines. BV173 (n=4) and SUP-B15 (n=4) cells' viability was assessed after 48h treatment with indicated concentrations of drugs combinations in the absence or presence of AUR by PI exclusion of dead cells in flow cytometry. Statistical differences between groups without distinction between AUR concentrations were assessed by a White-adjusted 2-way ANOVA: *p<0.05, ***p<0.001.

4.7.2. Lymphoid Ph+ PDXs

The cytotoxic effects of the 72h triple combination comprising AUR, TKIs and NHEJi have been evaluated in patient derived Ph^+ B-ALL PDX cells. For TKIs and NHEJi, concentrations corresponding to C_{max} in patients' serum were used, while a relatively low AUR concentration of 0.25µM was chosen, based on previous studies in B-ALL[74,120]. PDX cells were assigned into two groups, based on their sensitivity to TKIs – TKI sensitive (TKI^{sen}) and TKI resistant (TKI^{res}).

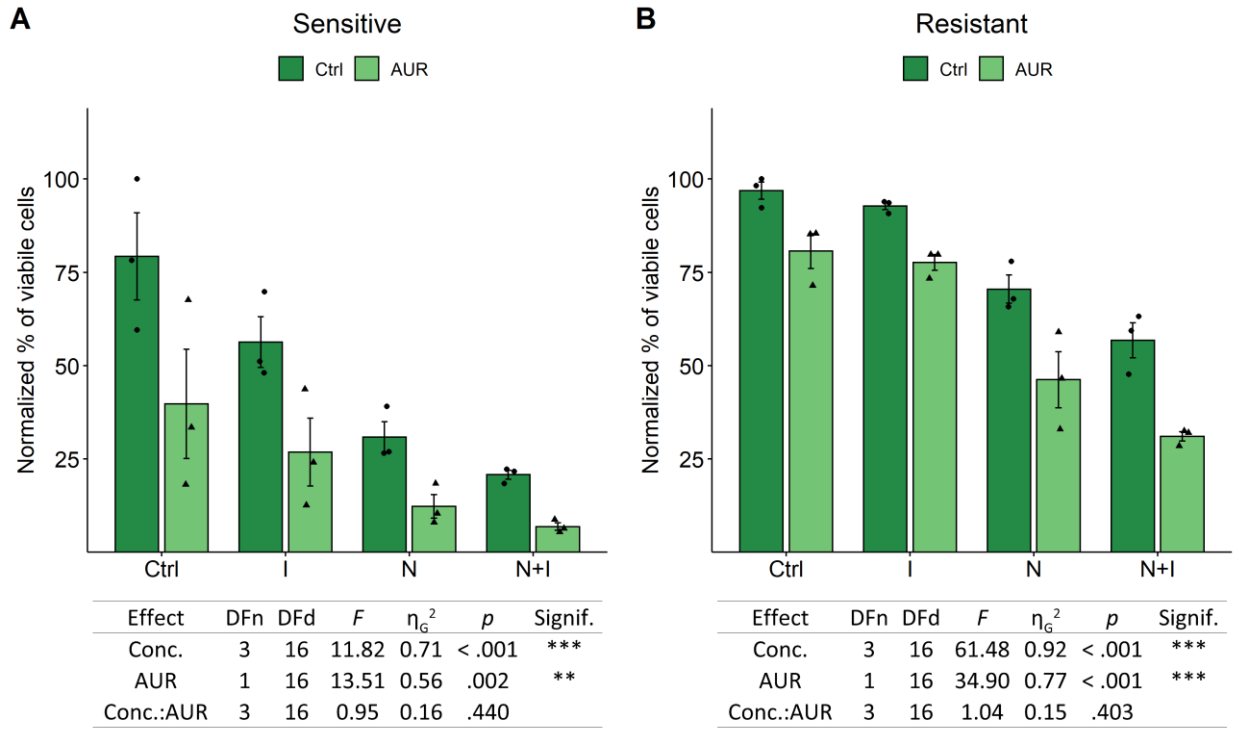

Effect	DFn	DFd	*F*	η_G^2	*p*	Signif.
Conc.	3	16	11.82	0.71	< .001	***
AUR	1	16	13.51	0.56	.002	**
Conc.:AUR	3	16	0.95	0.16	.440	

Effect	DFn	DFd	*F*	η_G^2	*p*	Signif.
Conc.	3	16	61.48	0.92	< .001	***
AUR	1	16	34.90	0.77	< .001	***
Conc.:AUR	3	16	1.04	0.15	.403	

Fig. 39. Triple combination of AUR, IMAT, and NEDI in Ph^+ PDX cells. PDXs were grouped according to their sensitivity to IMAT (panel A – sensitive, n=3; panel B – resistant, n=3), and their viability was assessed after 72h treatment with 8µM IMAT (I) in combination with 10µM NEDI (N) in the absence or presence of 0.25µM AUR by PI exclusion of dead cells in flow cytometry. Each point on the plot represents the mean of two independent measurements of an individual PDX sample. Viability of PDXs was normalized to PDX with highest % of viable cells in the control group, separately for TKI^{sen} and TKI^{res} PDXs. Means ± SD are presented. Statistical differences between groups were assessed by a White-adjusted 2-way ANOVA: ***p<0.001.

First, the cytotoxic effect of NEDI, IMAT, and AUR was assessed (Fig. 39). For TKI^{sen} samples (Fig. 39A), sensitivity to AUR only was very different among PDXs. Moreover, NEDI alone did eradicate ~50% of cells in all samples, while the addition of IMAT only improved that effect marginally. AUR decreased viability in all groups, with the most killed cells in the

group treated with all three drugs. Results for TKI^{res} samples (Fig. 39B) were very similar to the TKI^{sen} group, although overall cell viability in all of the groups was noticeably higher, even in triple combinations. Also, response to all drugs and combinations was consistent across different PDXs. A similar test was performed, using DASA instead of IMAT (Fig. 40), and the results were very similar as for IMAT.

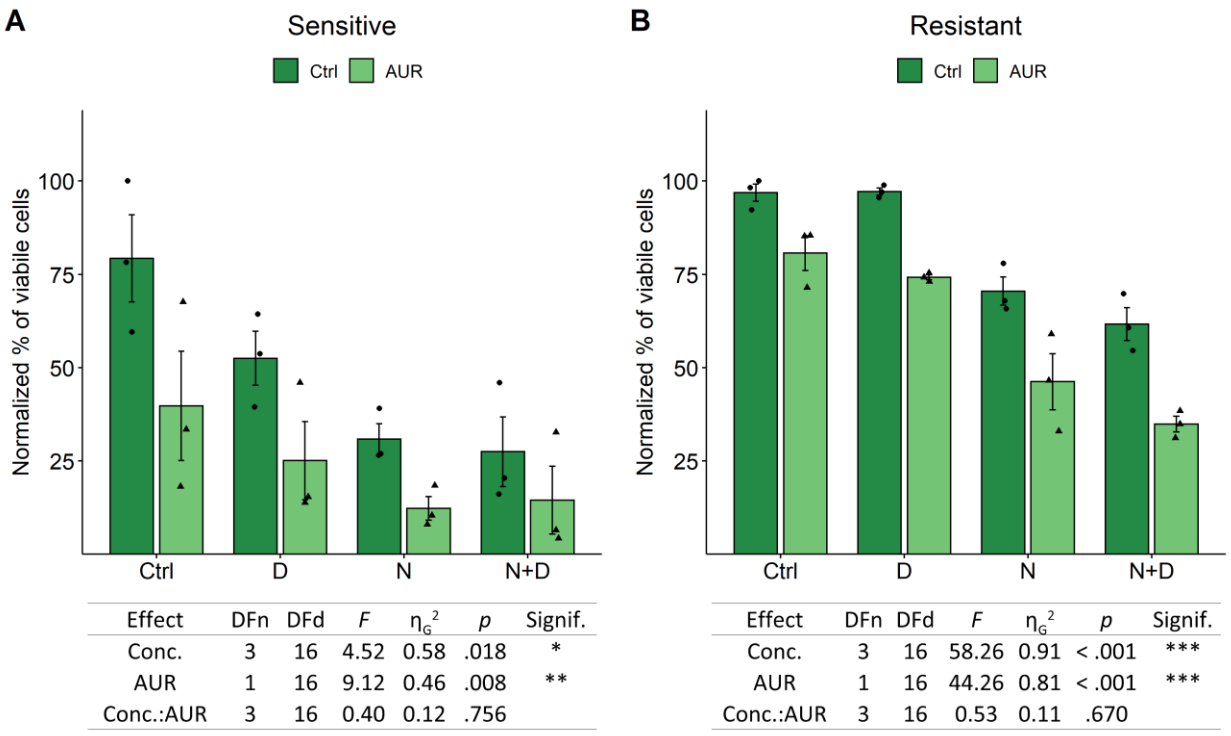

Effect	DFn	DFd	*F*	η_G^2	*p*	Signif.
Conc.	3	16	4.52	0.58	.018	*
AUR	1	16	9.12	0.46	.008	**
Conc.:AUR	3	16	0.40	0.12	.756	

Effect	DFn	DFd	*F*	η_G^2	*p*	Signif.
Conc.	3	16	58.26	0.91	< .001	***
AUR	1	16	44.26	0.81	< .001	***
Conc.:AUR	3	16	0.53	0.11	.670	

Fig. 40. Triple combination of AUR, DASA, and NEDI in Ph$^+$ PDX cells. PDXs were grouped according to their sensitivity to DASA (panel A – sensitive, n=3; panel B – resistant, n=3), and their viability was assessed after 72h treatment with 160nM DASA (D) in combination with 10µM NEDI (N) in the absence or presence of 0.25µM AUR by PI exclusion of dead cells in flow cytometry. Each point on the plot represents the mean of two independent measurements of an individual PDX sample. Viability of PDXs was normalized to PDX with highest % of viable cells in the control group. Normalization was performed for sensitive and insensitive cells separately. Means ± SD are presented. Statistical differences between groups were assessed by a White-adjusted 2-way ANOVA: ***p<0.001.

In the next tests, OLAP was used with AUR and TKIs. All PDXs were resistant to OLAP treatment, regardless of their sensitivity to TKIs, and its addition to groups treated with either IMAT or IMAT and AUR didn't decrease cells' viability (Fig. 41). The same results were obtained for combinations with DASA (Fig. 42). AUR addition to OLAP alone, or in combination

with IMAT, didn't show significant synergistic effect, as it exerted similar effect as in combination with IMAT only.

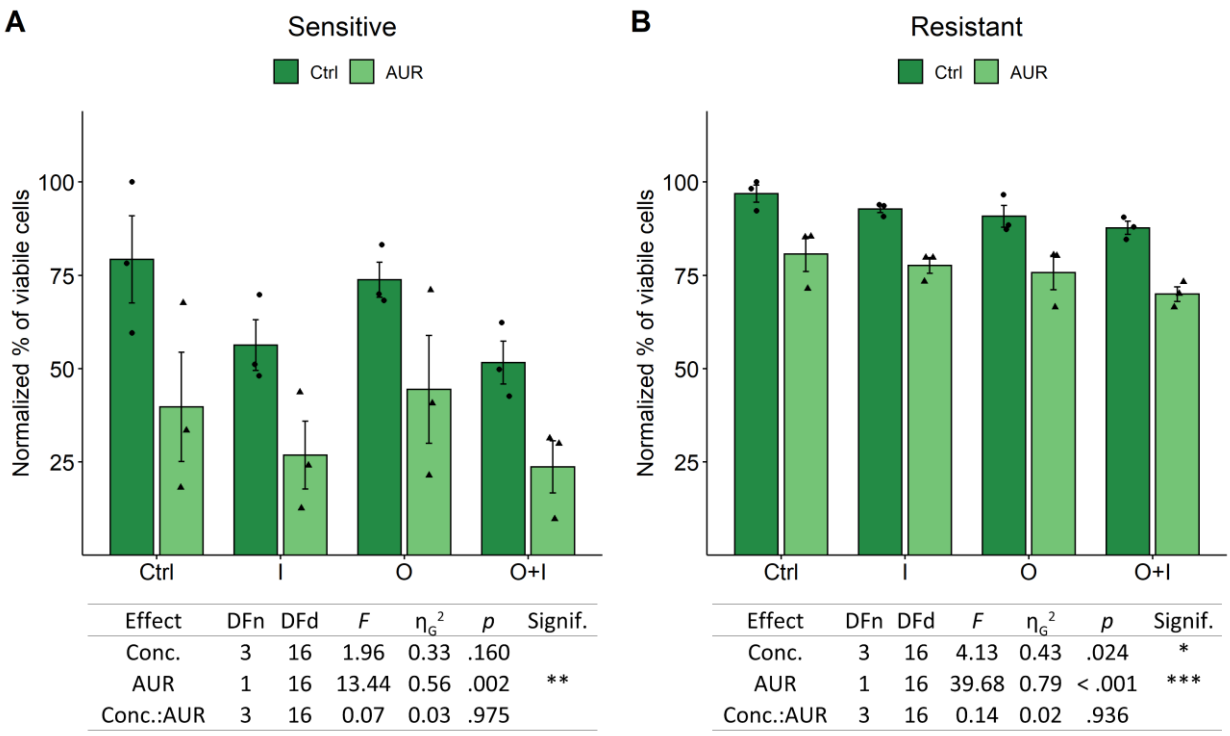

Effect	DFn	DFd	*F*	η_G^2	*p*	Signif.
Conc.	3	16	1.96	0.33	.160	
AUR	1	16	13.44	0.56	.002	**
Conc.:AUR	3	16	0.07	0.03	.975	

Effect	DFn	DFd	*F*	η_G^2	*p*	Signif.
Conc.	3	16	4.13	0.43	.024	*
AUR	1	16	39.68	0.79	< .001	***
Conc.:AUR	3	16	0.14	0.02	.936	

Fig. 41. Triple combination of AUR, IMAT, and OLAP in primary Ph$^+$ PDX cells. PDXs were grouped according to their sensitivity to IMAT (panel A – sensitive, n=3; panel B – resistant, n=3), and their viability was assessed after 72h treatment with 8µM IMAT (I) in combination with 5µM OLAP (O) in the absence or presence of 0.25µM AUR by PI exclusion of dead cells in flow cytometry. Each point on the plot represents the mean of two independent measurements of an individual PDX sample. Viability of PDXs was normalized to PDX with highest % of viable cells in the control group. Normalization was performed for sensitive and insensitive cells separately. Means ± SD are presented. Statistical differences between groups were assessed by a White-adjusted 2-way ANOVA: ***p<0.001.

Those results show the beneficial effect of pharmacological cNHEJ inhibition by NEDI in addition to TKIs and AUR combinations in both Ph$^+$ lymphoid cell lines and patient-derived PDXs. This reveals a potential of NEDI, TKIs, and AUR triple combinations for further pre-clinical research in the context of Ph$^+$ B-ALL. As for OLAP, while it potentiated cell death alone and in combination with TKIs and AUR in Ph$^+$ lymphoid cell lines, it showed no effect in PDX samples in a three-day assay.

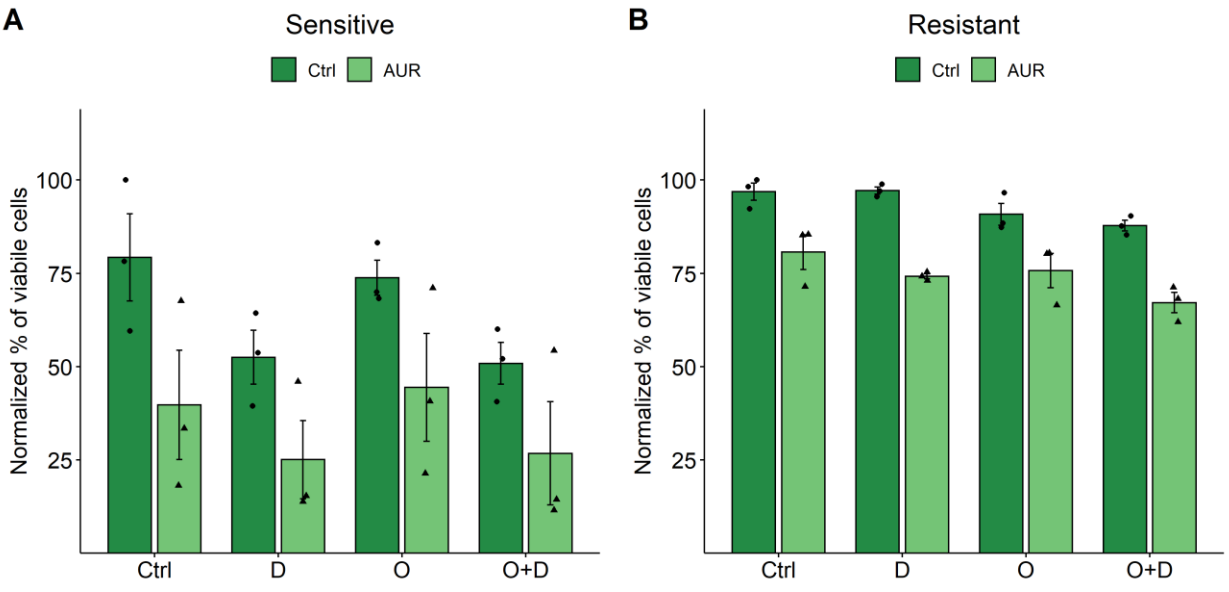

Effect	DFn	DFd	*F*	η_G^2	*p*	Signif.
Conc.	3	16	1.60	0.30	.230	
AUR	1	16	10.01	0.48	.006	**
Conc.:AUR	3	16	0.10	0.03	.961	

Effect	DFn	DFd	*F*	η_G^2	*p*	Signif.
Conc.	3	16	6.09	0.50	.006	**
AUR	1	16	55.18	0.84	< .001	***
Conc.:AUR	3	16	0.83	0.13	.497	

Fig. 42. Triple combination of AUR, DASA, and OLAP in primary Ph$^+$ PDX cells. PDXs were grouped according to their sensitivity to DASA (panel A – sensitive, n=3; panel B – resistant, n=3), and their viability was assessed after 72h treatment with 160nM DASA (D) in combination with 5μM OLAP (O) in the absence or presence of 0.25μM AUR by PI exclusion of dead cells in flow cytometry. Each point on the plot represents the mean of two independent measurements of an individual PDX sample. Viability of PDXs was normalized to PDX with highest % of viable cells in the control group. Normalization was performed for sensitive and insensitive cells separately. Means ± SD are presented. Statistical differences between groups were assessed by a White-adjusted 2-way ANOVA: ***p<0.001.

5. Discussion

Even though Ph+ B-ALL patients' prognosis has been vastly improved upon the introduction of TKIs to therapy, still a significant fraction of patients does not respond to treatment or relapses, worsening disease outcome in both children and adults [57]. To address this issue, multiple pre-clinical and clinical studies, aimed at the maximization of Ph+ B-ALL therapy outcomes with minimal side effects, are ongoing[30]. Tested approaches include combinations of clinically-approved TKIs with other therapies used in ALL, such as intensive chemotherapy (NCT05026229), or immunotherapy (NCT04722848)[69,70]. ASCI, a TKI with a novel allosteric mechanism of action is also being investigated in Ph+ B-ALL in either monotherapy or in combination with other TKIs, such as IMAT or DASA (NCT03595917, NCT02081378). Combination of blinatumomab with PONA is also tested in a phase III study (NCT04722848).

In the preclinical research, novel potential targets in Ph+ B-ALL are also seeked. One of proposed strategies is targeting DDR with OLAP in Ph+ B-ALL, exhibiting significant synergistic effect with IMAT[170]. Inhibition of TXN system was also shown to be efficient in B-ALL, including the Ph+ B-ALL subtype[74]. Another approach is targeting PKC with phospholipid conjugate of gemcitabine, showing promising selective effects in mice bearing Ph+ B-ALL cell lines[265].Even though some preclinical and preliminary results are promising, emerging therapy resistance warrants the need for a better understanding of Ph+ B-ALL biology and pathogenesis. This knowledge may allow for the identification of its specific vulnerabilities and may lead to the development of novel, targeted combination therapies with better efficacy and selectivity.

As Ph+ B-ALL patients respond much worse to TKIs treatment than those suffering from CML in CP[56], the main goal of this study was to propose a novel approach, allowing for a potential improvement of Ph+ B-ALL therapeutic outcomes in the future. Because the inhibition of the TXN system was shown to be beneficial in other B cell malignancies[74,74,120], it was initially selected as a promising target. Further investigation utilizing PRDX1-defiecent cell line models revealed NHEJ as the next pathway with prominent role in lymphoid Ph+ cells.

Taken together, these discoveries led to formulation of potentially beneficial triple combination targeting TXN system, BCR-ABL1 and NHEJ, the efficacy of which was confirmed in patient derived Ph^+ B-ALL PDXs.

5.1. Specific role of the TXN system in lymphoid Ph^+ leukemias

To counteract the effects of elevated OxS, cancer cells increase the activity of the antioxidant systems, mainly the GSH and TXN systems[98,99]. Increased expression of the TXN system elements were identified in lymphoid malignancies, including B-ALL[77,100], although a Ph^+ B-ALL subtype wasn't investigated in this context. The rationale for studying the TXN system in Ph^+ B-ALL was also provided by the analysis of a publicly available gene set, showing gene expression changes in pre-B cell line upon induction of BCR-ABL1 expression, which revealed tendency for downregulation of GSH-related genes, and a concomitant elevation of *PRDX1, TXN1* and *TXN-R1* (Table 7). This suggested that Ph^+ B cells may rely on the TXN1 system for the maintenance of redox homeostasis, with less significant role of the GSH system.

Considering the beforementioned points, the effects of the TXN system inhibition on the cytotoxicity of TKIs was tested in myeloid and lymphoid Ph^+ cell lines. Two TXN system inhibitors, AUR (targeting TXN-R1/2[266]) and ADE (inhibiting TXN-R, TXN, PRDX1/2[125,267]) were used. Inhibition of the TXN system alone or in combination with either IMAT or DASA, had significant cytotoxic effects mainly in Ph+ lymphoid cells (Figs. 3-6). Even though the cytotoxic effects of the TXN system inhibition were previously reported in other cancers including B-ALL, the synergistic effect between TKIs and the TXN system inhibitors in Ph^+ B-ALL is a novel discovery. Interestingly, the tested myeloid Ph^+ cell lines were insensitive to both AUR and ADE, less pronounced role of TXN system in cells of that lineage.

5.2. Role of PRDX1 in proliferation, survival, and drug sensitivity of lymphoid Ph+ cells

Moreover, in this study, the upregulation of PRDX1 in Ph^+ B-ALL was revealed, both at the protein (Fig. 7) and the mRNA levels (Fig. 8) in cell lines and primary material, respectively. As the mechanism of action of neither AUR nor ADE is specific for PRDX1, to investigate the role of PRDX1 in lymphoid and myeloid Ph^+ cells, two CRISPR-Cas9-mediated PRDX1 knockout

cell lines – K562 (CML) and BV173 (CML in LBC) - were generated. Similarly to the TXN system, PRDX1 was revealed to be crucial for lymphoid, but not myeloid, cells survival (Fig. 10) and sensitivity to TKIs (Figs. 11-13). PRDX1 knockout in lymphoid Ph^+ cells also potentiated IMAT-induced apoptotic signaling (Fig. 14). The most noticeable changes upon PRDX1 knockout were JNK and BIM overactivation with parallel BCL-W downregulation in PRDX1-deficient cells. This effect of the PRDX1 knockout in Ph^+ lymphoid cells could be explained by its known role in the protection of malignant cells from death through such mechanisms as activation of NF-κB[112] or preventing stress-mediated apoptosis dependent on JNK activation[107]. Moreover, BCL-W is also a known inhibitor of JNK[268], so its downregulation further overactivated JNK signaling.

5.3. Elucidation of the mechanisms of cell death induced by IMAT in PRDX1-deficientPh+ lymphoid cells

To elucidate the mechanisms of cell death triggered by IMAT in PRDX1-deficient Ph^+ lymphoid cells, an unbiased, RNAseq-based approach was employed. In IMAT-untreated cells, the PRDX1 knockout caused downregulation of several genes involved in the processes supporting malignant cells' survival and proliferation, including (1) the maintenance of DNA integrity (*SAMHD1*[224]), (2) TKI resistance (*CASD1*[219], *SPARC*[225]) or (3) survival promotion (*ANXA5*[231,232]). Also two tumor suppressors genes, *LRRC26* and *SRCIN1*[234,235], were upregulated (Table 8). This changes in gene expression could explain worse overall state and higher sensitivity to TKIs of PRDX1 knockout BV173 cells. Moreover, further analysis of changes in IMAT-induced signaling upon PRDX1 knockout was performed by a GSEA analysis, comparing activity of pathways in IMAT-treated control and PRDX1 knockout cells. GSEA revealed prominent early downregulation of several pathways linked to processes crucial for proper cell functions, such as oxidative phosphorylation, regulation of translation (Fig. 17), and later strong upregulation of pathways involved in apoptotic signal transduction and apoptosis (Fig. 18). Additionally, some changes were identified in UPR and OxS-induced pathways. Even though the observed UPR and OxS upregulation in PRDX1-deficient cells is in line with the well-known PRDX1 functions[108–110], the upregulation of UPR-related genes *ATF4* and *CHOP*, ROS, and OxS markers were not confirmed in the subsequent experiments (Figs.

19-22). Despite that, reconstitution of the catalytically active PRDX1, but not inactivated mutants, in PRDX1 knockout BV173 cells reversed the IMAT-sensitive phenotype (Fig. 24). Moreover, removal of ROS from the IMAT-treated cells through the addition of ROS scavengers partially reversed IMAT cytotoxic effect in both control and PRDX1 knockout cells alike, although significant viability differences between cell lines were still present (Fig. 25). This indicates that PRDX1 catalytic function is involved in lymphoid Ph^+ cells response to IMAT, although it is not exclusively responsible for IMAT sensitivity of the PRDX1-deficient cells, suggesting additional PRDX1's role in those cells.

5.4. Increased levels of DNA DSB upon PRDX1 knockout BV173 cells upon IMAT treatment

As neither UPR nor OxS were identified major factors responsible for the sensitization of PRDX1-deficient Ph^+ lymphoid cells to TKIs, the exact mechanism of observed PRDX1 knockout effect was still elusive. GSEA revealed upregulation of DDR-related pathways in PRDX1 deficient cells upon IMAT-treatment, possibly due to the accumulation of DNA lesions. Indeed, assessment of the DSB in IMAT-treated, PRDX1-defiecient cells revealed accumulation of DNA lesions in those cells in comparison to control ones, as shown by γH2AX levels (Fig. 26) and TUNEL assay (Fig. 27). A parallel increased mRNA levels of both HR and cNHEJ elements were also observed in PRDX1 knockout cell subjected to IMAT (Fig. 28), suggesting that upregulation of DDR wasn't sufficient to repair IMAT-induced DNA damage. Moreover, PRDX1 knockout caused significant sensitization to inhibitors of either cNHEJ or altNHEJ in a lymphoid-specific manner, as this effect was observed only in BV173 cells, while K562 weren't affected by PRDX1 knockout (Fig. 29 and Fig. 30). This led to a hypothesis that inhibition of DSB repair in PRDX1-deficient BV173 cells could exert further potentiate imatinib cytotoxicity.

5.5. Sensitization of lymphoid Ph+ cells to IMAT by inhibition of NHEJ

More effective NHEJ inhibition in cells with PRDX1 knockout provided rationale for the addition of NHEJi to TKIs and AUR combination. Before that, interaction of TKIs and NHEJi had to be investigated. Although synergistic effects of OLAP and TKIs were observed previously[170],

the referenced study was more focused on myeloid malignancies, and not many Ph$^+$ B-ALL samples were tested and no DNA-PKcs inhibitors were investigated. To test the proof of concept of targeting NHEJ in Ph+ B-ALL, the efficacy of inhibitors of cNHEJ (NEDI) and altNHEJ (OLAP) in combination with IMAT was tested in both myeloid and lymphoid Ph$^+$ cell lines. More consistent synergism of NHEJ inhibitors was observed in lymphoid cells. These results may be explained by the previously shown upregulation of NHEJ elements in all tested B-ALL patients[166,182]. This indicates that NHEJ may be a crucial DSB repair pathway in lymphoid malignancies, making them susceptible to its inhibition. On the other hand, inK562 myeloid cell line a very strong synergistic effect of NEDI and IMAT was identified (Figs. 31-34). K562 cell line was shown to exhibit impaired end joining activity[269,270], possibly making it susceptible to further NHEJ inhibition. Surprisingly, low synergistic effects of OLAP and IMAT in K562 cells are in opposition to the results of previously shown potentiation of IMAT effects by OLAP in CML primary samples[170]. This may be due to differential genetic background of K562 and samples tested in the cited study, as OLAP effect was shown for CML in CP and AP, while K562 is a model of highly mutated, aggressive CML in MBP.

5.6. Sensitization of Ph+ lymphoid cell lines and PDXs to TKIs and NHEJi combination by inhibition of the TXN system

As the inhibition of NHEJ enhanced the effectiveness of IMAT in both K562 and BV173 cell lines, the effect of PRDX1 knockout on the sensitivity of the combination of NHEJi and IMAT was tested. PRDX1 knockout sensitized only BV173 cells to the treatment, especially with OLAP and IMAT combination, allowing for killing almost all cells in the highest tested drugs concentration. K562 cells were mostly unaffected by the PRDX1 knockout (Fig. 35 and Fig. 36). Those results, taken together with much stronger synergistic effect of the TXN system inhibition with TKIs in lymphoid Ph$^+$ cell lines (Figs. 3-6) prompted further investigation of the triple combinations of AUR, TKIs and NHEJi solely in Ph$^+$ lymphoid cells (Figs. 37-42). Both NHEJi were effective in triple combinations in cell lines, with more pronounced effect of NEDI than OLAP. On the other hand, in PDXs only NEDI addition was effective in both TKI^{sen} and TKI^{res} samples, while all PDXs were insensitive to OLAP, regardless of their TKI sensitivity. This discrepancy of results in cell lines and PDXs might be caused by the fact that both BV173 and

SUP-B15 cell lines are proliferating, progressing through subsequent phases of cell cycle, while PDXs are in large part non-proliferating cells in an *ex vivo* setting. This may be of importance, as altNHEJ was shown to be most active in S and G_2 phases of cell cycle[271] and its activity decreased when cells entered plateau phase[272]. On the other hand, cNHEJ is known to be active throughout all of the cell cycle phases, including G_0/G_1 phase[271,273]. Moreover, PARP1 was shown to play more pronounced role in proliferating cells, promoting their progression through cell cycle and its inhibition caused arrest in G1/G0 phase[274,275], possibly further explaining differences in OLAP efficacy in proliferating cell lines and resting PDX cells. The limitation of this study is the lack of characterization of the functionality of subsequent DDR pathways in the investigated model cells. This will be further studied to allow for the full interpretation of these results.

The selective sensitivity of Ph+ PDXs to cNHEJ, but not altNHEJ, inhibition could also be potentially explained by their B cell origin. RAG1/2 expression and activity, characteristic only for lymphoid cells, causes elevated DSB occurrence[144,176]. As Ph^+ B-ALL cells are stalled at pre-B stage, an ongoing V(D)J recombination and RAG1/2 activity were identified in the majority of the tested B-ALL cases[177,178], yet limited to G_0/G_1 phase of the cell cycle[179]. Also, RAG1/2 promotes cNHEJ activity over altNHEJ, with HR normally unattainable during V(D)J recombination, although exact mechanism of favoring cNHEJ over altNHEJ by RAGs isn't fully elucidated[144,176]. Among proposed explanations of this phenomena is low polymerase theta expression in G_0 and G_1 phases, limiting altNHEJ activity[176]. Moreover, RAG1 was also shown to bind Ku70-containing complexes[176], and lately Ku70 was discovered to repress altNHEJ repair of RAG induced DSBs in G_1-arrested progenitor B cells[144]. Therefore, in non-proliferating, Ph+ B-ALL cells, cNHEJ is most likely the dominant mechanism of DDR.

PRDX1 was shown to promote NF-κB signaling[112], possibly also contributing to RAGs downregulation. This indicates that PRDX1 knockout or inhibition might promote RAGs activity, possibly explaining observed accumulation of DSBs in PRDX1-deficient cells. Moreover, BCR-ABL1 inhibition by IMAT in Ph^+ B-ALL was discovered to downregulate BCR-ABL1's downstream signaling involving AKT and NF-kB, subsequently activating RAGs, regardless of the cell cycle phase[179]. Those results taken together with the results obtained

in this PhD thesis, led to formulation of possible mechanism of action of the triple combination composed of TXN system, BCR-ABL1 and NHEJ inhibition (Fig. 43). It is hypothesized that the observed effect of triple combination is caused by concomitant activation of RAG1/2 activity by PRDX1 knockout and BCR-ABL1 inhibition, leading to generation of DSBs that can't be efficiently repaired due to NHEJ inhibition. Even though, this is only a hypothesis, and more in-depth study of RAG1/2 involvement in those processes is needed to elucidate the exact mechanism behind cytotoxic effect of triple combination.

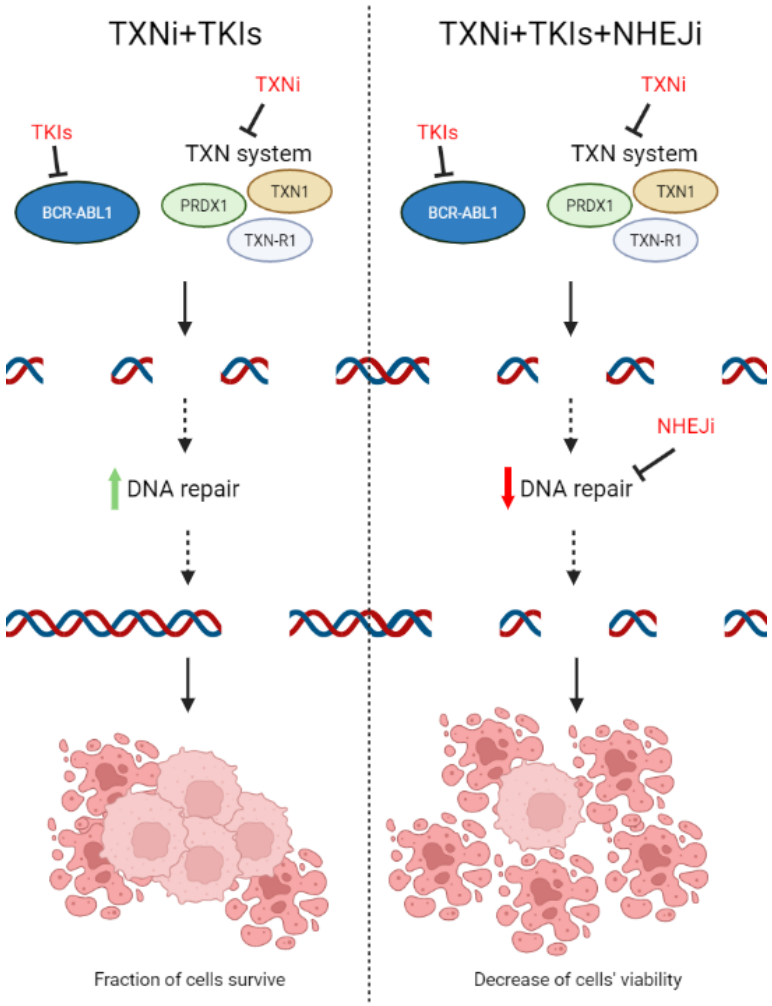

Fig. 43. Proposed mechanism of triple AUR, TKIs and NEDI effect on Ph+ lymphoid cells. In short, inhibition of TXN system and BCR-ABL1 (left) generates DSBs, which are partly repaired by the elevated DNA repair, allowing a fraction of cells to survive. Additional inhibition of NHEJ (right) decreases repair of therapy-induced DSBs, causing increased cell death. Indicated in red are the inhibitors used for treatment. Dashed arrows indicate omitted intermediary states, not relevant to the proposed mechanism. NHEJi – non-homologous recombination inhibitors, PRDX1 – peroxiredoxin 1, TKIs – tyrosine kinase inhibitors, TXN1 – thioredoxin 1, TXNi – thioredoxin system inhibitors, TXN-R1 – thioredoxin reductase 1.

Even though results presented in this thesis are encouraging, further research is still needed. Investigation triple combination's mechanisms, including explanation for its lymphoid specificity and RAGs involvement, and extensive studies in more pre-clinical models, including leukemia xenografts *in vivo* models, are still necessary.

6. Conclusions

- Inhibition of the TXN system ameliorates IMAT and DASA cytotoxicity in Ph^+ cell lines, in a lymphoid-specific manner;
- PRDX1 expression is upregulated in lymphoid Ph^+ primary cells (CML in LBP and Ph^+ B-ALL) in comparison to their myeloid counterparts (CML in CP and MBP);
- PRDX1 supports growth and resistance to TKIs specifically in Ph+ lymphoid cells;
- PRDX1-deficient Ph^+ lymphoid cells upregulate several stress- and apoptosis-related pathways and accumulate greater amounts of DNA DSB upon IMAT treatment;
- Inhibition of altNHEJ, TXN system, and BCR-ABL1 by a triple combination of OLAP, AUR and IMAT exerts potent cytotoxic effects in lymphoid Ph^+ cell lines;
- Inhibition of cNHEJ, TXN system, and BCR-ABL1 by a triple combination of NEDI, AUR, and TKIs exerts potent cytotoxic effects both in lymphoid Ph^+ cell lines and patient-derived Ph^+ B-ALL PDXs.

7. References

1. Melo, J. V., Hughes, T. P. & Apperley, J. F. Chronic Myeloid Leukemia. *Hematology* **2003**, 132–152 (2003).

2. Zhang, X. & Ren, R. Bcr-Abl efficiently induces a myeloproliferative disease and production of excess interleukin-3 and granulocyte-macrophage colony-stimulating factor in mice: a novel model for chronic myelogenous leukemia. *Blood* **92**, 3829–3840 (1998).

3. Gong, Z. *et al.* Clinical and prognostic significance of e1a2 BCR-ABL1 transcript subtype in chronic myeloid leukemia. *Blood Cancer J.* **7**, e583 (2017).

4. Reckel, S. *et al.* Structural and functional dissection of the DH and PH domains of oncogenic Bcr-Abl tyrosine kinase. *Nat. Commun.* **8**, 2101 (2017).

5. Mizuno, S. *et al.* Allogeneic hematopoietic cell transplantation efficacy in patients with Philadelphia chromosome-positive acute myeloid leukemia in complete remission. *Bone Marrow Transplant.* **56**, 232–242 (2021).

6. Qasrawi, A., Ramlal, R., Munker, R. & Hildebrandt, G. C. Prognostic impact of Philadelphia chromosome in mixed phenotype acute leukemia (MPAL): A cancer registry analysis on real-world outcome. *Am. J. Hematol.* **95**, 1015–1021 (2020).

7. Komorowski, L., Fidyt, K., Patkowska, E. & Firczuk, M. Philadelphia Chromosome-Positive Leukemia in the Lymphoid Lineage—Similarities and Differences with the Myeloid Lineage and Specific Vulnerabilities. *Int. J. Mol. Sci.* **21**, 5776 (2020).

8. Hunger, S. P. & Mullighan, C. G. Redefining ALL classification: toward detecting high-risk ALL and implementing precision medicine. *Blood* **125**, 3977–3987 (2015).

9. Yeung, D. T. O., Osborn, M. P. & White, D. L. B-cell acute lymphoblastic leukaemia: recent discoveries in molecular pathology, their prognostic significance, and a review of the current classification. *Br. J. Haematol.* **197**, 13–27 (2022).

10. Kang, Z.-J. *et al.* The Philadelphia chromosome in leukemogenesis. *Chin. J. Cancer* **35**, 48 (2016).

11. Mattarucchi, E. *et al.* Microhomologies and interspersed repeat elements at genomic breakpoints in chronic myeloid leukemia. *Genes. Chromosomes Cancer* **47**, 625–632 (2008).

12. Score, J. *et al.* Analysis of genomic breakpoints in p190 and p210 BCR–ABL indicate distinct mechanisms of formation. *Leukemia* **24**, 1742–1750 (2010).

13. Greuber, E. K., Smith-Pearson, P., Wang, J. & Pendergast, A. M. Role of ABL Family Kinases in Cancer: from Leukemia to Solid Tumors. *Nat. Rev. Cancer* **13**, 559–571 (2013).

14. Dasgupta, Y. *et al.* Normal ABL1 is a tumor suppressor and therapeutic target in human and mouse leukemias expressing oncogenic ABL1 kinases. *Blood* **127**, 2131–2143 (2016).

15. Aloisi, A. *et al.* BCR-ABL nuclear entrapment kills human CML cells: ex vivo study on 35 patients with the combination of imatinib mesylate and leptomycin B. *Blood* **107**, 1591–1598 (2006).

16. Cilloni, D. & Saglio, G. Molecular pathways: BCR-ABL. *Clin. Cancer Res. Off. J. Am. Assoc. Cancer Res.* **18**, 930–937 (2012).

17. Li, S., Ilaria, R. L., Million, R. P., Daley, G. Q. & Van Etten, R. A. The P190, P210, and P230 Forms of the BCR/ABL Oncogene Induce a Similar Chronic Myeloid Leukemia–like Syndrome in Mice but Have Different Lymphoid Leukemogenic Activity. *J. Exp. Med.* **189**, 1399–1412 (1999).

18. Reckel, S. *et al.* Differential signaling networks of Bcr–Abl p210 and p190 kinases in leukemia cells defined by functional proteomics. *Leukemia* **31**, 1502–1512 (2017).

19. Chen, Z. *et al.* Differential impact of additional chromosomal abnormalities in myeloid vs lymphoid blast phase of chronic myelogenous leukemia in the era of tyrosine kinase inhibitor therapy. *Leukemia* **30**, 1606–1609 (2016).

20. Foulon, S. *et al.* Using healthcare claims data to analyze the prevalence of BCR-ABL-positive chronic myeloid leukemia in France: A nationwide population-based study. *Cancer Med.* **8**, 3296–3304 (2019).

21. Clarkson, B., Strife, A., Wisniewski, D., Lambek, C. L. & Liu, C. Chronic myelogenous leukemia as a paradigm of early cancer and possible curative strategies. *Leukemia* **17**, 1211–1262 (2003).

22. Togasaki, E. *et al.* Frequent somatic mutations in epigenetic regulators in newly diagnosed chronic myeloid leukemia. *Blood Cancer J.* **7**, e559 (2017).

23. Schmidt, M. *et al.* Molecular-defined clonal evolution in patients with chronic myeloid leukemia independent of the BCR-ABL status. *Leukemia* **28**, 2292–2299 (2014).

24. Reid, A. G. *et al.* Phenotype of blasts in chronic myeloid leukemia in blastic phase-Analysis of bone marrow trephine biopsies and correlation with cytogenetics. *Leuk. Res.* **33**, 418–425 (2009).

25. Soverini, S., Mancini, M., Bavaro, L., Cavo, M. & Martinelli, G. Chronic myeloid leukemia: the paradigm of targeting oncogenic tyrosine kinase signaling and counteracting resistance for successful cancer therapy. *Mol. Cancer* **17**, 49 (2018).

26. Perrotti, D., Jamieson, C., Goldman, J. & Skorski, T. Chronic myeloid leukemia: mechanisms of blastic transformation. *J. Clin. Invest.* **120**, 2254–2264 (2010).

27. Branford, S. *et al.* Integrative genomic analysis reveals cancer-associated mutations at diagnosis of CML in patients with high-risk disease. *Blood* **132**, 948–961 (2018).

28. Adnan Awad, S. *et al.* Mutation accumulation in cancer genes relates to nonoptimal outcome in chronic myeloid leukemia. *Blood Adv.* **4**, 546–559 (2020).

29. Hunger, S. P. CML in blast crisis: more common than we think? *Blood* **129**, 2713–2714 (2017).

30. Saleh, K., Fernandez, A. & Pasquier, F. Treatment of Philadelphia Chromosome-Positive Acute Lymphoblastic Leukemia in Adults. *Cancers* **14**, 1805 (2022).

31. EMA. EU/3/20/2261. *European Medicines Agency* https://www.ema.europa.eu/en/medicines/human/orphan-designations/eu3202261 (2020).

32. Research, C. for D. E. and. FDA approves asciminib for Philadelphia chromosome-positive chronic myeloid leukemia. *FDA* (2021).

33. Hoelzer, D. *et al.* Acute lymphoblastic leukaemia in adult patients: ESMO Clinical Practice Guidelines for diagnosis, treatment and follow-up †. *Ann. Oncol.* **27**, v69–v82 (2016).

34. Acute Lymphocytic Leukemia - Cancer Stat Facts. *SEER* https://seer.cancer.gov/statfacts/html/alyl.html.

35. Rehe, K. *et al.* Acute B lymphoblastic leukaemia-propagating cells are present at high frequency in diverse lymphoblast populations. *EMBO Mol. Med.* **5**, 38–51 (2013).

36. Terwilliger, T. & Abdul-Hay, M. Acute lymphoblastic leukemia: a comprehensive review and 2017 update. *Blood Cancer J.* **7**, e577 (2017).

37. Klco, J. M. & Mullighan, C. G. Advances in germline predisposition to acute leukemias and myeloid neoplasms. *Nat. Rev. Cancer* **21**, 122–137 (2021).

38. Pui, C.-H., Nichols, K. E. & Yang, J. J. Somatic and germline genomics in paediatric acute lymphoblastic leukaemia. *Nat. Rev. Clin. Oncol.* **16**, 227–240 (2019).

39. Inaba, H. & Mullighan, C. G. Pediatric acute lymphoblastic leukemia. *Haematologica* **105**, 2524–2539 (2020).

40. Locatelli, F., Schrappe, M., Bernardo, M. E. & Rutella, S. How I treat relapsed childhood acute lymphoblastic leukemia. *Blood* **120**, 2807–2816 (2012).

41. Samra, B., Jabbour, E., Ravandi, F., Kantarjian, H. & Short, N. J. Evolving therapy of adult acute lymphoblastic leukemia: state-of-the-art treatment and future directions. *J. Hematol. Oncol.J Hematol Oncol* **13**, 70 (2020).

42. Primo, D. *et al.* Genetic heterogeneity of BCR/ABL+ adult B-cell precursor acute lymphoblastic leukemia: impact on the clinical, biological and immunophenotypical disease characteristics. *Leukemia* **19**, 713–720 (2005).

43. Dupuis, A. *et al.* Biclonal and biallelic deletions occur in 20% of B-ALL cases with IKZF1 mutations. *Leukemia* **27**, 503–507 (2013).

44. Mullighan, C. G. *et al.* BCR-ABL1 lymphoblastic leukaemia is characterized by the deletion of Ikaros. *Nature* **453**, 110–114 (2008).

45. Dong, Y. *et al.* Illegitimate RAG-mediated recombination events are involved in IKZF1 Δ3–6 deletion in BCR-ABL1 lymphoblastic leukaemia. *Clin. Exp. Immunol.* **185**, 320–331 (2016).

46. Yao, L. *et al.* IK6 isoform with associated cytogenetic and molecular abnormalities in Chinese patients with Philadelphia chromosome-positive adult acute lymphoblastic leukemia. *Leuk. Lymphoma* **54**, 1626–1632 (2013).

47. Chan, L. N. *et al.* Metabolic gatekeeper function of B-lymphoid transcription factors. *Nature* **542**, 479–483 (2017).

48. Pfeifer, H. *et al.* Genomic CDKN2A/2B deletions in adult Ph+ ALL are adverse despite allogeneic stem cell transplantation. *Blood* **131**, 1464–1475 (2018).

49. Martín-Lorenzo, A. *et al.* Loss of Pax5 exploits Sca1-BCR-ABLp190 susceptibility to confer the metabolic shift essential for pB-ALL. *Cancer Res.* **78**, 2669–2679 (2018).

50. Xu, N. *et al.* Correlation between deletion of the CDKN2 gene and tyrosine kinase inhibitor resistance in adult Philadelphia chromosome-positive acute lymphoblastic leukemia. *J. Hematol. Oncol.J Hematol Oncol* **9**, 40 (2016).

51. Xu, N. *et al.* CDKN2 Gene Deletion as Poor Prognosis Predictor Involved in the Progression of Adult B-Lineage Acute Lymphoblastic Leukemia Patients. *J. Cancer* **6**, 1114–1120 (2015).

52. Kim, M. *et al.* PAX5 deletion is common and concurrently occurs with CDKN2A deletion in B-lineage acute lymphoblastic leukemia. *Blood Cells. Mol. Dis.* **47**, 62–66 (2011).

53. LeBien, T. W. Fates of human B-cell precursors. *Blood* **96**, 9–23 (2000).

54. Chen, Z. *et al.* Signaling thresholds and negative B cell selection in acute lymphoblastic leukemia. *Nature* **521**, 357–361 (2015).

55. Shojaee, S. *et al.* PTEN opposes negative selection and enables oncogenic transformation of pre-B cells. *Nat. Med.* **22**, 379–387 (2016).

56. Fielding, A. K. Curing Ph+ ALL: assessing the relative contributions of chemotherapy, TKIs, and allogeneic stem cell transplant. *Hematol. Am. Soc. Hematol. Educ. Program* **2019**, 24–29 (2019).

57. Boer, J. M. & den Boer, M. L. BCR-ABL1-like acute lymphoblastic leukaemia: From bench to bedside. *Eur. J. Cancer Oxf. Engl. 1990* **82**, 203–218 (2017).

58. Maude, S. L. *et al.* Tisagenlecleucel in Children and Young Adults with B-Cell Lymphoblastic Leukemia. *N. Engl. J. Med.* **378**, 439–448 (2018).

59. Martinelli, G. *et al.* Complete Hematologic and Molecular Response in Adult Patients With Relapsed/Refractory Philadelphia Chromosome-Positive B-Precursor Acute Lymphoblastic Leukemia Following Treatment With Blinatumomab: Results From a Phase II, Single-Arm, Multicenter Study. *J. Clin. Oncol. Off. J. Am. Soc. Clin. Oncol.* **35**, 1795–1802 (2017).

60. Chen, J. *et al.* Dynamic evolution of ponatinib-resistant mutations in BCR-ABL1-positive leukaemias revealed by next-generation sequencing. *Br. J. Haematol.* **191**, e113–e116 (2020).

61. Miller, G. D., Bruno, B. J. & Lim, C. S. Resistant mutations in CML and Ph(+)ALL - role of ponatinib. *Biol. Targets Ther.* **8**, 243–254 (2014).

62. Suzuki, M. *et al.* BCR-ABL-independent and RAS / MAPK pathway-dependent form of imatinib resistance in Ph-positive acute lymphoblastic leukemia cell line with activation of EphB4. *Eur. J. Haematol.* **84**, 229–238 (2010).

63. Mian, A. A., Zafar, U., Ahmed, S. M. A., Ottmann, O. G. & Lalani, E.-N. M. A. Oncogene-independent resistance in Philadelphia chromosome - positive (Ph+) acute lymphoblastic leukemia (ALL) is mediated by activation of AKT/mTOR pathway. *Neoplasia N. Y. N* **23**, 1016–1027 (2021).

64. Mian, A. A., Zafar, U., Ottmann, O., Ruthardt, M. & Lalani, E.-N. M. A. Activation of AKT/mTOR Pathway in Ph+ Acute Lymphoblastic Leukemia (ALL) Leads to Non-Mutational Resistance. *Blood* **134**, 2570–2570 (2019).

65. S, M. *et al.* Tyrosine kinase inhibitors induce mesenchymal stem cell-mediated resistance in BCR-ABL+ acute lymphoblastic leukemia. *Blood* **125**, (2015).

66. Vignetti, M. *et al.* Imatinib plus steroids induces complete remissions and prolonged survival in elderly Philadelphia chromosome-positive patients with acute lymphoblastic leukemia without additional chemotherapy: results of the Gruppo Italiano Malattie Ematologiche dell'Adulto (GIMEMA) LAL0201-B protocol. *Blood* **109**, 3676–3678 (2007).

67. Papayannidis, C. *et al.* Rate of complete hematological response of elderly Ph+ acute lymphoblastic leukemia (ALL) patients by sequential use of nilotinib and imatinib: A GIMEMA protocol LAL 1408. *J. Clin. Oncol.* **31**, 7025–7025 (2013).

68. Martinelli, G. *et al.* INCB84344-201: Ponatinib and steroids in frontline therapy for unfit patients with Ph+ acute lymphoblastic leukemia. *Blood Adv.* **6**, 1742–1753 (2022).

69. Foà, R. *et al.* Dasatinib–Blinatumomab for Ph-Positive Acute Lymphoblastic Leukemia in Adults. *N. Engl. J. Med.* **383**, 1613–1623 (2020).

70. Advani, A. *et al.* A Phase 2 Study of Dasatinib, Prednisone, and Blinatumomab for Older Patients with Philadelphia-Chromosome (Ph) Positive or Ph-like Acute Lymphoblastic Leukemia (ALL) (with Dasatinib Sensitive Fusions/ Mutations). *Blood* **138**, 3397 (2021).

71. Leonard, J. T. *et al.* Concomitant use of a dual Src/ABL kinase inhibitor eliminates the in vitro efficacy of blinatumomab against Ph+ ALL. *Blood* **137**, 939–944 (2021).

72. Xiao, G. *et al.* B cell-specific diversion of glucose carbon utilization reveals a unique vulnerability in B cell malignancies. *Cell* **173**, 470-484.e18 (2018).

73. Graczyk-Jarzynka, A. *et al.* Inhibition of thioredoxin-dependent H2O2 removal sensitizes malignant B-cells to pharmacological ascorbate. *Redox Biol.* **21**, 101062 (2019).

74. Fidyt, K. *et al.* Targeting the thioredoxin system as a novel strategy against B-cell acute lymphoblastic leukemia. *Mol. Oncol.* **13**, 1180–1195 (2019).

75. Gorrini, C., Harris, I. S. & Mak, T. W. Modulation of oxidative stress as an anticancer strategy. *Nat. Rev. Drug Discov.* **12**, 931–947 (2013).

76. Firczuk, M. *et al.* Harnessing altered oxidative metabolism in cancer by augmented prooxidant therapy. *Cancer Lett.* **471**, 1–11 (2020).

77. Graczyk-Jarzynka, A. *et al.* New insights into redox homeostasis as a therapeutic target in B-cell malignancies. *Curr. Opin. Hematol.* **24**, 393–401 (2017).

78. Nathan, C. & Cunningham-Bussel, A. Beyond oxidative stress: an immunologist's guide to reactive oxygen species. *Nat. Rev. Immunol.* **13**, 349–361 (2013).

79. Sies, H. & Jones, D. P. Reactive oxygen species (ROS) as pleiotropic physiological signalling agents. *Nat. Rev. Mol. Cell Biol.* **21**, 363–383 (2020).

80. Rasool, M. *et al.* Assessment of circulating biochemical markers and antioxidative status in acute lymphoblastic leukemia (ALL) and acute myeloid leukemia (AML) patients. *Saudi J. Biol. Sci.* **22**, 106–111 (2015).

81. Almondes, K. G. de S. *et al.* Selenium inadequacy is not associated with oxidative stress in child and adolescent acute lymphocytic leukemia survivors. *Nutr. Burbank Los Angel. Cty. Calif* **30**, 563–568 (2014).

82. Yang, Y. *et al.* Determinants of urinary 8-hydroxy-2'-deoxyguanosine in Chinese children with acute leukemia. *Environ. Toxicol.* **24**, 446–452 (2009).

83. Domka, K., Goral, A. & Firczuk, M. cROSsing the Line: Between Beneficial and Harmful Effects of Reactive Oxygen Species in B-Cell Malignancies. *Front. Immunol.* **11**, 1538 (2020).

84. Chen, Y., Li, J. & Zhao, Z. Redox Control in Acute Lymphoblastic Leukemia: From Physiology to Pathology and Therapeutic Opportunities. *Cells* **10**, 1218 (2021).

85. Prieto-Bermejo, R., Romo-González, M., Pérez-Fernández, A., Ijurko, C. & Hernández-Hernández, Á. Reactive oxygen species in haematopoiesis: leukaemic cells take a walk on the wild side. *J. Exp. Clin. Cancer Res. CR* **37**, 125 (2018).

86. Steelman, L. S. *et al.* Contributions of the Raf/MEK/ERK, PI3K/PTEN/Akt/mTOR and Jak/STAT pathways to leukemia. *Leukemia* **22**, 686–707 (2008).

87. Chen, C., Liu, Y., Liu, Y. & Zheng, P. The axis of mTOR-mitochondria-ROS and stemness of the hematopoietic stem cells. *Cell Cycle Georget. Tex* **8**, 1158–1160 (2009).

88. Mannan, A. *et al.* Reactive Oxygen Species in Acute Lymphoblastic Leukaemia: Reducing Radicals to Refine Responses. *Antioxidants* **10**, 1616 (2021).

89. Naughton, R., Quiney, C., Turner, S. D. & Cotter, T. G. Bcr-Abl-mediated redox regulation of the PI3K/AKT pathway. *Leukemia* **23**, 1432–1440 (2009).

90. Sattler, M. *et al.* The BCR/ABL tyrosine kinase induces production of reactive oxygen species in hematopoietic cells. *J. Biol. Chem.* **275**, 24273–24278 (2000).

91. Koundouros, N. & Poulogiannis, G. Phosphoinositide 3-Kinase/Akt Signaling and Redox Metabolism in Cancer. *Front. Oncol.* **8**, 160 (2018).

92. Koptyra, M., Cramer, K., Slupianek, A., Richardson, C. & Skorski, T. BCR/ABL promotes accumulation of chromosomal aberrations induced by oxidative and genotoxic stress. *Leukemia* **22**, 10.1038/leu.2008.78 (2008).

93. Koptyra, M. *et al.* BCR/ABL kinase induces self-mutagenesis via reactive oxygen species to encode imatinib resistance. *Blood* **108**, 319–327 (2006).

94. Fan, P. *et al.* Modulation of nuclear factor-kappa B activation by the endoplasmic reticulum stress sensor PERK to mediate estrogen-induced apoptosis in breast cancer cells. *Cell Death Discov.* **4**, 1–14 (2018).

95. Yin, Z., Machius, M., Nestler, E. J. & Rudenko, G. Activator Protein-1: redox switch controlling structure and DNA-binding. *Nucleic Acids Res.* **45**, 11425–11436 (2017).

96. Samanta, D. & Semenza, G. L. Maintenance of redox homeostasis by hypoxia-inducible factors. *Redox Biol.* **13**, 331 (2017).

97. Eriksson, S. E., Ceder, S., Bykov, V. J. N. & Wiman, K. G. p53 as a hub in cellular redox regulation and therapeutic target in cancer. *J. Mol. Cell Biol.* **11**, 330–341 (2019).

98. Miller, C. G., Holmgren, A., Arnér, E. S. J. & Schmidt, E. E. NADPH-dependent and -independent disulfide reductase systems. *Free Radic. Biol. Med.* **127**, 248–261 (2018).

99. Espinosa-Diez, C. *et al.* Antioxidant responses and cellular adjustments to oxidative stress. *Redox Biol.* **6**, 183–197 (2015).

100. Trzeciecka, A. *et al.* Dimeric peroxiredoxins are druggable targets in human Burkitt lymphoma. *Oncotarget* **7**, 1717 (2016).

101. Karlenius, T. C. & Tonissen, K. F. Thioredoxin and Cancer: A Role for Thioredoxin in all States of Tumor Oxygenation. *Cancers* **2**, 209–232 (2010).

102. Muri, J. *et al.* The thioredoxin-1 system is essential for fueling DNA synthesis during T-cell metabolic reprogramming and proliferation. *Nat. Commun.* **9**, 1851 (2018).

103. Matthews, J. R., Wakasugi, N., Virelizier, J. L., Yodoi, J. & Hay, R. T. Thioredoxin regulates the DNA binding activity of NF-kappa B by reduction of a disulphide bond involving cysteine 62. *Nucleic Acids Res.* **20**, 3821–3830 (1992).

104. Kylarova, S. *et al.* Cysteine residues mediate high-affinity binding of thioredoxin to ASK1. *FEBS J.* **283**, 3821–3838 (2016).

105. Mitchell, D. A., Morton, S. U., Fernhoff, N. B. & Marletta, M. A. Thioredoxin is required for S-nitrosation of procaspase-3 and the inhibition of apoptosis in Jurkat cells. *Proc. Natl. Acad. Sci. U. S. A.* **104**, 11609–11614 (2007).

106. Meuillet, E. J., Mahadevan, D., Berggren, M., Coon, A. & Powis, G. Thioredoxin-1 binds to the C2 domain of PTEN inhibiting PTEN's lipid phosphatase activity and membrane binding: a mechanism for the functional loss of PTEN's tumor suppressor activity. *Arch. Biochem. Biophys.* **429**, 123–133 (2004).

107. Neumann, C. A., Cao, J. & Manevich, Y. Peroxiredoxin 1 and its role in cell signaling. *Cell Cycle Georget. Tex* **8**, 4072–4078 (2009).

108. Lim, J. C. *et al.* Irreversible oxidation of the active-site cysteine of peroxiredoxin to cysteine sulfonic acid for enhanced molecular chaperone activity. *J. Biol. Chem.* **283**, 28873–28880 (2008).

109. Teixeira, F. *et al.* Chaperone activation and client binding of a 2-cysteine peroxiredoxin. *Nat. Commun.* **10**, 659 (2019).

110. Troussicot, L., Burmann, B. M. & Molin, M. Structural determinants of multimerization and dissociation in 2-Cys peroxiredoxin chaperone function. *Structure* **29**, 640–654 (2021).

111. Wen, S. T. & Van Etten, R. A. The PAG gene product, a stress-induced protein with antioxidant properties, is an Abl SH3-binding protein and a physiological inhibitor of c-Abl tyrosine kinase activity. *Genes Dev.* **11**, 2456–2467 (1997).

112. Ding, C., Fan, X. & Wu, G. Peroxiredoxin 1 – an antioxidant enzyme in cancer. *J. Cell. Mol. Med.* **21**, 193–202 (2017).

113. McDonald, C., Muhlbauer, J., Perlmutter, G., Taparra, K. & Phelan, S. A. Peroxiredoxin proteins protect MCF-7 breast cancer cells from doxorubicin-induced toxicity. *Int. J. Oncol.* **45**, 219–226 (2014).

114. Turner-Ivey, B. *et al.* Role for Prdx1 as a specific sensor in redox-regulated senescence in breast cancer. *Oncogene* **32**, 5302–5314 (2013).

115. Kalinina, E. V. *et al.* Expression of peroxiredoxin 1, 2, 3, and 6 genes in cancer cells during drug resistance formation. *Bull. Exp. Biol. Med.* **153**, 878–881 (2012).

116. Hwang, K.-E. *et al.* Prx1 modulates the chemosensitivity of lung cancer to docetaxel through suppression of FOXO1-induced apoptosis. *Int. J. Oncol.* **43**, 72–78 (2013).

117. Peroja, P. *et al.* Total peroxiredoxin expression is associated with survival in patients with follicular lymphoma. *Virchows Arch. Int. J. Pathol.* **468**, 623–630 (2016).

118. Cramer, S. L. *et al.* Systemic depletion of serum l-Cyst(e)ine with an engineered human enzyme induces production of reactive oxygen species and suppresses tumor growth in mice. *Nat. Med.* **23**, 120–127 (2017).

119. Barr, P. M. *et al.* Phase 2 study of imexon, a prooxidant molecule, in relapsed and refractory B-cell non-Hodgkin lymphoma. *Blood* **124**, 1259–1265 (2014).

120. Fidyt, K. *et al.* Potent, p53-independent induction of NOXA sensitizes MLL-rearranged B-cell acute lymphoblastic leukemia cells to venetoclax. *Oncogene* **41**, 1600–1609 (2022).

121. Abdalbari, F. H. & Telleria, C. M. The gold complex auranofin: new perspectives for cancer therapy. *Discov. Oncol.* **12**, 42 (2021).

122. Li, H. *et al.* Auranofin-mediated inhibition of PI3K/AKT/mTOR axis and anticancer activity in non-small cell lung cancer cells. *Oncotarget* **7**, 3548–3558 (2016).

123. Rios Perez, M. V. *et al.* Antineoplastic effects of auranofin in human pancreatic adenocarcinoma preclinical models. *Surg. Open Sci.* **1**, 56–63 (2019).

124. Pfoh, R., Lacdao, I. K. & Saridakis, V. Deubiquitinases and the new therapeutic opportunities offered to cancer. *Endocr. Relat. Cancer* **22**, T35–T54 (2015).

125. Muchowicz, A. *et al.* Adenanthin targets proteins involved in the regulation of disulphide bonds. *Biochem. Pharmacol.* **89**, 210–216 (2014).

126. Bajor, M. *et al.* Abstract P5-07-09: Adenanthin, a new peroxiredoxin inhibitor, induces a switch between estrogen receptor alpha-mediated and Src/Akt-driven signaling in breast cancer cells. *Cancer Res.* **75**, P5-07–09 (2015).

127. Hou, J.-K. *et al.* Adenanthin targets peroxiredoxin I/II to kill hepatocellular carcinoma cells. *Cell Death Dis.* **5**, e1400–e1400 (2014).

128. Siernicka, M. *et al.* Adenanthin, a new inhibitor of thiol-dependent antioxidant enzymes, impairs the effector functions of human natural killer cells. *Immunology* **146**, 173–183 (2015).

129. O'Connor, M. J. Targeting the DNA Damage Response in Cancer. *Mol. Cell* **60**, 547–560 (2015).

130. Phan, L. M. & Rezaeian, A.-H. ATM: Main Features, Signaling Pathways, and Its Diverse Roles in DNA Damage Response, Tumor Suppression, and Cancer Development. *Genes* **12**, 845 (2021).

131. Lee, J.-H. & Paull, T. T. Cellular functions of the protein kinase ATM and their relevance to human disease. *Nat. Rev. Mol. Cell Biol.* **22**, 796–814 (2021).

132. Mah, L.-J., El-Osta, A. & Karagiannis, T. C. γH2AX: a sensitive molecular marker of DNA damage and repair. *Leukemia* **24**, 679–686 (2010).

133. Blackford, A. N. & Jackson, S. P. ATM, ATR, and DNA-PK: The Trinity at the Heart of the DNA Damage Response. *Mol. Cell* **66**, 801–817 (2017).

134. Huang, R. & Zhou, P.-K. DNA damage repair: historical perspectives, mechanistic pathways and clinical translation for targeted cancer therapy. *Signal Transduct. Target. Ther.* **6**, 1–35 (2021).

135. Yao, Y. *et al.* ATM Promotes RAD51-Mediated Meiotic DSB Repair by Inter-Sister-Chromatid Recombination in Arabidopsis. *Front. Plant Sci.* **11**, 839 (2020).

136. Kumar, A., Purohit, S. & Sharma, N. K. Aberrant DNA Double-strand Break Repair Threads in Breast Carcinoma: Orchestrating Genomic Insult Survival. *J. Cancer Prev.* **21**, 227–234 (2016).

137. Trenner, A. & Sartori, A. A. Harnessing DNA Double-Strand Break Repair for Cancer Treatment. *Front. Oncol.* **9**, 1388 (2019).

138. Allera-Moreau, C. *et al.* DNA replication stress response involving PLK1, CDC6, POLQ, RAD51 and CLASPIN upregulation prognoses the outcome of early/mid-stage non-small cell lung cancer patients. *Oncogenesis* **1**, e30 (2012).

139. Scully, R., Panday, A., Elango, R. & Willis, N. A. DNA double-strand break repair-pathway choice in somatic mammalian cells. *Nat. Rev. Mol. Cell Biol.* **20**, 698–714 (2019).

140. Caston, R. A. *et al.* The multifunctional APE1 DNA repair-redox signaling protein as a drug target in human disease. *Drug Discov. Today* **26**, 218–228 (2021).

141. Graham, T. G. W., Walter, J. C. & Loparo, J. J. Two-Stage Synapsis of DNA Ends during Non-homologous End Joining. *Mol. Cell* **61**, 850–858 (2016).

142. Perkhofer, L. *et al.* DNA damage repair as a target in pancreatic cancer: state-of-the-art and future perspectives. *Gut* **70**, 606–617 (2021).

143. Zhao, L. *et al.* The Determinant of DNA Repair Pathway Choices in Ionising Radiation-Induced DNA Double-Strand Breaks. *BioMed Res. Int.* **2020**, 4834965 (2020).

144. Liang, Z. *et al.* Ku70 suppresses alternative end joining in G1-arrested progenitor B cells. *Proc. Natl. Acad. Sci. U. S. A.* **118**, e2103630118 (2021).

145. Ahrabi, S. *et al.* A role for human homologous recombination factors in suppressing microhomology-mediated end joining. *Nucleic Acids Res.* **44**, 5743–5757 (2016).

146. Ray Chaudhuri, A. & Nussenzweig, A. The multifaceted roles of PARP1 in DNA repair and chromatin remodelling. *Nat. Rev. Mol. Cell Biol.* **18**, 610–621 (2017).

147. Cohen-Armon, M. A Long-Lasting PARP1-Activation Mediates Signal-Induced Gene Expression. *Cells* **11**, 1576 (2022).

148. Huang, D. & Kraus, W. L. The expanding universe of PARP1-mediated molecular and therapeutic mechanisms. *Mol. Cell* (2022) doi:10.1016/j.molcel.2022.02.021.

149. Muoio, D., Laspata, N. & Fouquerel, E. Functions of ADP-ribose transferases in the maintenance of telomere integrity. *Cell. Mol. Life Sci.* **79**, 215 (2022).

150. Padella, A. *et al.* Targeting PARP proteins in acute leukemia: DNA damage response inhibition and therapeutic strategies. *J. Hematol. Oncol.J Hematol Oncol* **15**, 10 (2022).

151. Han, Y. *et al.* DNA-PKcs PARylation regulates DNA-PK kinase activity in the DNA damage response. *Mol. Med. Rep.* **20**, 3609–3616 (2019).

152. Li, L., Guan, Y., Chen, X., Yang, J. & Cheng, Y. DNA Repair Pathways in Cancer Therapy and Resistance. *Front. Pharmacol.* **11**, (2021).

153. Sishc, B. J. & Davis, A. J. The Role of the Core Non-Homologous End Joining Factors in Carcinogenesis and Cancer. *Cancers* **9**, 81 (2017).

154. Jonsson, P. *et al.* Tumor lineage shapes BRCA-mediated phenotypes. *Nature* **571**, 576 (2019).

155. Riaz, N. *et al.* Pan-cancer analysis of bi-allelic alterations in homologous recombination DNA repair genes. *Nat. Commun.* **8**, 857 (2017).

156. Deutsch, E. *et al.* Down-regulation of BRCA1 in BCR-ABL-expressing hematopoietic cells. *Blood* **101**, 4583–4588 (2003).

157. Scardocci, A. *et al.* Reduced BRCA1 expression due to promoter hypermethylation in therapy-related acute myeloid leukaemia. *Br. J. Cancer* **95**, 1108–1113 (2006).

158. Knijnenburg, T. A. *et al.* Genomic and Molecular Landscape of DNA Damage Repair Deficiency across The Cancer Genome Atlas. *Cell Rep.* **23**, 239-254.e6 (2018).

159. Bartkova, J. *et al.* Aberrations of the MRE11–RAD50–NBS1 DNA damage sensor complex in human breast cancer: MRE11 as a candidate familial cancer-predisposing gene. *Mol. Oncol.* **2**, 296–316 (2008).

160. Yin, J. *et al.* Revisiting Non-BRCA1/2 Familial Whole Exome Sequencing Datasets Implicates NCK1 as a Cancer Gene. *Front. Genet.* **10**, (2019).

161. Lord, C. J. & Ashworth, A. BRCAness revisited. *Nat. Rev. Cancer* **16**, 110–120 (2016).

162. Wang, Y., Ghosh, G. & Hendrickson, E. A. Ku86 represses lethal telomere deletion events in human somatic cells. *Proc. Natl. Acad. Sci. U. S. A.* **106**, 12430–12435 (2009).

163. Lomnytska, M. I. *et al.* Impact of genomic stability on protein expression in endometrioid endometrial cancer. *Br. J. Cancer* **106**, 1297–1305 (2012).

164. Pozniak, Y. *et al.* System-wide Clinical Proteomics of Breast Cancer Reveals Global Remodeling of Tissue Homeostasis. *Cell Syst.* **2**, 172–184 (2016).

165. Someya, M. *et al.* The association of DNA-dependent protein kinase activity with chromosomal instability and risk of cancer. *Carcinogenesis* **27**, 117–122 (2006).

166. Nilles, N. & Fahrenkrog, B. Taking a Bad Turn: Compromised DNA Damage Response in Leukemia. *Cells* **6**, 11 (2017).

167. Tobin, L. A. *et al.* Targeting abnormal DNA double-strand break repair in tyrosine kinase inhibitor-resistant chronic myeloid leukemias. *Oncogene* **32**, 1784–1793 (2013).

168. Gaymes, T. J., Mufti, G. J. & Rassool, F. V. Myeloid leukemias have increased activity of the nonhomologous end-joining pathway and concomitant DNA misrepair that is dependent on the Ku70/86 heterodimer. *Cancer Res.* **62**, 2791–2797 (2002).

169. Deriano, L. *et al.* Human chronic lymphocytic leukemia B cells can escape DNA damage-induced apoptosis through the nonhomologous end-joining DNA repair pathway. *Blood* **105**, 4776–4783 (2005).

170. Nieborowska-Skorska, M. *et al.* Gene expression and mutation-guided synthetic lethality eradicates proliferating and quiescent leukemia cells. *J. Clin. Invest.* **127**, 2392–2406.

171. Podszywalow-Bartnicka, P. *et al.* Downregulation of BRCA1 protein in BCR-ABL1 leukemia cells depends on stress-triggered TIAR-mediated suppression of translation. *Cell Cycle Georget. Tex* **13**, 3727–3741 (2014).

172. Deutsch, E. *et al.* BCR-ABL down-regulates the DNA repair protein DNA-PKcs. *Blood* **97**, 2084–2090 (2001).

173. Choudhury, A. *et al.* Targeting homologous recombination using imatinib results in enhanced tumor cell chemosensitivity and radiosensitivity. *Mol. Cancer Ther.* **8**, 203–213 (2009).

174. Slupianek, A. *et al.* BCR/ABL stimulates WRN to promote survival and genomic instability. *Cancer Res.* **71**, 842–851 (2011).

175. Hähnel, P. S. *et al.* Targeting components of the alternative NHEJ pathway sensitizes KRAS mutant leukemic cells to chemotherapy. *Blood* **123**, 2355–2366 (2014).

176. Christie, S. M., Fijen, C. & Rothenberg, E. V(D)J Recombination: Recent Insights in Formation of the Recombinase Complex and Recruitment of DNA Repair Machinery. *Front. Cell Dev. Biol.* **10**, 886718 (2022).

177. Steenbergen, E. J., Verhagen, O. J. H. M., van Leeuwen, E. F., von dem Borne, A. E. G. K. & van der Schoot, C. E. Distinct ongoing Ig heavy chain rearrangement processes in childhood B-precursor acute lymphoblastic leukemia. *Blood* **82**, 581–589 (1993).

178. Gawad, C. *et al.* Massive evolution of the immunoglobulin heavy chain locus in children with B precursor acute lymphoblastic leukemia. *Blood* **120**, 4407–4417 (2012).

179. Ochodnicka-Mackovicova, K. *et al.* NF-κB and AKT signaling prevent DNA damage in transformed pre-B cells by suppressing RAG1/2 expression and activity. *Blood* **126**, 1324–1335 (2015).

180. Zhang, L., Reynolds, T. L., Shan, X. & Desiderio, S. Coupling of V(D)J recombination to the cell cycle suppresses genomic instability and lymphoid tumorigenesis. *Immunity* **34**, 163–174 (2011).

181. Bahjat, M. & Guikema, J. E. J. The Complex Interplay between DNA Injury and Repair in Enzymatically Induced Mutagenesis and DNA Damage in B Lymphocytes. *Int. J. Mol. Sci.* **18**, 1876 (2017).

182. Chiou, S.-S. *et al.* Elevated mRNA transcripts of non-homologous end-joining genes in pediatric acute lymphoblastic leukemia. *Leukemia* **21**, 2061–2064 (2007).

183. Coleman, R. L. *et al.* Veliparib with First-Line Chemotherapy and as Maintenance Therapy in Ovarian Cancer. *N. Engl. J. Med.* **381**, 2403–2415 (2019).

184. Robson, M. *et al.* Olaparib for Metastatic Breast Cancer in Patients with a Germline BRCA Mutation. *N. Engl. J. Med.* **377**, 523–533 (2017).

185. Morice, P.-M. *et al.* Myelodysplastic syndrome and acute myeloid leukaemia in patients treated with PARP inhibitors: a safety meta-analysis of randomised controlled trials and a retrospective study of the WHO pharmacovigilance database. *Lancet Haematol.* **8**, e122–e134 (2021).

186. Rose, M., Burgess, J. T., O'Byrne, K., Richard, D. J. & Bolderson, E. PARP Inhibitors: Clinical Relevance, Mechanisms of Action and Tumor Resistance. *Front. Cell Dev. Biol.* **8**, 564601 (2020).

187. Research, C. for D. E. and. FDA approves olaparib tablets for maintenance treatment in ovarian cancer. *FDA* (2019).

188. Research, C. for D. E. and. FDA approves talazoparib for gBRCAm HER2-negative locally advanced or metastatic breast cancer. *FDA* (2019).

189. Research, C. for D. E. and. FDA approves niraparib for first-line maintenance of advanced ovarian cancer. *FDA* (2021).

190. Research, C. for D. E. and. FDA grants accelerated approval to rucaparib for BRCA-mutated metastatic castration-resistant prostate cancer. *FDA* (2021).

191. Dolman, M. E. M. *et al.* DNA-Dependent Protein Kinase As Molecular Target for Radiosensitization of Neuroblastoma Cells. *PloS One* **10**, e0145744 (2015).

192. Yang, C. *et al.* NU7441 Enhances the Radiosensitivity of Liver Cancer Cells. *Cell. Physiol. Biochem. Int. J. Exp. Cell. Physiol. Biochem. Pharmacol.* **38**, 1897–1905 (2016).

193. LaFargue, C. J., Dal Molin, G. Z., Sood, A. K. & Coleman, R. L. Exploring and comparing adverse events between PARP inhibitors. *Lancet Oncol.* **20**, e15–e28 (2019).

194. Li, H. *et al.* PARP inhibitor resistance: the underlying mechanisms and clinical implications. *Mol. Cancer* **19**, 107 (2020).

195. Choi, Y. E. *et al.* Platinum and PARP Inhibitor Resistance Due to Overexpression of MicroRNA-622 in BRCA1-Mutant Ovarian Cancer. *Cell Rep.* **14**, 429–439 (2016).

196. D'Andrea, A. D. Mechanisms of PARP inhibitor sensitivity and resistance. *DNA Repair* **71**, 172–176 (2018).

197. Gogola, E. *et al.* Selective Loss of PARG Restores PARylation and Counteracts PARP Inhibitor-Mediated Synthetic Lethality. *Cancer Cell* **33**, 1078-1093.e12 (2018).

198. Noordermeer, S. M. & Attikum, H. van. PARP Inhibitor Resistance: A Tug-of-War in BRCA-Mutated Cells. *Trends Cell Biol.* **29**, 820–834 (2019).

199. Dietlein, F. *et al.* A functional cancer genomics screen identifies a druggable synthetic lethal interaction between MSH3 and PRKDC. *Cancer Discov.* **4**, 592–605 (2014).

200. Wu, Z.-X. *et al.* M3814, a DNA-PK Inhibitor, Modulates ABCG2-Mediated Multidrug Resistance in Lung Cancer Cells. *Front. Oncol.* **10**, (2020).

201. van Bussel, M. T. J. *et al.* A first-in-man phase 1 study of the DNA-dependent protein kinase inhibitor peposertib (formerly M3814) in patients with advanced solid tumours. *Br. J. Cancer* **124**, 728–735 (2021).

202. Thijssen, R. *et al.* Dual TORK/DNA-PK inhibition blocks critical signaling pathways in chronic lymphocytic leukemia. *Blood* **128**, 574–583 (2016).

203. Munster, P. *et al.* First-In-Human Phase I Study Of A Dual mTOR Kinase And DNA-PK Inhibitor (CC-115) In Advanced Malignancy. *Cancer Manag. Res.* **11**, 10463–10476 (2019).

204. Biddlestone-Thorpe, L. *et al.* ATM kinase inhibition preferentially sensitizes p53-mutant glioma to ionizing radiation. *Clin. Cancer Res. Off. J. Am. Assoc. Cancer Res.* **19**, 3189–3200 (2013).

205. Hoey, C. *et al.* miRNA-106a and prostate cancer radioresistance: a novel role for LITAF in ATM regulation. *Mol. Oncol.* **12**, 1324–1341 (2018).

206. Durant, S. T. *et al.* The brain-penetrant clinical ATM inhibitor AZD1390 radiosensitizes and improves survival of preclinical brain tumor models. *Sci. Adv.* **4**, eaat1719 (2018).

207. Knegtel, R. *et al.* Rational Design of 5-(4-(Isopropylsulfonyl)phenyl)-3-(3-(4-((methylamino)methyl)phenyl)isoxazol-5-yl)pyrazin-2-amine (VX-970, M6620): Optimization of Intra- and Intermolecular Polar Interactions of a New Ataxia Telangiectasia Mutated and Rad3-Related (ATR) Kinase Inhibitor. *J. Med. Chem.* (2019) doi:10.1021/acs.jmedchem.9b00426.

208. Middleton, M. R. *et al.* Phase 1 study of the ATR inhibitor berzosertib (formerly M6620, VX-970) combined with gemcitabine ± cisplatin in patients with advanced solid tumours. *Br. J. Cancer* **125**, 510–519 (2021).

209. Barnieh, F. M., Loadman, P. M. & Falconer, R. A. Progress towards a clinically-successful ATR inhibitor for cancer therapy. *Curr. Res. Pharmacol. Drug Discov.* **2**, 100017 (2021).

210. Reich, M. *et al.* GenePattern 2.0. *Nat. Genet.* **38**, 500–501 (2006).

211. Subramanian, A. *et al.* Gene set enrichment analysis: A knowledge-based approach for interpreting genome-wide expression profiles. *Proc. Natl. Acad. Sci.* **102**, 15545–15550 (2005).

212. Kesarwani, M. *et al.* c-Fos and Dusp1 confer non-oncogene addiction in BCR-ABL induced leukemia. *Nat. Med.* **23**, 472–482 (2017).

213. Zheng, S. & Tang, J. *synergyfinder: Calculate and Visualize Synergy Scores for Drug Combinations*. (Bioconductor version: Release (3.14), 2022). doi:10.18129/B9.bioc.synergyfinder.

214. Takahashi, N., Miura, M., Scott, S. A., Niioka, T. & Sawada, K. Pharmacokinetics of dasatinib for Philadelphia-positive acute lymphocytic leukemia with acquired T315I mutation. *J. Hematol. Oncol.J Hematol Oncol* **5**, 23 (2012).

215. Voeltzel, T. *et al.* A new signaling cascade linking BMP4, BMPR1A, ΔNp73 and NANOG impacts on stem-like human cell properties and patient outcome. *Cell Death Dis.* **9**, 1011 (2018).

216. Bras, S. *et al.* Myeloid leukemia factor is a conserved regulator of RUNX transcription factor activity involved in hematopoiesis. *Proc. Natl. Acad. Sci. U. S. A.* **109**, 4986–4991 (2012).

217. Sood, R., Kamikubo, Y. & Liu, P. Role of RUNX1 in hematological malignancies. *Blood* **129**, 2070–2082 (2017).

218. Jakobczyk, H. *et al.* Reduction of RUNX1 transcription factor activity by a CBFA2T3-mimicking peptide: application to B cell precursor acute lymphoblastic leukemia. *J. Hematol. Oncol.J Hematol Oncol* **14**, 47 (2021).

219. Baumann, A.-M. T. *et al.* 9-O-Acetylation of sialic acids is catalysed by CASD1 via a covalent acetyl-enzyme intermediate. *Nat. Commun.* **6**, 7673 (2015).

220. Mok, S. C. *et al.* DOC-2, a candidate tumor suppressor gene in human epithelial ovarian cancer. *Oncogene* **16**, 2381–2387 (1998).

221. Itami, Y. *et al.* Disabled Homolog 2 (DAB2) Protein in Tumor Microenvironment Correlates with Aggressive Phenotype in Human Urothelial Carcinoma of the Bladder. *Diagnostics* **10**, 54 (2020).

222. Xie, Y. *et al.* Disabled homolog 2 is required for migration and invasion of prostate cancer cells. *Front. Med.* **9**, 312–321 (2015).

223. Matsumoto, Y., Itou, J., Sato, F. & Toi, M. SALL4 - KHDRBS3 network enhances stemness by modulating CD44 splicing in basal-like breast cancer. *Cancer Med.* **7**, 454–462 (2018).

224. Coquel, F. *et al.* SAMHD1 acts at stalled replication forks to prevent interferon induction. *Nature* **557**, 57–61 (2018).

225. Fenouille, N. *et al.* Persistent activation of the Fyn/ERK kinase signaling axis mediates imatinib resistance in chronic myelogenous leukemia cells through upregulation of intracellular SPARC. *Cancer Res.* **70**, 9659–9670 (2010).

226. Cao, Z. *et al.* ZMYND8-regulated IRF8 transcription axis is an acute myeloid leukemia dependency. *Mol. Cell* **81**, 3604-3622.e10 (2021).

227. Tanaka, N., Wang, Y.-H., Shiseki, M., Takanashi, M. & Motoji, T. Inhibition of PRAME expression causes cell cycle arrest and apoptosis in leukemic cells. *Leuk. Res.* **35**, 1219–1225 (2011).

228. Zhang, T. *et al.* APOC2 Is Upregulated in Acute Myeloid Leukemia and Presents a Novel Therapeutic Target. *Blood* **130**, 2483 (2017).

229. Zhang, T. *et al.* Apolipoprotein C2 - CD36 Promotes Leukemia Growth and Presents a Targetable Axis in Acute Myeloid Leukemia. *Blood Cancer Discov.* **1**, 198–213 (2020).

230. Adane, B. *et al.* The Hematopoietic Oxidase NOX2 Regulates Self-Renewal of Leukemic Stem Cells. *Cell Rep.* **27**, 238-254.e6 (2019).

231. Kheifets, V., Bright, R., Inagaki, K., Schechtman, D. & Mochly-Rosen, D. Protein kinase C delta (deltaPKC)-annexin V interaction: a required step in deltaPKC translocation and function. *J. Biol. Chem.* **281**, 23218–23226 (2006).

232. Nayak, R. C. *et al.* The signaling axis atypical protein kinase C λ/ι-Satb2 mediates leukemic transformation of B-cell progenitors. *Nat. Commun.* **10**, 46 (2019).

233. Zhang, T. *et al.* H19 overexpression promotes leukemogenesis and predicts unfavorable prognosis in acute myeloid leukemia. *Clin. Epigenetics* **10**, 47 (2018).

234. Miyagawa, Y. *et al.* Frequent downregulation of LRRC26 by epigenetic alterations is involved in the malignant progression of triple-negative breast cancer. *Int. J. Oncol.* **52**, 1539–1558 (2018).

235. Grasso, S. *et al.* The SRCIN1/p140Cap adaptor protein negatively regulates the aggressiveness of neuroblastoma. *Cell Death Differ.* **27**, 790–807 (2020).

236. Li, J. *et al.* Up-regulated expression of phospholipase C, β1 is associated with tumor cell proliferation and poor prognosis in hepatocellular carcinoma. *OncoTargets Ther.* **9**, 1697–1706 (2016).

237. Xia, L. *et al.* Transcriptional regulation of PRKAR2B by miR-200b-3p/200c-3p and XBP1 in human prostate cancer. *Biomed. Pharmacother.* **124**, 109863 (2020).

238. Sha, J. *et al.* PRKAR2B promotes prostate cancer metastasis by activating Wnt/β-catenin and inducing epithelial-mesenchymal transition. *J. Cell. Biochem.* **119**, 7319–7327 (2018).

239. Alachkar, H. *et al.* SPARC promotes leukemic cell growth and predicts acute myeloid leukemia outcome. *J. Clin. Invest.* **124**, 1512–1524 (2014).

240. DiMartino, J. F. *et al.* Low or absent SPARC expression in acute myeloid leukemia with MLL rearrangements is associated with sensitivity to growth inhibition by exogenous SPARC protein. *Leukemia* **20**, 426–432 (2006).

241. Gaillard, C. *et al.* Identification of IRF8 as a potent tumor suppressor in murine acute promyelocytic leukemia. *Blood Adv.* **2**, 2462–2466 (2018).

242. Sharma, A. *et al.* Constitutive IRF8 expression inhibits AML by activation of repressed immune response signaling. *Leukemia* **29**, 157–168 (2015).

243. Liu, Y., Meng, Y., Zhang, T. & Alachkar, H. Deregulation of apolipoprotein C2 gene in cancer: A potential metabolic vulnerability. *Clin. Transl. Med.* **11**, e406 (2021).

244. Figueroa, M. E. *et al.* Integrated genetic and epigenetic analysis of childhood acute lymphoblastic leukemia. *J. Clin. Invest.* **123**, 3099–3111 (2013).

245. Paolillo, R. *et al.* The NADPH oxidase NOX2 is a marker of adverse prognosis involved in chemoresistance of acute myeloid leukemias. *Haematologica* (2020) doi:10.3324/haematol.2021.279889.

246. Aydin, E. *et al.* NOX2 inhibition reduces oxidative stress and prolongs survival in murine KRAS-induced myeloproliferative disease. *Oncogene* **38**, 1534–1543 (2019).

247. Leong, C. T. C., Ong, C. K., Tay, S. K. & Huynh, H. Silencing expression of UO-44 (CUZD1) using small interfering RNA sensitizes human ovarian cancer cells to cisplatin in vitro. *Oncogene* **26**, 870–880 (2007).

248. Guérin, A. *et al.* LIX1 regulates YAP activity and controls gastrointestinal cancer cell plasticity. *J. Cell. Mol. Med.* **24**, 9244–9254 (2020).

249. Cornish, A. J. *et al.* Identification of recurrent noncoding mutations in B-cell lymphoma using capture Hi-C. *Blood Adv.* **3**, 21–32 (2019).

250. Dallosso, A. R. *et al.* Long-range epigenetic silencing of chromosome 5q31 protocadherins is involved in early and late stages of colorectal tumorigenesis through modulation of oncogenic pathways. *Oncogene* **31**, 4409–4419 (2012).

251. Wang, Z. & Bunting, K. D. STAT5 activation in B-cell acute lymphoblastic leukemia: damned if you do, damned if you don't. *Cancer Cell Microenviron.* **3**, e1186 (2016).

252. Hipp, N. *et al.* IL-2 imprints human naive B cell fate towards plasma cell through ERK/ELK1-mediated BACH2 repression. *Nat. Commun.* **8**, 1443 (2017).

253. Ding, J. *et al.* Inhibition of PI3K/mTOR Overcomes Nilotinib Resistance in BCR-ABL1 Positive Leukemia Cells through Translational Down-Regulation of MDM2. *PLOS ONE* **8**, e83510 (2013).

254. Li, Q. *et al.* BCR/ABL oncogene-induced PI3K signaling pathway leads to chronic myeloid leukemia pathogenesis by impairing immuno-modulatory function of hemangioblasts. *Cancer Gene Ther.* **22**, 227–237 (2015).

255. Hart, L. S. *et al.* ER stress-mediated autophagy promotes Myc-dependent transformation and tumor growth. *J. Clin. Invest.* **122**, 4621–4634 (2012).

256. Zinszner, H. *et al.* CHOP is implicated in programmed cell death in response to impaired function of the endoplasmic reticulum. *Genes Dev.* **12**, 982–995 (1998).

257. Wortel, I. M. N., van der Meer, L. T., Kilberg, M. S. & van Leeuwen, F. N. Surviving Stress: Modulation of ATF4-Mediated Stress Responses in Normal and Malignant Cells. *Trends Endocrinol. Metab. TEM* **28**, 794–806 (2017).

258. Rhee, S. G. & Kil, I. S. Multiple Functions and Regulation of Mammalian Peroxiredoxins. *Annu. Rev. Biochem.* **86**, 749–775 (2017).

259. Barranco-Medina, S., Lázaro, J.-J. & Dietz, K.-J. The oligomeric conformation of peroxiredoxins links redox state to function. *FEBS Lett.* **583**, 1809–1816 (2009).

260. Lee, W. *et al.* Human peroxiredoxin 1 and 2 are not duplicate proteins: the unique presence of CYS83 in Prx1 underscores the structural and functional differences between Prx1 and Prx2. *J. Biol. Chem.* **282**, 22011–22022 (2007).

261. Kim, H. *et al.* Stable maintenance of the Mre11-Rad50-Nbs1 complex is sufficient to restore the DNA double-strand break response in cells lacking RecQL4 helicase activity. *J. Biol. Chem.* **297**, 101148 (2021).

262. Tang, J. *et al.* Role of Paralogue of XRCC4 and XLF in DNA Damage Repair and Cancer Development. *Front. Immunol.* **13**, (2022).

263. De Gregoriis, G. *et al.* DNA repair genes PAXIP1 and TP53BP1 expression is associated with breast cancer prognosis. *Cancer Biol. Ther.* **18**, 439–449 (2017).

264. Liu, Y. & Lu, L.-Y. BRCA1 and homologous recombination: implications from mouse embryonic development. *Cell Biosci.* **10**, 49 (2020).

265. Alexander, P. M., Caudell, D. L., Kucera, G. L., Pladna, K. M. & Pardee, T. S. The novel phospholipid mimetic KPC34 is highly active against preclinical models of Philadelphia chromosome positive acute lymphoblastic leukemia. *PLOS ONE* **12**, e0179798 (2017).

266. Fiskus, W. *et al.* Auranofin induces lethal oxidative and endoplasmic reticulum stress and exerts potent preclinical activity against chronic lymphocytic leukemia. *Cancer Res.* **74**, 2520–2532 (2014).

267. Liu, C.-X. *et al.* Adenanthin targets peroxiredoxin I and II to induce differentiation of leukemic cells. *Nat. Chem. Biol.* **8**, 486–493 (2012).

268. Hartman, M. L. & Czyz, M. BCL-w: apoptotic and non-apoptotic role in health and disease. *Cell Death Dis.* **11**, 1–16 (2020).

269. Poplawski, T., Pastwa, E. & Blasiak, J. Non-homologous DNA end joining in normal and cancer cells and its dependence on break structures. *Genet. Mol. Biol.* **33**, 368–373 (2010).

270. Fu, Y.-W. *et al.* Dynamics and competition of CRISPR–Cas9 ribonucleoproteins and AAV donor-mediated NHEJ, MMEJ and HDR editing. *Nucleic Acids Res.* **49**, 969–985 (2021).

271. Yu, W. *et al.* Repair of G1 induced DNA double-strand breaks in S-G2/M by alternative NHEJ. *Nat. Commun.* **11**, 5239 (2020).

272. Iliakis, G. Backup pathways of NHEJ in cells of higher eukaryotes: Cell cycle dependence. *Radiother. Oncol.* **92**, 310–315 (2009).

273. Hustedt, N. & Durocher, D. The control of DNA repair by the cell cycle. *Nat. Cell Biol.* **19**, 1–9 (2017).

274. Yang, L. *et al.* Identification of Poly(ADP-Ribose) Polymerase-1 as a Cell Cycle Regulator through Modulating Sp1 Mediated Transcription in Human Hepatoma Cells. *PLOS ONE* **8**, e82872 (2013).

275. Weaver, A. & Yang, E. Beyond DNA Repair: Additional Functions of PARP-1 in Cancer. *Front. Oncol.* **3**, (2013).

Komisja Bioetyczna
przy Warszawskim Uniwersytecie Medycznym

Tel.: 022/ 57 - 20 -303
Fax: 022/ 57 - 20 -165

ul. Żwirki i Wigury nr 61
02-091 Warszawa

e-mail: komisja.bioetyczna@wum.edu.pl
www.komisja-bioetyczna.wum.edu.pl

KB/.....44...../2015

Komisja Bioetyczna przy Warszawskim Uniwersytecie Medycznym
po zapoznaniu się z wnioskiem /wymienić wnioskodawcę/ - **w dniu 10 marca 2015r.**
Prof.dr hab. Jakub Gołąb, Zakład Immunologii,
ul. Chałubińskiego 5,02-004 Warszawa,

dotyczącym: wyrażenia opinii w sprawie badania pt.: „ Rola peroksyredoksyny 1 i innych białek antyoksydacyjnych w ostrej białaczce limfoblastycznej B komórkowej."

wyraża następującą
o p i n i ę

- stwierdza, że jest ono dopuszczalne i zgodne z zasadami naukowo-etycznymi*.
- ~~stwierdza, że jest ono niedopuszczalne i niezgodne z zasadami naukowo-etycznymi.*~~

Uwagi Komisji-verte

Pouczenie-w ciągu 14 dni od otrzymania decyzji wnioskodawcy przysługuje Prawo odwołania do Komisji Odwoławczej za pośrednictwem Komisji Bioetycznej przy Warszawskim Uniwersytecie Medycznym.
Komisja działa na podstawie art.29 ustawy z dnia 5.12.1996r. o zawodzie lekarza /Dz.U.nr 28/97 poz.152 wraz z późn.zm./, zarządzenia MZiOS z dn.11.05.1999r. w sprawie szczegółowych zasad powoływania i finansowania oraz trybu działania komisji bioetycznych /Dz.U.nr 47 poz.480/, Ustawy prawo farmaceutyczne z dnia 6 września 2001r. (Dz.U.Nr 126, poz. 1381 z późn. zm.) Zarządzenie nr 56/2007 z dnia 15 października 2007 r.w sprawie działania Komisji Bioetycznej przy Warszawskim Uniwersytecie Medycznym /Regulamin Komisji Bioetycznej przy Warszawskim Uniwersytecie Medycznym/. Komisja działa zgodnie z zasadami GCP.
W załączeniu- skład Komisji oraz lista obecności.

Przewodnicząca
Komisji Bioetycznej

Prof. dr hab. n .med. Maria Roszkowska-Blaim

*niepotrzebne skreślić

UCHWAŁA NR WAW2/095/2019

z dnia 28 czerwca 2019 r.

II Lokalnej Komisji Etycznej do spraw doświadczeń na zwierzętach w Warszawie

§ 1

Na podstawie art. 48 ust. 1 pkt. 1[1] ustawy z dnia 15 stycznia 2015r. o ochronie zwierząt wykorzystywanych do celów naukowych lub edukacyjnych (Dz. U. poz. 266), zwanej dalej „ustawą" po rozpatrzeniu wniosku pt.: „Namnażanie ludzkich komórek białaczkowych w myszach z niedoborem odporności oraz ocena skuteczności immunoterapii" z dnia 04 czerwca 2019 roku, złożonego przez Warszawski Uniwersytet Medyczny, I Wydział Lekarski, adres: ul. Żwirki i Wigury 61, 02-091 Warszawa, zaplanowanego przez Małgorzatę Firczuk[2]

przy udziale[3] -

Lokalna Komisja Etyczna:

WYRAŻA ZGODĘ

na przeprowadzenie doświadczeń na zwierzętach w zakresie wniosku.

§ 2

W wyniku rozpatrzenia wniosku o którym mowa w § , Lokalna Komisja Etyczna ustaliła, że:

1. Wniosek należy przypisać do kategorii: badania podstawowe, onkologia.
2. Najwyższy stopień dotkliwości proponowanych procedur to: umiarkowana.
3. Doświadczenia będą przeprowadzane na gatunkach lub grupach gatunków[4]:

Gatunek	Wiek/stadium rozwoju	Liczba
Mysz domowa NOD/ShiLtJ (NSG)	8-12 tygodni	342

4. Doświadczenia będą przeprowadzane przez: Małgorzata Firczuk, Angelika Muchowicz, Klaudyna Fidyt, Łukasz Komorowski, Łukasz Cheda.
5. Doświadczenie będzie przeprowadzane w terminie[5] od 01.07.2019 do 30.06.2023 r.
6. Doświadczenie będzie przeprowadzone w ośrodku[6]: Centrum Badań Przedklinicznych i Technologii WUM, Banacha 1B, 02-097 Warszawa.
7. Doświadczenie będzie przeprowadzone poza ośrodkiem, w: Centrum Nauk Biologiczno-Chemicznych, Uniwersytet Warszawski, Żwirki i Wigury 101, 02-089 Warszawa.
8. Użyte do procedur zwierzęta dzikie zostaną odłowione przez: nie dotyczy.
9. Doświadczenie ~~zostanie~~/nie zostanie ~~poddane ocenie retrospektywnej w terminie do 6 miesięcy od dnia przekazania przez użytkownika dokumentacji, mającej stanowić podstawę~~

---

[1] Niewłaściwy zapis usunąć

[2] imię i nazwisko osoby, która zaplanowała i jest odpowiedzialna za przeprowadzenie doświadczenia

[3] Wypełnić w przypadku dopuszczenia do postępowania organizacji społecznej.

[4] Podać liczbę, szczep/stado, wiek/stadium rozwoju

[5] Nie dłużej niż 5 lat

[6] Podać jeśli jest to inny ośrodek niż użytkownik

~~dokonania oceny retrospektywnej. Użytkownik jest zobowiązany do przekazania ww. dokumentacji niezwłocznie, tj. w terminie, o którym mowa w art. 52 ust. 2 ustawy.~~

§ 3

Uzasadnienie:

Komisja oceniła wniosek zgodnie z kryteriami zawartymi w art. 47.1. ustawy z dnia 15 stycznia 2015 r. o ochronie zwierząt wykorzystywanych do celów naukowych lub edukacyjnych (Dz. U. poz. 266). Po zapoznaniu się z problematyką badawczą przedstawioną we wniosku komisja stwierdza, że przedstawiony projekt spełnia zasady dopuszczenia doświadczeń na zwierzętach. Na podstawie art. 107 § 4 ustawy z dnia 14 czerwca 1960 r. – Kodeks postępowania administracyjnego z późniejszymi zmianami (Dz. U. z 2017 poz. 1257) odstąpiono od sporządzania uzasadnienia decyzji, gdyż uwzględnia ona w całości żądanie strony.

§ 4

Integralną część niniejszej uchwały stanowi kopia wniosku, o którym mowa w § 1.

Szkoła Główna Gospodarstwa Wiejskiego
w Warszawie
II Lokalna Komisja Etyczna
ds. Doświadczeń na Zwierzętach
02-786 Warszawa, ul. Ciszewskiego 8
tel. 22 59-36522

(Pieczęć lokalnej komisji etycznej)

PRZEWODNICZĄCA
II Lokalnej Komisji Etycznej
ds. Doświadczeń na Zwierzętach przy SGGW
/ Prof. dr hab. Joanna Gromadzka-Ostrowska /

(Podpis Przewodniczącej komisji)

Pouczenie:

Zgodnie z art. 33 ust. 3 i art. 40 ustawy w zw. z art. 127 § 1 i 2 oraz 129 § 2 ustawy z dnia z dnia 14 czerwca 1960 r. Kodeks postępowania administracyjnego (Dz. U. 2017, poz. 1257 – tj.; dalej KPA) od uchwały Lokalnej Komisji Etycznej strona może wnieść, za jej pośrednictwem, odwołanie do Krajowej Komisji Etycznej do Spraw Doświadczeń na Zwierzętach w terminie 14 od dnia doręczenia uchwały.

Na podstawie art. 127a KPA w trakcie biegu terminu do wniesienia odwołania strona może zrzec się prawa do jego wniesienia, co należy uczynić wobec Lokalnej Komisji Etycznej, która wydała uchwałę. Z dniem doręczenia Lokalnej Komisji Etycznej oświadczenia o zrzeczeniu się prawa do wniesienia odwołania przez ostatnią ze stron postępowania, decyzja staje się ostateczna i prawomocna.

Otrzymuje:

1) Użytkownik,
2) Organizacja społeczna dopuszczona do udziału w postępowaniu (jeśli dotyczy)
3) a/a

Użytkownik kopie przekazuje:

- Osoba planująca doświadczenie
- Zespół ds. dobrostanu